The Role of Neutral Donor Ligands in the Isoselective Ring-Opening Polymerization of *rac*-β-Butyrolactone

Xiang Dong,[a] Jerome R. Robinson*[a]

[a] 324 Brook St., Department of Chemistry, Brown University, Providence, RI 02912, United States
Phone: (+1)-401-863-3249; e-mail: jerome_robinson@brown.edu

Supporting Information

1. General Methods.

Instruments and measurements: Unless specified, all reactions were performed under inert conditions (N_2) using standard Schlenk techniques or in a MBraun drybox equipped with a standard catalyst purifier and solvent trap. Glassware was oven-dried for at least 2 h at 150 °C prior to use. Celite and 3 Å molecular sieves were heated under reduced pressure at 300 °C for at least 24 h and then cooled under vacuum prior to use. The following spectrometers were used for NMR characterization: Bruker Avance III HD Ascend (^{1}H: 600 MHz, ^{13}C: 152 MHz, ^{31}P: 243 MHz) and a Bruker DRX (^{1}H: 400 MHz, ^{13}C: 101 MHz, ^{31}P: 162 MHz). ^{1}H- and ^{13}C-NMR shifts are referenced relative to the solvent signal ($CDCl_3$: ^{1}H: 7.26 ppm, ^{13}C: 77.16 ppm; C_6D_6: ^{1}H: 7.16 ppm, ^{13}C: 128.06 ppm), while ^{31}P-NMR shifts are referenced relative to external solution standards (H_3PO_4, 0 ppm). Both instruments were equipped with Z-gradient BBFO probes. Probe temperatures were calibrated using ethylene glycol and methanol as previously described.[1] Polymer tacticity (P_m, percentage of *meso* diads) was measured using a ^{13}C inverse-gated pulse sequence, followed by integration of the <u>*C*</u>=O resonances (Figure S21). The mechanism for stereocontrol was determined by statistical analysis of stereochemical triads in P3HB (*rr, mm,* and *rm*/*mr*; integration of <u>*C*</u>H_2 resonances from ^{13}C-NMR using an inverse-gated pulse sequence) as described by Thomas and Carpentier.[2]

Gel permeation chromatography (GPC) measurements were performed using an Agilent 1260 equipped with two Poroshell 120 EC-C18 columns heated at 35 °C (4.6 x 100 mm, 2.7 µm) and a UV-vis diode-array detector and refractive detector. The eluent was inhibitor-free THF, and the system was calibrated with standard polystyrene standards ranging from 580 to 1,500,000 Da. Reported molecular weights are those obtained from GPC corrected by a Mark-Houwink factor of 0.54.[3] Unless stated otherwise, all GPC samples were of the quenched crude reaction mixtures (not precipitated or purified polymers). P3HB samples (10 mg/mL in THF) using a DCTB/NaTFA matrix (v/v, 10:1) were analysed using MALDI TOF MS under positive-ion reflectron mode on a Bruker Ultraflex III ToF/ToF mass spectrometer at the University of Akron. IR spectra were recorded on Jasco 4100 FTIR spectrometers using Nujol mulls sandwiched between KBr plates. Elemental analyses were performed by Robertson Microlit Laboratories (Ledgewood, NJ) and Midwest Microlab, LLC (Indianapolis, IN) for bench-stable (**^{1}L**) and air-sensitive compounds (**1-RE** and **1-RE(TPPO)$_2$**) respectively. Samples were shipped in a sealed 2 mL vial that was placed in a 20 mL scintillation vial and sealed, which were then placed in a vacuum-sealed plastic bag.

Materials: Tetrahydrofuran, diethyl ether, toluene, hexanes, and pentane were purchased from Fisher Scientific. Solvents were sparged for 20 min with dry Ar and dried using a commercial two-column solvent purification system (LC Technologies). Solvents were further dried by storing them over 3 Å molecular sieves for at least 48 h prior to use. Ultrapure, deionized water (18.2 MΩ) was obtained from a Millipore Direct-Q 3 UV Water Purification System. Deuterated solvents were purchased from Cambridge Isotope Laboratories, Inc. C_6D_6 was degassed with 3 freeze-pump-thaw cycles and stored over 3 Å molecular sieves for at least 48 h prior to use. Qualitative assessment of moisture-content in these solvents was performed by adding 1 drop of a concentrated solution of a sodium benzophenone radical anion (purple) to 10 mL of solvent where maintenance of a dark blue color for at least 5 minutes was sufficient for use.

2,6-ditertbutyl phenol (Oakwood Chemical; 99% purity), para-formaldehyde (Alfa Aesar; 97% purity), benzylamine (TCI; 99% purity), 2-methoxyethylamine (Sigma-Aldrich; 99% purity), triphenylphosphine oxide (Acros; 99% purity), trioctylphosphine oxide (Sigma-Aldrich; 99% purity), hexamethylphosphoramide (TCI; 98% purity), triphenylphosphate (Sigma-Aldrich; 99% purity), triphenyl phosphine (Sigma-Aldrich; 99% purity), 4-dimethylaminopyridine (Chem-Impex; 99% purity), 1,4-diazabicyclo[2.2.2]octane (Sigma-Aldrich; 99% purity), potassium hexamethyldisilazide (Sigma-Aldrich; 95% purity), 1,1,3,3-tetramethyldisilazane (TCI, 97% purity), $RECl_3$ (Strem; RE = La, Y; 99.9% purity), (*R*)-methyl 3-hydroxybutanoate (Oakwood; 99% purity), acetyl chloride (Acros; 99% purity), 2-propanol (Alfa-Aesar, Anhydrous, 99.5% purity), and pyridine (Sigma-Aldrich; 99% purity) were purchased and used as received. Racemic butyrolactone (Sigma-Aldrich; 98% purity) was freshly distilled from CaH_2 under nitrogen and degassed by freeze-pump-thaw cycles prior to use. $RE[N(SiMe_3)_2]_3$ (RE = La and Y),[4] $RE[N(SiHMe_2)_2]_3(THF)_2$ (RE = La and Y),[5] 6,6'-(((2-methoxyethyl)azanediyl)bis-(methylene))bis(2,4-di-tert-butylphenol) (^{2}L),[6] RE(^{2}L)THF (RE = La[6] and Y[7]) were prepared according to reported procedures.

X-ray Crystallography: Samples were collected in Paraton™ oil on a petri dish in a glovebox and then quickly evaluated and mounted with the assistance of an optical microcope. X-ray reflection intensity data were collected on a Bruker D8 Quest with a Photon 100 CMOS detector employing graphite-monochromated Mo-Kα radiation (λ = 0.71073 Å) at a temperature of 173(1) K. Rotation frames were integrated using SAINT,[8] producing a listing of unaveraged F^2 and $\sigma(F^2)$ values which were then passed to the SHELXT[9] program package for further processing and structure solution. The intensity data were corrected for Lorentz and polarization effects and for absorption using SADABS.[10] The structures were solved by direct methods (SHELXT).[9] Refinement was by full-matrix least squares based on F^2 using SHELXL.[11] All reflections were used during refinements. Non-hydrogen atoms were refined anisotropically and hydrogen atoms were refined using a riding model. Two tert-butyl groups and one of the $Si(HMe_2)$ groups were found to be disordered over two positions in [La(^{1}L)($N(SiHMe_2)_2$)$(TPPO)_2$] (**1-La(TPPO)$_2$**). Two tert-butyl groups were found to be disordered over two positions in [Y(^{1}L)($N(SiHMe_2)_2$)$(TPPO)_2$] (**1-Y(TPPO)$_2$**). Disorders were refined with the help of similarity restraints using standard/default values on 1,2 and 1,3 distances (SADI) and rigid bond restraints (RIGU) of the disordered groups.[12,13] For the structures [La(^{1}L)($N(SiHMe_2)_2$)$(TPPO)_2$] (**1-La(TPPO)$_2$**) and [Y(^{1}L)($N(SiHMe_2)_2$)$(TPPO)_2$] (**1-Y(TPPO)$_2$**) there were areas of disordered solvent (toluene, 2 molecules in the asymmetric unit) for which reliable disorder models could not be devised; the X-ray data were corrected for the presence of disordered solvent using SQUEEZE.[14] Crystallographic parameters are summarized in Table S5, bond distances and angles are summarized in Tables S6-S8, and thermal ellipsoid plots (50 % probability) are shown in Figures S26-S28.

2. Synthetic Details and Characterization.

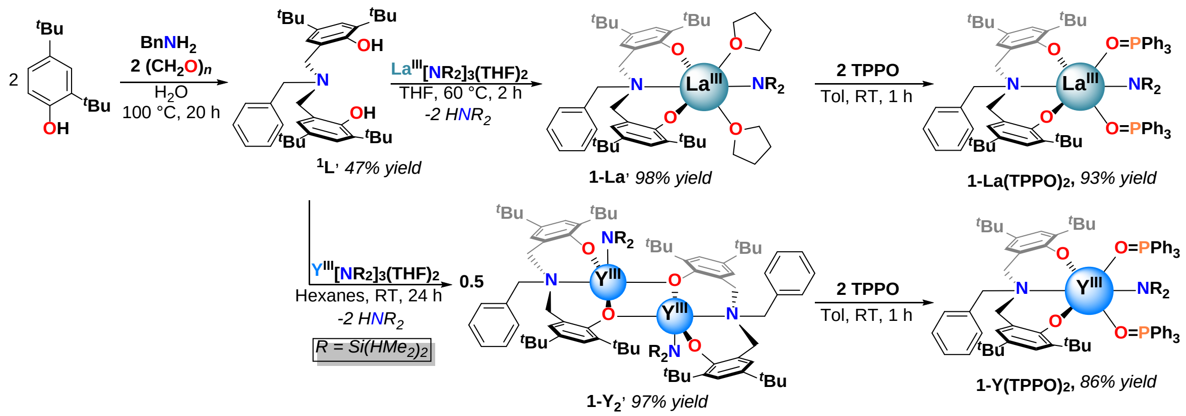

Scheme S1. Synthesis of benzyl-amino bisphenol and corresponding rare-earth complexes.

6,6'-((benzylazanediyl)bis(methylene))bis(2,4-di-tert-butylphenol), (^{1}L)

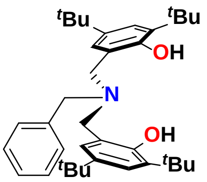

^{1}L

A 250 mL round-bottomed flask was charged with benzyl amine (3.27 g, 30.5 mmol, 1.0 equiv.; MW: 107.16 g•mol^{-1}), DI water (50 mL), a Teflon-coated stir bar, and paraformaldehyde (1.83 g; 30.5 mmol; 2.0 equiv.; MW: 30.03 g•mol^{-1}) paraformaldehyde, resulting in a colorless solution. To the stirring mixture, 2,6-ditertbutyl phenol (12.59 g, 30.5 mmol, 2.0 equiv.; MW: 206.33 g•mol^{-1}) was added and floated on the top of the solution. The reaction was heated in an oil bath at 110 °C for 20 h. The mixture became a yellow emulsion during heating. After cooling to RT, a solid was formed out of the cooled liquid. The aqueous layer was decanted. The residual solid was dissolved in EtOH (20 mL) at 60 °C and then cooled to RT, affording a colorless crystalline solid after standing overnight. The solid was isolated by vacuum filtration over a course porosity fritted filter, washed with EtOH (2 × 10 mL), and dried under reduced pressure to furnish compound **^{1}L** as a white solid. Yield: 7.8 g (14.3 mmol, 47% yield; MW: 543.84 g•mol^{-1}).

^{1}H-NMR (400 MHz, $CDCl_3$, 298 K): δ = 1.28 (s, 18H; 2-^{t}Bu), 1.42 (s, 18H; 4-^{t}Bu), 3.60 (s, 2H; N<u>*CH*</u>$_2$Bn), 3.66 (s, 4H; N<u>*CH*</u>$_2$ArOH), 6.94 (d, *J* = 2.4 Hz, 2H; 5-H_{Ar}), 7.22 (d, *J* = 2.4 Hz, 2H; 3-H_{Ar}), 7.30-7.42 ppm (m, 7H; Bn, OH);

^{13}C{^{1}H}-NMR (101 MHz, $CDCl_3$, 298 K): δ = 29.8 (C<u>*Me*</u>$_3$), 31.8 (C<u>*Me*</u>$_3$), 34.3 (<u>*C*</u>Me$_3$), 35.0 (<u>*C*</u>Me$_3$), 57.0 (N<u>CH</u>$_2$ArOH), 58.6 (N<u>CH</u>$_2$Bn), 121.5, 123.7, 125.3, 128.0, 129.1, 129.7, 136.1, 137.6, 141.6, 152.3 ppm (<u>C</u>$_{Ar}$–OH);

^{1}H-NMR (400 MHz, C_6D_6, 298 K): δ = 1.34 (s, 18H; 2-^{t}Bu), 1.62 (s, 18H; 4-^{t}Bu), 3.29 (s, 2H; N<u>*CH*</u>$_2$Bn), 3.39 (s, 4H; N<u>*CH*</u>$_2$ArOH), 6.96 (d, *J* = 2.4 Hz, 2H; 5-H_{Ar}), 7.02 (t, *J* = 7.2 Hz, 1H;

p-H$_{Bn}$), 7.11 (t, J = 7.2 Hz, 2H; m-H$_{Bn}$), 7.26 (d, J = 7.2 Hz, 2H; o-H$_{Bn}$), 7.49 (d, J = 2.4 Hz, 2H; 3-H$_{Ar}$), 7.69 ppm (m, 2H; OH);

Elemental Analysis calcd. (%) for $C_{37}H_{53}NO_2$: C 81.72, H 9.82, N 2.58; found: C 81.94, H 9.78, N 2.56.

La(^{1}L)[N(SiHMe$_2$)$_2$](THF)$_2$ (1-La)

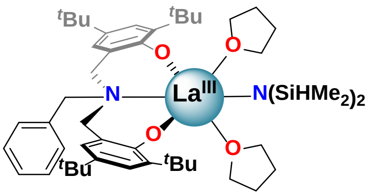

1-La

A 20 mL scintillation vial was charged with **^{1}L** (335 mg, 0.62 mmol, 1.0 equiv.; MW: 543.84 g•mol^{-1}), a Teflon-coated stir-bar, and THF (2 mL). To the stirring, clear, and colorless solution, La[N(SiHMe$_2$)$_2$]$_3$(THF)$_2$ (419 mg, 0.62 mmol, 1.0 equiv.; MW: 680.12 g•mol^{-1}) was added. The solution was heated at 60 °C for 2 h. All volatiles were removed under reduced pressure, affording **1-La** as a white solid. Yield: 580 mg (0.61 mmol, 98% yield; MW: 957.27 g•mol^{-1}).

^{1}H-NMR (600 MHz, C_6D_6, 298 K): δ = 0.42 (d, ^3J = 3.0 Hz, 12H; SiH<u>*Me*$_2$</u>), 1.23 (s, 8H; 3,4-H$_{THF}$), 1.46 (s, 18H; 2-^{t}Bu), 1.74 (s, 18H; 4-^{t}Bu), 3.45 (d, ^2J = 12.8 Hz, 2H; N<u>C*H*$_2$</u>ArO), 3.65 (s, 8H; 2,5-H$_{THF}$), 3.79 (s, 2H; N<u>C*H*$_2$</u>Bn), 4.00 (d, ^2J = 12.8 Hz, 2H; NC*H*$_2$ArO), 5.21 (quint, ^3J = 3.0 Hz, $^1J_{Si(29)\text{-}H}$ = 167 Hz, 2H; Si-H), 7.04 (t, J = 7.2 Hz, 1H; p-H$_{Bn}$), 7.15 (t, J = 7.2 Hz, 2H; m-H$_{Bn}$), 7.19 (d, J = 7.2 Hz, 2H; o-H$_{Bn}$), 7.20 (d, J = 2.4 Hz, 2H; 5-H$_{ArO}$), 7.62 ppm (d, J = 2.4 Hz, 2H; 3-H$_{ArO}$);

^{13}C{^{1}H}-NMR (152 MHz, C_6D_6, 298 K): δ = 4.0 (SiH<u>*Me*$_2$</u>), 25.3 (β-C$_{THF}$), 30.5 (C<u>*Me*$_3$</u>), 32.3 (C<u>*Me*$_3$</u>), 34.3 (<u>*C*</u>Me$_3$), 35.6 (<u>*C*</u>Me$_3$), 52.0 (N<u>*C*H$_2$</u>Bn), 61.6 (N<u>*C*H$_2$</u>ArO), 69.7 (α-C$_{THF}$), 124.0, 125.0, 127.8, 128.3, 128.7, 131.6, 135.7, 135.9, 136.9, 162.6 ppm (<u>C$_{Ar}$</u>–O);

IR (Nujol): 2075 [m, ν(SiH)], 2011 [w, ν(La←<u>*H–Si*</u>)], 1774 (w), 1602 (w), 1414 (m), 1305 (s), 1279 (s), 1241 (s), 1232 (s), 1201 (m), 1165 (m), 1133 (m), 1051 (m), 1030 (m), 962 (m), 899 (s), 883 (s), 835 (s), 802 (m), 787 (m), 762 (m), 700 (m), 644 (w), 629 (m), 598 (m), 528 (m), 489 (w), 444 (m) cm^{-1};

Elemental Analysis calcd. (%) for $C_{49}H_{81}LaN_2O_4Si_2$: C 61.75, H 8.30, N 2.92; found: C 61.48, H 8.53, N 2.93.

{Y(^{1}L)[N(SiHMe$_2$)$_2$]}$_2$ (1-Y$_2$)

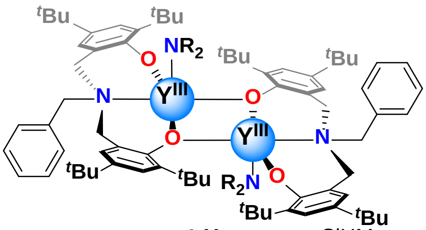

1-Y$_2$ R = SiHMe$_2$

A 20 mL scintillation vial was charged with **^{1}L** (253 mg, 0.47 mmol, 1.0 equiv.; MW: 543.84 g•mol^{-1}), a Teflon-coated stir-bar, and hexanes (2 mL). To the stirring, clear, and colorless solution, Y[N(SiHMe$_2$)$_2$]$_3$(THF)$_2$ (294 mg, 0.47 mmol, 1.0 equiv.; MW: 630.12 g•mol^{-1}) was added. The solution was stirred at ambient temperature for 24 h. All volatiles were removed under reduced pressure, affording **1-Y$_2$** as a white solid. Yield: 345 mg (0.23 mmol, 97% yield; MW: 1526.12 g•mol^{-1}).

^{1}H-NMR (600 MHz, C_6D_6, 298 K): δ = -0.09 (d, ^3J = 2.9 Hz, 12H; SiH<u>*Me$_2$*</u>), 0.18 (d, ^3J = 2.9 Hz, 12H; SiH<u>*Me$_2$*</u>), 1.23 (s, 18H; 2-^{t}Bu), 1.32 (s, 18H; 4-^{t}Bu) , 1.37 (s, 18H; 4-^{t}Bu) , 1.62 (s, 18H; 2-^{t}Bu), 3.79 (d, ^2J = 13.2 Hz, 2H; N<u>C*H$_2$*</u>ArO), 3.93 (d, ^2J = 14.4 Hz, 2H; N<u>C*H$_2$*</u>ArO), 4.40 (d, ^2J = 14.4 Hz, 2H; N<u>C*H$_2$*</u>Bn), 4.55 (d, ^2J = 14.4 Hz, 2H; N<u>C*H$_2$*</u>Bn), 4.73 (d, ^2J = 13.2 Hz, 2H; N<u>C*H$_2$*</u>ArO), 4.94 (d, ^2J = 14.4 Hz, 2H; N<u>C*H$_2$*</u>ArO), 5.00-5.03 (m, 4H; Si-H), 7.06 (d, J = 2.4 Hz, 2H; 5-H$_{ArO}$), 7.17 (t, J = 7.2 Hz, 2H; *p*-H$_{Bn}$), 7.22 (d, J = 2.4 Hz, 2H; 5-H$_{ArO}$), 7.27 (t, J = 7.2 Hz, 4H; *m*-H$_{Bn}$), 7.38 (d, J = 2.4 Hz, 4H; 3-H$_{ArO}$), 7.47 (d, J = 2.4 Hz, 4H; 3-H$_{ArO}$), 7.60 ppm (d, J = 7.2 Hz, 4H; *o*-H$_{Bn}$);

^{13}C{^{1}H}-NMR (152 MHz, C_6D_6, 298 K): δ = 2.6 (SiH<u>*Me$_2$*</u>), 3.1 (SiH<u>*Me$_2$*</u>), 29.6 (C<u>*Me$_3$*</u>), 31.6 (C<u>*Me$_3$*</u>), 32.0 (C<u>*Me$_3$*</u>), 34.22 (<u>*C*</u>Me$_3$), 34.26 (<u>*C*</u>Me$_3$), 34.33 (C<u>*Me$_3$*</u>), 35.1 (<u>*C*</u>Me$_3$), 36.7 (<u>*C*</u>Me$_3$), 52.1 (N<u>*C*H$_2$</u>Bn), 59.3 (N<u>*C*H$_2$</u>ArO), 62.1 (N<u>*C*H$_2$</u>ArO), 123.3, 123.8, 125.5, 126.7, 128.29, 128.31, 128.34, 129.4, 132.8, 133.4, 136.4, 137.7, 137.9, 142.6, 155.0 (<u>C$_{Ar}$</u>–O), 161.1 ppm (d, $J_{Y\text{-}C}$ = 3.3 Hz, <u>C$_{Ar}$</u>–O);

IR (Nujol): 2096 [m, ν(SiH)], 2054 [w, ν(SiH)], 1936 [br, m, ν(Y←<u>*H–Si*</u>)], 1605 (w), 1415 (m), 1307 (m), 1279 (m), 1248 (m), 1246 (m), 1225 (m), 1201 (m), 1165 (m), 1128 (m), 1086 (w), 1012 (s), 964 (m), 901 (s), 877 (s), 834 (s), 802 (m), 768 (m), 746 (m), 704 (m), 648 (w), 631 (m), 613 (m), 534 (m), 521 (w), 501 (w), 455 (m) cm^{-1};

Elemental Analysis calcd. (%) for $C_{82}H_{130}N_4O_4Si_4Y_2$: C 64.76, H 8.63, N 3.63; found: C 64.54, H 8.59, N 3.67.

The assignment of the ^{1}H- and ^{13}C{^{1}H}-NMR spectrum for **1-Y$_2$** was made by heteronuclear multiple bond correlation (HMBC) spectroscopy. Assignment for the bridging versus terminal phenolate in the ^{13}C-NMR was made based on comparison of the mononuclear **1-La**. The bridging phenolate <u>*C$_{Ar}$*</u>–O is significantly shifted up-field (155.0 ppm) in comparison to the corresponding terminal <u>C$_{Ar}$</u>–O (**1-Y$_2$**: 161.1 ppm; **1-La**: 162.6 ppm). The HMBC experiment was done at 600 MHz, with filtered ^1J coupling constant (cnst2) = 145 Hz, long rang ^nJ coupling constant (cnst13) = 10 Hz.

La(^{1}L)[N(SiHMe$_2$)$_2$](TPPO)$_2$ (1-La(TPPO)$_2$)

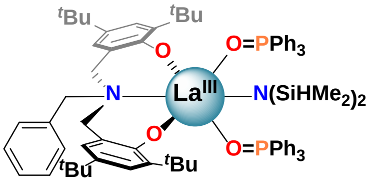

1-La(TPPO)$_2$

A 20 mL scintillation vial was charged with **1-La** (173 mg, 0.18 mmol, 1.0 equiv.; MW: 957.27 g•mol^{-1}), TPPO (101 mg, 0.36 mmol, 2.0 equiv.; MW: 278.29 g•mol^{-1}) and toluene (0.5 mL). After all solids were dissolved, hexane (3 mL) was layered on top of the toluene solution. After the two layers mixed (~ 1 h), the vial was cooled in the glovebox freezer at –35 °C for 3 h, affording a white crystalline solid. The mother liquor was decanted and volatiles were removed under reduced pressure, affording **1-La(TPPO)$_2$** as a white solid. Yield: 230 mg (0.17 mmol, 93% yield; MW: 1369.64 g•mol^{-1}). X-ray quality crystals were grown by layering hexane (2 mL) on top of a solution of **1-La(TPPO)$_2$** (200 mg / 0.5 mL toluene) and allowing the solution to stand and mix undisturbed at RT.

^{1}H-NMR (600 MHz, C_6D_6, 298 K): δ = 0.50 (d, J_3 = 3.0 Hz, 12H; SiH$\underline{Me_2}$), 1.51 (s, 18H; 2-^{t}Bu), 1.81 (s, 18H; 4-^{t}Bu), 2.95 (br, 2H; N$\underline{CH_2}$ArO), 3.74 (s, 2H; N$\underline{CH_2}$Bn), 3.78 (br, 2H; N$\underline{CH_2}$ArO), 5.63 (quint, ^3J = 3.0 Hz, $^1J_{Si(29)\text{-}H}$ = 174 Hz, 2H; Si-H), 6.94 (d, J = 2.4 Hz, 2H; 5-H_{ArO}), 6.96-7.04 (m, 19H; *p*-H_{Bn}, *m,p*-H_{TPPO}), 7.12 (t, J = 7.5 Hz, 2H; *m*-H_{Bn}), 7.19 (d, J = 7.5 Hz, 2H; *o*-H_{Bn}), 7.63 (d, J = 2.4 Hz, 2H; 3-H_{ArO}), 7.65 ppm (br, 12H; *o*-H_{TPPO});

^{13}C{^{1}H}-NMR (152 MHz, C_6D_6, 298 K): δ = 5.0 (SiH$\underline{Me_2}$), 31.0 (C$\underline{Me_3}$), 32.5 (C$\underline{Me_3}$), 34.3 ($\underline{C}$Me$_3$), 36.0 ($\underline{C}$Me$_3$), 51.2 (N$\underline{CH_2}$Bn), 61.0 (N$\underline{CH_2}$ArO), 123.1, 125.5, 127.0, 127.3, 128.3, 128.5, 128.9 (d, $J_{P(31)\text{-}C(13)}$ = 12.5 Hz; *m*-C_{TPPO}), 130.3 (d, $J_{P(31)\text{-}C(13)}$ = 107 Hz; C–P), 132.5 (*p*-C_{TPPO}), 133.0 (d, $J_{P(31)\text{-}C(13)}$ = 10.5 Hz; *o*-C_{TPPO}), 134.2, 135.5, 135.8, 164.3 ppm (C_{Ar}–O);

^{31}P{^{1}H}-NMR (243 MHz, C_6D_6, 298 K): δ = 33.3 (br) ppm;

IR (Nujol): 2048 [m, ν(Si-H)], 1959 (w), 1593(w), 1414 (m), 1331 (m), 1298 (m), 1259 (w), 1236 (m), 1200 (w), 1155 [s, ν(P=O)], 1120 (m), 1089(m), 1074 (w), 1043 (m), 1024 (m), 999 (w), 937 (m), 883 (m), 741 (m), 694 (m), 673 (w), 648 (w), 625 (w), 606 (w), 542 [s, ν(P-C)], 461 (w), 440 (w), 426 (w) cm^{-1};

Elemental Analysis calcd. (%) for $C_{77}H_{95}LaN_2O_4P_2Si_2$: C 66.98, H 6.77, N 1.86; found: C 67.52, H 6.99, N 2.05.

Y(^{1}L)[N(SiHMe$_2$)$_2$](TPPO)$_2$ (1-Y(TPPO)$_2$)

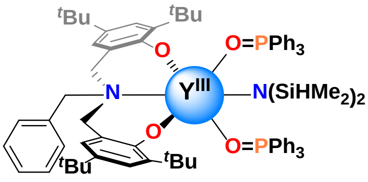

1-Y(TPPO)$_2$

A 20 mL scintillation vial was charged with **1-Y$_2$** (129 mg, 0.085 mmol, 1.0 equiv.; MW: 1526.12 g•mol^{-1}), TPPO (94 mg, 0.34 mmol, 4.0 equiv.; MW: 278.29 g•mol^{-1}) and toluene (0.5 mL). After all solids were dissolved, hexane (3 mL) was layered on top of the toluene solution. After the two layers mixed (~ 1 h), the vial was cooled in the glovebox freezer at –35 ^{o}C for 3 h, affording a white crystalline solid. The mother liquor was decanted, and volatiles were removed under reduced pressure, affording **1-Y(TPPO)$_2$** as a white solid. Yield: 192 mg (0.15 mmol, 86% yield; MW: 1319.64 g•mol^{-1}). X-ray quality crystals were grown by layering hexanes (1 mL) on top of a solution of **1-Y(TPPO)$_2$** (100 mg / 0.2 mL toluene) and allowing the solution to stand and mix undisturbed at RT.

Note: The solution behaviour of **1-Y(TPPO)$_2$** and **1-Y** + 2 TPPO is complex and concentration-dependent. Crystallized **1-Y(TPPO)$_2$** has limited solubility in C_6D_6, and some TPPO dissociation was observed by ^{1}H- and ^{31}P-NMR. The major species observed at low concentration ([Y] = 25 mM) correspond to monomeric and dimeric Y-TPPO adducts (1:2). Concentrated ([Y] = 75 mM) C_6D_6 solutions of **1-Y(TPPO)$_2$** were made by adding 4 equiv. TPPO to C_6D_6 solution of **1-Y$_2$**, in which **1-Y(TPPO)$_2$**, **[1-Y(TPPO)$_2$]$_2$** and **1-Y(TPPO)** was observed. The speciation is readily seen from DOSY NMR spectra (Figures S13 and S14).

^{1}H-NMR (400 MHz, C_6D_6, 298 K, 25 mM): δ = 0.10 (d, ^{3}J = 2.9 Hz, 12H; SiH<u>*Me$_2$*</u> of **[1-Y(TPPO)$_2$]$_2$**), 1.37-1.85 (m; ^{t}Bu), 2.72 (d, J = 13.7 Hz, 2H; N<u>*CH$_2$*</u>ArO of **1-Y(TPPO)**), 2.95 (br), 3.22 (d, J = 13.7 Hz, 2H; N<u>*CH$_2$*</u>ArO of **1-Y(TPPO)**), 3.50 (s, 2H; N<u>*CH$_2$*</u>Bn of **1-Y(TPPO)**), 3.66 (br; **1-Y(TPPO)$_2$**), 3.76 (d, J = 15.3 Hz, 1H; N<u>*CH$_2$*</u>ArO), 3.78 (d, J = 13.7 Hz, 1H; N<u>*CH$_2$*</u>ArO), 4.04 (br; **1-Y(TPPO)$_2$**), 4.64 (d, J = 14.1 Hz, 1H; N<u>*CH$_2$*</u>Bn), 4.70 (br; **1-Y(TPPO)$_2$**), 4.77 (d, J = 14.1 Hz, 1H; N<u>*CH$_2$*</u>Bn), 4.99 (quint, ^{3}J = 3.0 Hz, 2H; Si-H), 5.16 (d, J = 15.3 Hz, 1H; N<u>*CH$_2$*</u>ArO), 5.17 (d, J = 13.7 Hz, 1H; N<u>*CH$_2$*</u>ArO), 5.49 (br; Si-H of **1-Y(TPPO)$_2$**), 6.62-6.68 (m), 7.01-7.16 (m), 7.29-7.36 (m), 7.44-7.82 (m),;

^{31}P{^{1}H}-NMR (162 MHz, C_6D_6, 298 K, 15 mM): δ = 25.2 (br, free TPPO), 25.2 (br, **1-Y(TPPO)$_2$**), 34.6 (d, $J_{Y\text{-}P(31)}$ = 12.6 Hz; **1-Y(TPPO)**), 38.4 (d, $J_{Y\text{-}P(31)}$ = 11.1 Hz; [**1-Y(TPPO)$_2$]$_2$**), 39.1 (d, $J_{Y\text{-}P(31)}$ = 10.9 Hz; **1-Y(TPPO)**) ppm;

IR (Nujol): 2081 [m, ν(SiH)], 2015 (w), 1959 (w), 1591(w), 1416 (m), 1331 (m), 1300 (m), 1259 (m), 1240 (m), 1201 (w), 1153 [s, ν(P=O)], 1120 (m), 1090 (m), 1018 (m), 997 (m), 933 (m), 897 (m), 885 (m), 835 (m), 802 (w), 789 (w), 744 (m), 694 (m), 671 (w), 646 (w), 629 (w), 540 [s, ν(P-C)], 464 (m), 447 (m) cm^{-1};

Elemental Analysis calcd. (%) for $C_{77}H_{95}YN_2O_4P_2Si_2$: C 69.75, H 7.59, N 1.65; found: C 70.08, H 7.26, N 2.12.

^{1}H-NMR (600 MHz, C_6D_6, 298 K, 75 mM, prepared *in-situ*): δ = 0.09 (d, ^{3}J = 3.0 Hz, 12H; SiH*Me*$_2$), 1.45 (s, 9H; ^{t}Bu), 1.49 (s, 9H; ^{t}Bu), 1.58 (s, 9H; ^{t}Bu), 1.69 (s, 9H; ^{t}Bu), 3.76 (d, *J* = 15.3 Hz, 1H; NC*H*$_2$ArO), 3.78 (d, *J* = 13.7 Hz, 1H; NC*H*$_2$ArO), 4.64 (d, *J* = 14.1 Hz, 1H; NC*H*$_2$Bn), 4.77 (d, *J* = 14.1 Hz, 1H; NC*H*$_2$Bn), 4.99 (quint, ^{3}J = 3.0 Hz, 2H; Si-H), 5.16 (d, *J* = 15.3 Hz, 1H; NC*H*$_2$ArO), 5.17 (d, *J* = 13.7 Hz, 1H; NC*H*$_2$ArO), 6.86 (t, *J* = 6.0 Hz, 6H; *p*-H$_{TPPO}$), 6.99-7.09 (m, 12H), 7.13 (t, *J* = 7.5 Hz, 1H; *p*-H$_{Bn}$), 7.17-7.22 (m, 10H), 7.33 (t, *J* = 7.5 Hz, 2H; *m*-H$_{Bn}$), 7.46 (d, *J* = 2.4 Hz, 1H; 3-H$_{ArO}$), 7.50 (d, *J* = 2.4 Hz, 1H; 3-H$_{ArO}$), 7.73 (br, 4H), 7.79 ppm (d, *J* = 7.5 Hz, 2H; *o*-H$_{Bn}$);

^{13}C{^{1}H}-NMR (152 MHz, C_6D_6, 298 K, 75 mM, prepared *in-situ*): δ = 3.7 (SiH*Me*$_2$), 30.6 (C*Me*$_3$), 30.8 (C*Me*$_3$), 32.6 (C*Me*$_3$), 32.7 (C*Me*$_3$), 34.2 (*C*Me$_3$), 34.3 (*C*Me$_3$), 35.6 (*C*Me$_3$), 35.7 (*C*Me$_3$), 50.6 (N*C*H$_2$Bn), 61.67 (N*C*H$_2$ArO), 61.7 (N*C*H$_2$ArO), 122.8, 122.9, 123.4, 124.3, 127.2, 127.3, 127.4, 127.6, 128.3 (*p*-C$_{TPPO}$), 128.9 (d, $J_{P(31)-C(13)}$ = 115 Hz; P-C), 129.1 (d, $J_{P(31)-C(13)}$ = 12.6 Hz; *m*-C$_{TPPO}$), 132.9 (d, $J_{P(31)-C(13)}$ = 10.9 Hz; *o*-C$_{TPPO}$), 133.1, 133.4, 133.8, 135.7, 136.0, 136.4, 164.3 (O-C),164.6 ppm (O-C);

^{31}P{^{1}H}-NMR (243 MHz, C_6D_6, 298 K, 75 mM, prepared *in-situ*): δ = 25.0 (br, free TPPO), 34.6 (d, $J_{Y-P(31)}$ = 10.4 Hz; **1-Y(TPPO)**), 38.3 (d, $J_{Y-P(31)}$ = 12.8 Hz; [**1-Y(TPPO)$_2$]$_2$**), 38.9 (d, $J_{Y-P(31)}$ = 10.3 Hz; **1-Y(TPPO)**) ppm;

(*R*)-3-acetoxybutyric acid methylester [(*R*)-3-OAcB^{Me}]

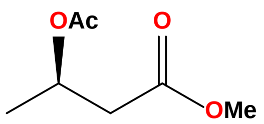

In a 50 mL flask, acetyl chloride (2.40 g, 30.6 mmol, 1.2 equiv.; MW = 78.50) was added to a solution of (*R*)-Methyl 3-hydroxybutanoate (3.01 g, 25.5 mmol, 1.0 equiv.) and pyridine (3.02 g, 38.2 mmol, 1.5 equiv.) in CH_2Cl_2 (15 mL). The reaction was stirred at ambient temperature for 6 h. Saturated NH_4Cl solution (15 mL) was added to the reaction, followed by deionized water (15 mL) to dissolve all solids. The organic phase was isolated and washed with saturated NH_4Cl solution (3 x 10 mL). The combined organic layer was evaporated under reduced pressure and redissolved with Et_2O (20 mL). The mixture was dried with Na_2SO_4, filtrated through activated carbon and Celite®, and dried under reduced pressure to yield **(*R*)-3-OAcB^{Me}** as a colorless oil. Yield: 3.25 g (20.3 mmol, 80% yield; MW: 160.17 g•mol^{-1}). The ^{1}H-NMR spectrum is in agreement with the previous report.[15]

^{1}H-NMR (400 MHz, $CDCl_3$, 298 K): δ = 1.29 (d, *J* = 6.3 Hz, 3H; CH*Me*), 2.02 (s, 3H; CO*Me*), 2.50 (dd, *J* = 15.6, 5.8 Hz, 1H; COC*H*$_2$), 2.64 (dd, *J* = 15.6, 7.4 Hz, 1H; COC*H*$_2$), 3.68 (s, 3H; O*Me*), 5.26 ppm (hex, *J* = 6.2 Hz, 1H; C*H*);

^{1}H-NMR (400 MHz, C_6D_6, 298 K): δ = 1.05 (d, *J* = 6.3 Hz, 3H; CH*Me*), 1.64 (s, 3H; CO*Me*), 2.14 (dd, *J* = 15.6, 5.6 Hz, 1H; COC*H*$_2$), 2.40 (dd, *J* = 15.6, 7.4 Hz, 1H; COC*H*$_2$), 3.30 (s, 3H; O*Me*), 5.33 ppm (hex, *J* = 6.2 Hz, 1H; C*H*).

3. Experimental Procedures

Typical polymerization procedures

Reactions at ambient temperature:

In a glovebox, a 2 mL scintillation vial was charged with Rare-earth catalyst [e.g. **1-La(TPPO)$_2$** (5.7 mg, 0.0060 mmol, 1.0 equiv.; MW: 957.27 g•mol^{-1})], neutral ligand [if needed, e.g. TPPO (3.4 mg, 0.012 mmol, 2.0 equiv.; MW: 278.29 g•mol^{-1})] and toluene (0.382 mL). A toluene solution of ^{i}PrOH (2% m/m, 0.021 mL, ρ = 0.867 g/mL; 0.36 mg, 0.0060 mmol, 1.0 equiv.; MW: 60.10 g•mol^{-1}) was then added to the clear colorless solution. After approximately one minute, *rac*-BBL (103 mg, 1.20 mmol, 200 equiv.; MW: 86.09 g•mol^{-1}) was added to the catalyst solution. After 1 h, the reaction was quenched by a methanol solution of AcOH (10% v/v, ca. 0.1 mL), and volatiles were removed under reduced pressure.

Analysis of reaction progress prior to quenching:

An aliquot of the reaction was removed and dissolved in $CDCl_3$ for NMR analysis without additional quenching. The $CDCl_3$ solution was evaporated in vacuo and the sample was redissolved in THF for GPC analysis.

Reactions at 0 and –30 °C:

In a glovebox, a J-Young NMR tube was charged with **1-La(TPPO)$_2$** (8.2 mg, 0.0060 mmol, 1.0 equiv.; MW: 1369.64 g•mol^{-1}) and toluene (0.382 mL). A toluene solution of ^{i}PrOH (2% m/m, 0.021 mL, ρ = 0.867 g/mL; 0.36 mg, 0.0060 mmol, 1.0 equiv.; MW: 60.10 g•mol^{-1}) was then added to the clear colorless solution. After approximately one minute, the solution was then chilled to –30 °C in the glovebox freezer and pre-chilled (–30 °C) *rac*-BBL (103 mg, 1.20 mmol, 200 equiv.; MW: 86.09 g•mol^{-1}) was added to the catalyst solution. The tube was then immediately removed from the glovebox and reacted in a 0 ^{o}C or –30 ^{o}C bath. After 1 h, the reaction was quenched by a methanol solution of AcOH (10% v/v, ca. 0.1 mL), and all volatiles were removed under reduced pressure.

NMR studies of relevant catalyst species in the ROP of *rac*-BBL

Room Temperature (**1–La** + 1 ^{i}PrOH + 1 or 2 equiv. TPPO)

A screw-capped NMR tube was charged with **1-La** (5.7 mg, 0.0060 mmol, 1.0 equiv.; MW: 957.27 g•mol^{-1}), TPPO (1.7 mg, 0.0060 mmol, 1.0 equiv.; 3.4 mg, 0.012 mmol, 2.0 equiv.; MW: 278.29 g•mol^{-1}), toluene (0.382 mL), and C_6D_6 (0.025 mL). The sample was removed from the glovebox and NMR spectra were taken. A toluene solution of ^{i}PrOH (2% m/m, 0.021 mL, ρ = 0.867 g/mL; 0.36 mg, 0.0060 mmol, 1.0 equiv.; MW: 60.10 g•mol^{-1}) was added inside the glovebox, and NMR spectra were recorded. *rac*-BBL (103 mg, 1.20 mmol, 200 equiv.; MW: 86.09 g•mol^{-1}) was then added to catalyst solution and NMR spectra were recorded at varying time points. Reaction conversion was determined by ^{1}H-NMR taken immediately before and after the ^{31}P{^{1}H}-NMR spectra were taken. The ^{31}P{^{1}H}-NMR spectra are displayed as Figure S15a and S15b. The ^{1}H-NMR of reaction of 2equiv. TPPO is displayed as Figure S15c.

*–30 °C (**1-La(TPPO)$_2$** + 1 ^{i}PrOH)*

A J-Young NMR tube was charged with **1-La(TPPO)$_2$** (12.0 mg, 0.0088 mmol, 1.0 equiv.; MW: 1369.64 g•mol^{-1}) and toluene-*d$_8$* (0.350 mL). PPh_3 (1.0 mg, 0.0040 mmol, 0.45 equiv.; MW: 262.29 g•mol^{-1}) was also added to calibrate line width in the ^{31}P-NMR spectra. The sample was removed from the glovebox, cooled to –30 °C in the NMR spectrometer, and spectra were taken. The sample was then brought inside of the glovebox, and a toluene solution of ^{i}PrOH (2% m/m, 0.031 mL, ρ = 0.867 g/mL; 0.53 mg, 0.0088 mmol, 1.0 equiv; MW: 60.10 g•mol^{-1}) was added to the tube. The sample was cooled to –30 °C in the NMR spectrometer, and spectra were recorded. The sample was then brought inside of the glovebox and chilled in the glovebox freezer to –30 °C. *rac*-BBL (75 mg, 0.88 mmol, 100 equiv.; MW: 86.09 g•mol^{-1}) was chilled at –30 °C, and then added to the NMR tube. The tube was immediately removed from the glovebox and chilled to –78 °C (^{i}PrOH-dry ice bath) for the brief period of time needed to transport the sample to the spectrometer. The sample was then loaded to the pre-cooled spectrometer (–30 °C) and spectra were taken immediately. The ^{1}H- and ^{31}P{^{1}H}-NMR spectra are displayed as Figure S16a and S16b.

After 25 min, the spectrometer was warmed to –15 °C and 0 °C and spectra were recorded after 5 min of thermal equilibration. The total warming process was 30 min, and corresponded to an increase in reaction conversion from 48 to 67% during this time. ^{31}P{^{1}H}-NMR are displayed as Figure S17.

Sample for end-group analysis (MALDI-TOF and NMR)

In a glovebox, a 2 mL scintillation vial was charged with **1-La** (37 mg, 0.031 mmol, 1.0 equiv.; MW: 1369.64 g•mol^{-1}) and toluene (0.310 mL). A toluene solution of ^{i}PrOH (2% m/m, 0.109 mL, ρ = 0.867 g/mL; 1.86 mg, 0.031 mmol, 1.0 equiv.; MW: 60.10 g•mol^{-1}) was then added to the clear colorless solution. After approximately one minute, *rac*-BBL (108 mg, 1.25 mmol, 40 equiv.; MW: 86.09 g•mol^{-1}) was added to the catalyst solution. After 1 h, the reaction reached full conversion, was quenched by a drop of acetic acid, and all volatiles were removed under reduced pressure. ^{i}PrOH (1 mL) was added to the residual material precipitating the polymer and the liquid was decanted. The polymer was washed with ^{i}PrOH (1 mL) and dried under reduced pressure. This material was used for NMR, GPC and MALDI analysis. The ^{1}H-NMR and MALDI-TOF spectra are displayed as Figure S22 and S23.

Measurement of M_n and *Đ* as a function of conversion

In a glovebox, a 20 mL scintillation vial was charged with **1-La(TPPO)$_2$** (16.4 mg, 0.012 mmol, 1.0 equiv.; MW: 1369.64 g•mol^{-1}), a Teflon-coated stirbar, and toluene (0.763 mL). A toluene solution of ^{i}PrOH (2% m/m, 0.042 mL, ρ = 0.867 g/mL; 0.72 mg, 0.012 mmol, 1.0 equiv.; MW: 60.10 g•mol^{-1}) was added to the clear colorless solution. After approximately one minute, *rac*-BBL (207 mg, 2.40 mmol, 200 equiv.; MW: 86.09 g•mol^{-1}) was added to the stirring catalyst solution. After various time, 0.050 mL reaction solution was added to 0.050 mL 5%(m/m) benzoic acid solution in toluene to quench. The quenched mixture was dissolved in 0.5 mL $CDCl_3$ for NMR analysis. The NMR sample was evaporated under reduced pressure and dissolved in 1 mL THF for GPC analysis. The conversions, M_n and *Đ* are displayed as Table S4 and Figure S24.

Reactivity studies of 1-La and 1-La(TPPO)$_2$ in the presence of 1 equiv ^{i}PrOH and 15 equiv. (*R*)-3-acetoxybutyric acid methylester [(*R*)-3-OAcB^{Me}]

A screw-capped NMR tube was charged with **1-La** (6.9 mg, 0.0072 mmol, 1.0 equiv.; MW: 957.27 g•mol^{-1}) or **1-La(TPPO)$_2$** (9.9 mg, 0.0072 mmol, 1.0 equiv.; MW: 1369.64 g•mol^{-1}) and C_6D_6 (0.558 mL). A toluene solution of ^{i}PrOH (2% m/m, 0.025 mL, ρ = 0.867 g/mL; 0.43 mg, 0.0072 mmol, 1.0 equiv.; MW: 60.10 g•mol^{-1}) and **(*R*)-3-OAcB^{Me}** (17.3 mg, 0.105 mmol, 15 equiv.; MW: 160.17 g•mol^{-1}) were added. NMR spectra were taken recorded at 0.5 h and 7 h. The ^{1}H-NMR spectra are displayed as Figure S25.

4. Supporting Data and Spectra

Table S1. Additional reaction optimization results (solvent screening, ligand equivalents, inclusion of alcohol) for the ROP of *rac*-BBL catalyzed by **1-La** and **1-Y$_2$**.

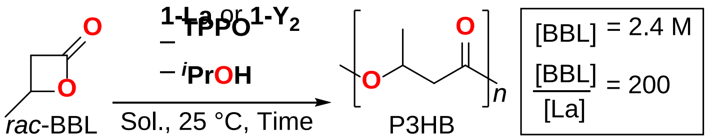

Entry	Cat.	[BBL]/[RE]/[TPPO]/[^{i}PrOH]	Solvent	Time (h)^a	Conv. (%)^b	$M_{n, calc}$^{c} (kg/mol)	$M_{n, exp}$^{d} (kg/mol)	$Đ$^{d,e}	P_m^{f}
1	**1-Y$_2$**	200/1/0/0	Tol	1	0	--	n.d.	n.d.	n.d.
2	**1-Y$_2$**	200/1/0/1	Tol	1	5	0.9	n.d.	n.d.	n.d.
3	**1-Y$_2$**	200/1/2/0	Tol	7	97	16.6	29.8	1.33	0.50
4	**1-Y$_2$**	200/1/2/1	Tol	3	95	16.4	14.0	1.18	0.51
5	**1-La**	200/1/0/0	Tol	48	35	5.9	2.1	1.46	0.54
6	**1-La**	200/1/0/1	Tol	1	21	3.6	2.9	1.04	0.57
7	**1-La**	200/1/1/1	Tol	6	71	12.2	4.7	1.04	0.67
8	**1-La**	200/1/2/1	Tol	1	97	16.7	9.6	1.18	0.71
9	**1-La**	200/1/3/1	Tol	1	97	16.7	9.1	1.27	0.71
10	**1-La**	200/1/2/0	THF	3	75	12.9	12.2	1.64	0.65
11	**1-La**	200/1/2/1	THF	3	84	14.5	8.7	1.10	0.68
12	**1-La**	200/1/2/0	CH_2Cl_2	3	53	9.1	8.2	1.76	0.64
13	**1-La**	200/1/2/1	CH_2Cl_2	3	82	14.1	8.2	1.17	0.64

a – Reaction times not optimized. *b* – Determined by ^{1}H-NMR integration of BBL and PHB methine resonances in the crude reaction mixture. *c* – [BBL]/[RE]/[^{i}PrOH] × Conv. × 0.08609 kg•mol^{-1}. When [^{i}PrOH] = 0, [BBL]/[La] × Conv. × 0.08609 kg•mol^{-1}. *d* – Determined by gel permeation chromatography (GPC) at 30 °C in THF using polystyrene standards and corrected by Mark-Houwink factor of 0.54.[16] *e* – M_w/M_n. *f* – Probability of *meso*-linkages between repeat units. Determined by integration of P3HB C=O resonances using inverse gated (IG) ^{13}C-NMR.

Table S2. Impact of alcohol equivalents on the ROP of *rac*-BBL catalyzed by **1-La(TPPO)$_2$**.

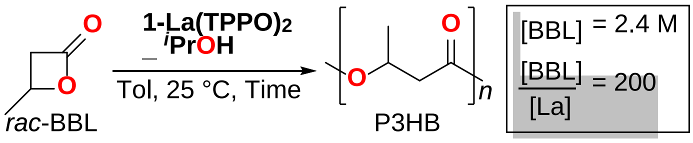

Entry	^{i}PrOH (equiv)	Time (h)^a	Conv. (%)^b	$M_{n,\,calc}$^{c} (kg/mol)	$M_{n,\,exp}$^{d} (kg/mol)	$Đ^{d,e}$	P_m^{f}
1	0	5	87	15.0	13.5	1.45	0.71
2	1	1	93	16.0	9.4	1.16	0.71
3	2	1	95	8.2	6.6	1.14	n.d.
4	4	1	93	4.0	3.3	1.07	0.70

a – Reaction times not optimized. *b* – Determined by ^{1}H-NMR integration of BBL and PHB methine resonances in the crude reaction mixture. *c* – [BBL]/[La]/[^{i}PrOH] × Conv. × 0.08609 kg•mol^{-1}. When [^{i}PrOH] = 0, [BBL]/[La] × Conv. × 0.08609 kg•mol^{-1}. *d* – Determined by gel permeation chromatography (GPC) at 30 °C in THF using polystyrene standards and corrected by Mark-Houwink factor of 0.54.[16] *e* – M_w/M_n. *f* – Probability of *meso*-linkages between repeat units. Determined by integration of P3HB $\underline{C}$=O resonances using inverse gated (IG) ^{13}C-NMR.

Discussion of stereocontrol mechanism (statistical analysis)

As described by Thomas and Carpentier,[2] diad and triad distribution can provide insight into the mechanism of stereocontrol for the ROP of *rac*-BBL. Two types of stereocontrol may contribute to the tacticity of BBL polymerization:

(1) *enantiomorphic site control*, under which the selectivity of incoming monomer is determined by the asymmetric environment of catalyst, and (2) *chain-end control*, in which the asymmetric nature of the active end of growing polymer differentiates the two enantiomers of the monomer.

In the context that the isotactic diad (meso diad) is dominant, one can consider a mis-insertion (e.g. …RRRR$\underline{S}$, where $\underline{S}$ is the mis-insertion) is immediately corrected and followed by insertions that are favored. For site control, error correction leads to propagation with the favored enantiomer (e.g., …RRR$\underline{S}$RRR, where $\underline{S}$ is the mis-insertion). For chain-end control, it will continue to propagate the meso diad and propagate the enantiomer that was mis-inserted (e.g. …RRR$\underline{S}$SSS). Therefore, the resulting minor triads for site control are 1 *mr*, 1 *rr* and 1 *rm*, while the minor triads for chain-end control are 1 *mr* and 1 *rm*. Therefore, the two methods of stereocontrol can be differentiated by their triad distribution.

The triad distribution was obtained from the $\underline{C}H_2$ signals of P3HB using IG-^{13}C-NMR. We fit the signals in the form of a Cauchy-Lorentz distribution. The result contains 4 components, each of which represents a triad ratio with its area (Figure S1). A representative example is P3HB obtained from Table 1, entry 6 (**1-La** + 2 TPPO + 1 ^{i}PrOH; P_m = 0.71).

For chain-end control, the triad distribution obeys a binominal distribution, i.e.: P (*mm*) = P_m^2, P(*rr*) = $(1-P_m)^2$, P (*mr*) = P (*rm*) = $P_m(1-P_m)$. Applying the Bernoulli model triad test, B = 4P(*mm*)P(*rr*)/[P(*mr*)+P(*rm*)]^2, where B = 1 for a purely chain-end controlled process. For

P3HB obtained from entry 6 in Table 1, B = (4*51.01*8.46)/(20.38+20.15)^2 = 1.05. This is close to the theoretical value and confirms chain-end control as the mechanism for stereocontrol.

triad	δ_0, Chemical Shift/ppm	γ, Width/ppm	I_0, Intensity	rel. Area (%)
rm	40.864(1)	0.025(4)	0.59(6)	20.38
mm	40.809(1)	0.026(2)	1.38(6)	51.01
rr	40.727(2)	0.019(6)	0.32(7)	8.46
mr	40.662(1)	0.021(3)	0.68(7)	20.15

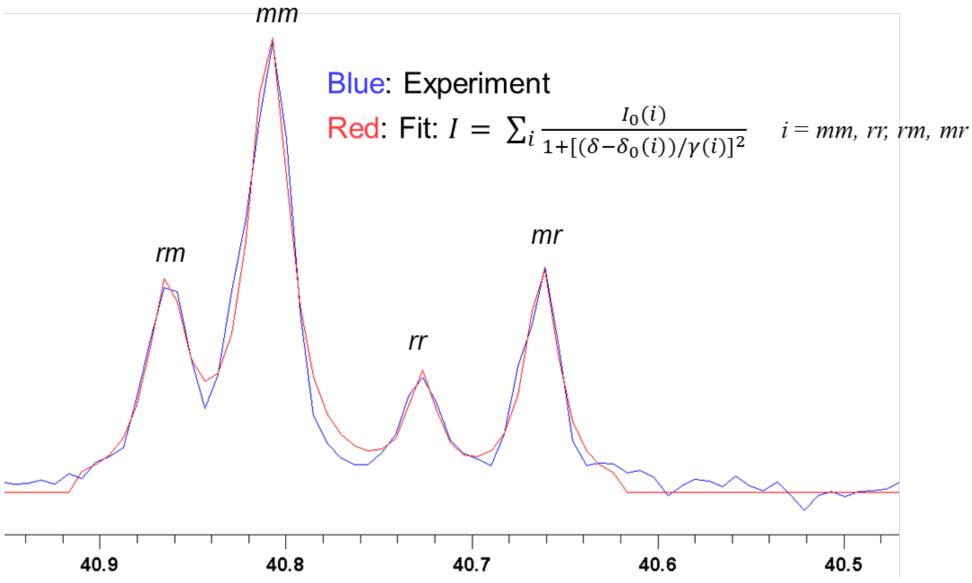

Figure S1. Experimental and fitted IG-^{13}C-NMR (152 MHz, $CDCl_3$) signal of P3HB (Table 1, entry 6; **1-La** + 2 TPPO + 1 ^{i}PrOH, P_m = 0.71)

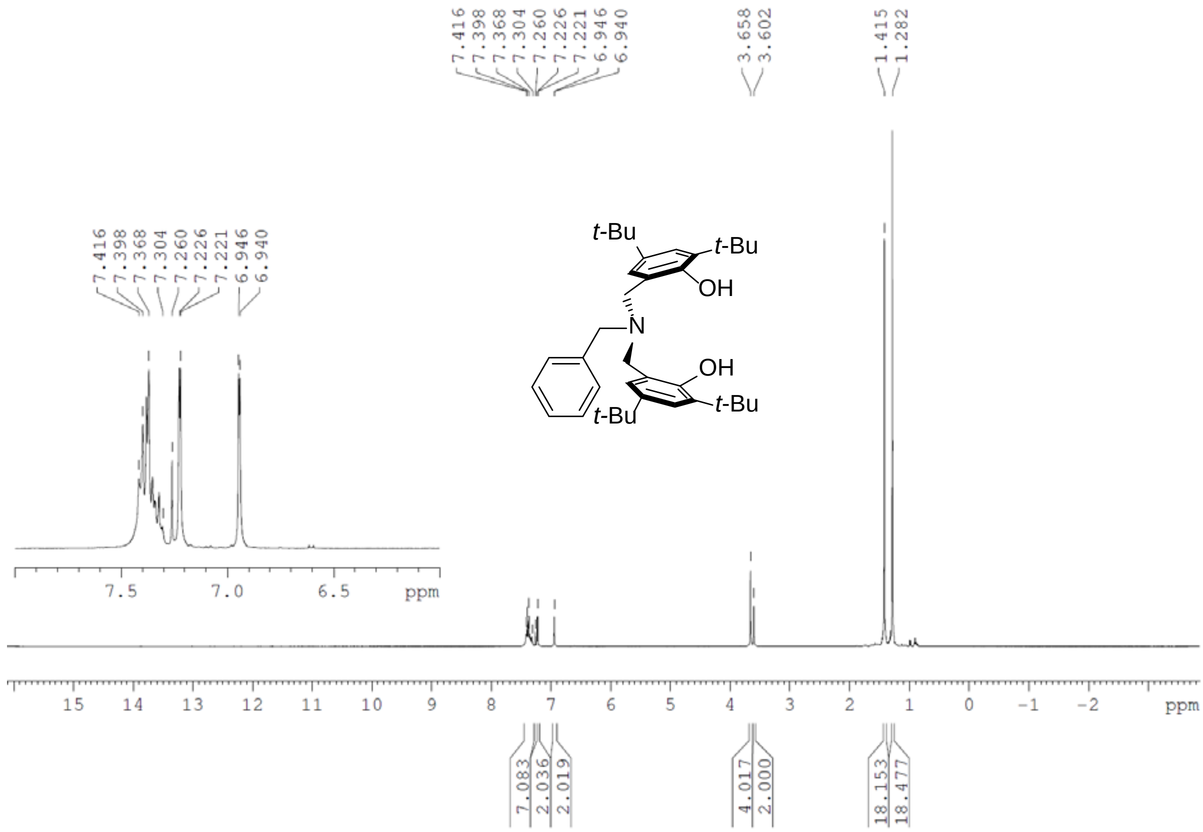

Figure S2a. [1]H-NMR ($CDCl_3$, 400 MHz) spectra of $\mathbf{H_2{}^1L}$.

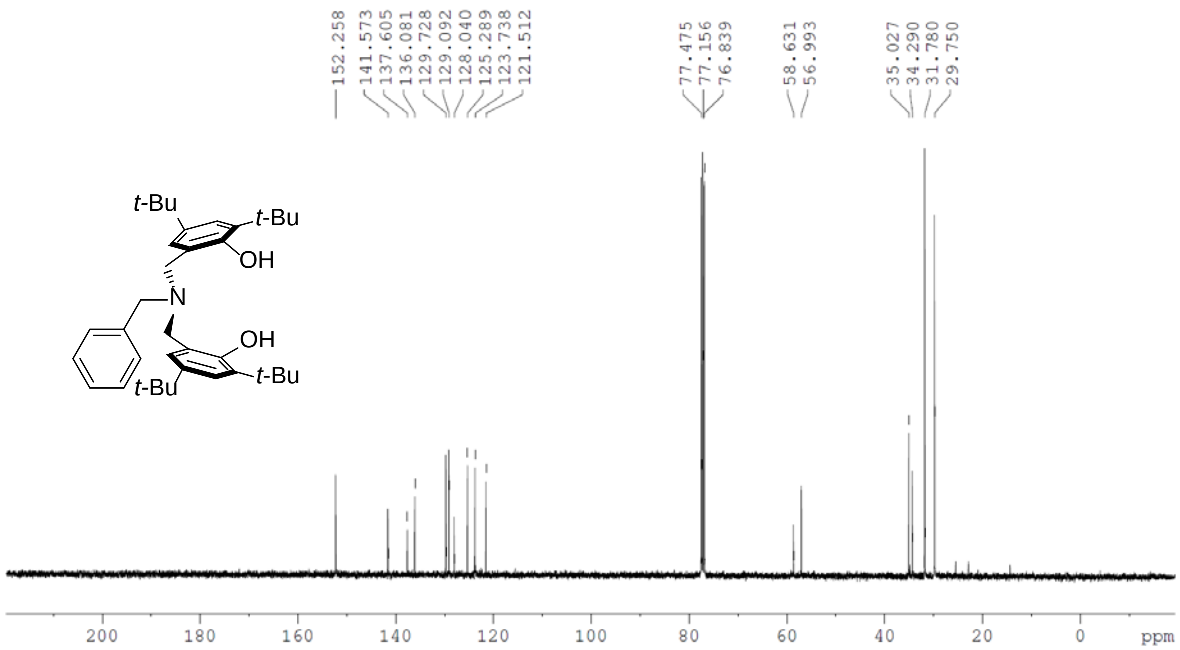

Figure S2b. [13]C-NMR ($CDCl_3$, 101 MHz) spectra of $\mathbf{H_2{}^1L}$.

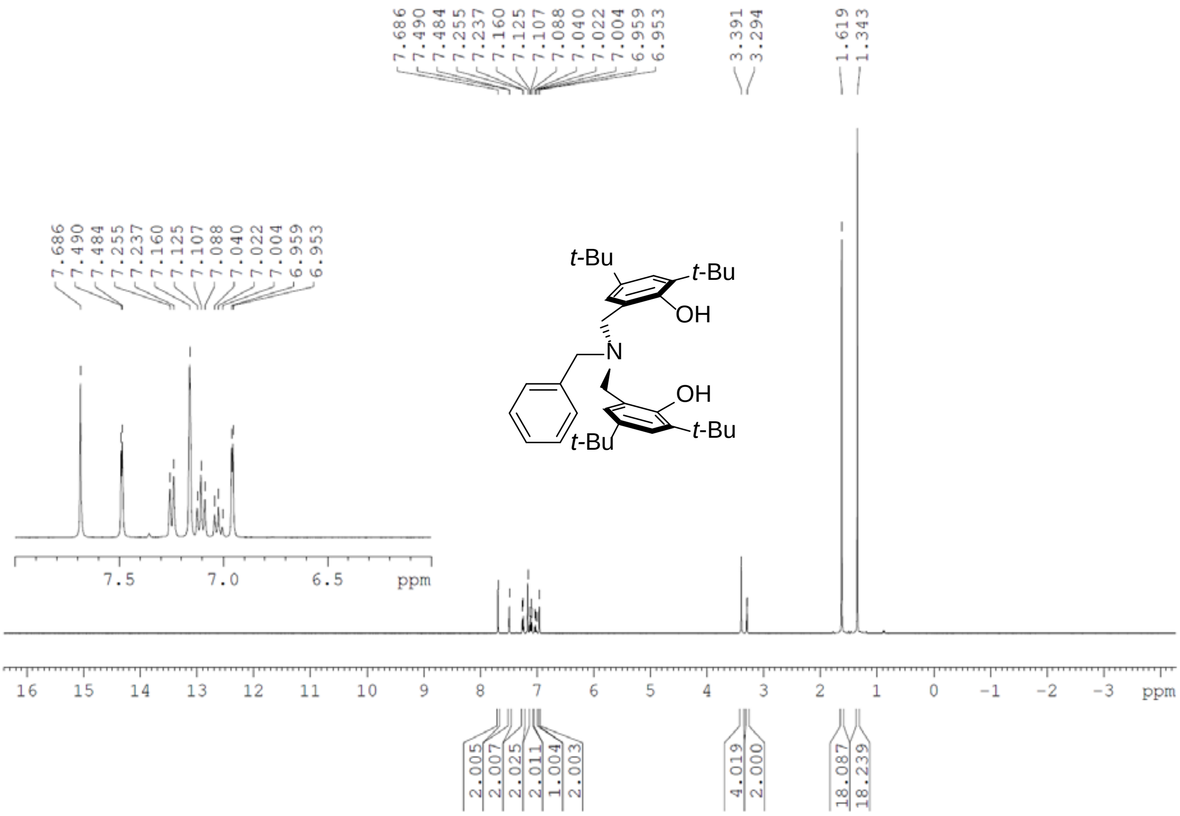

Figure S2c. ^{1}H-NMR (C_6D_6, 400 MHz) spectra of **$H_2{}^1L$**.

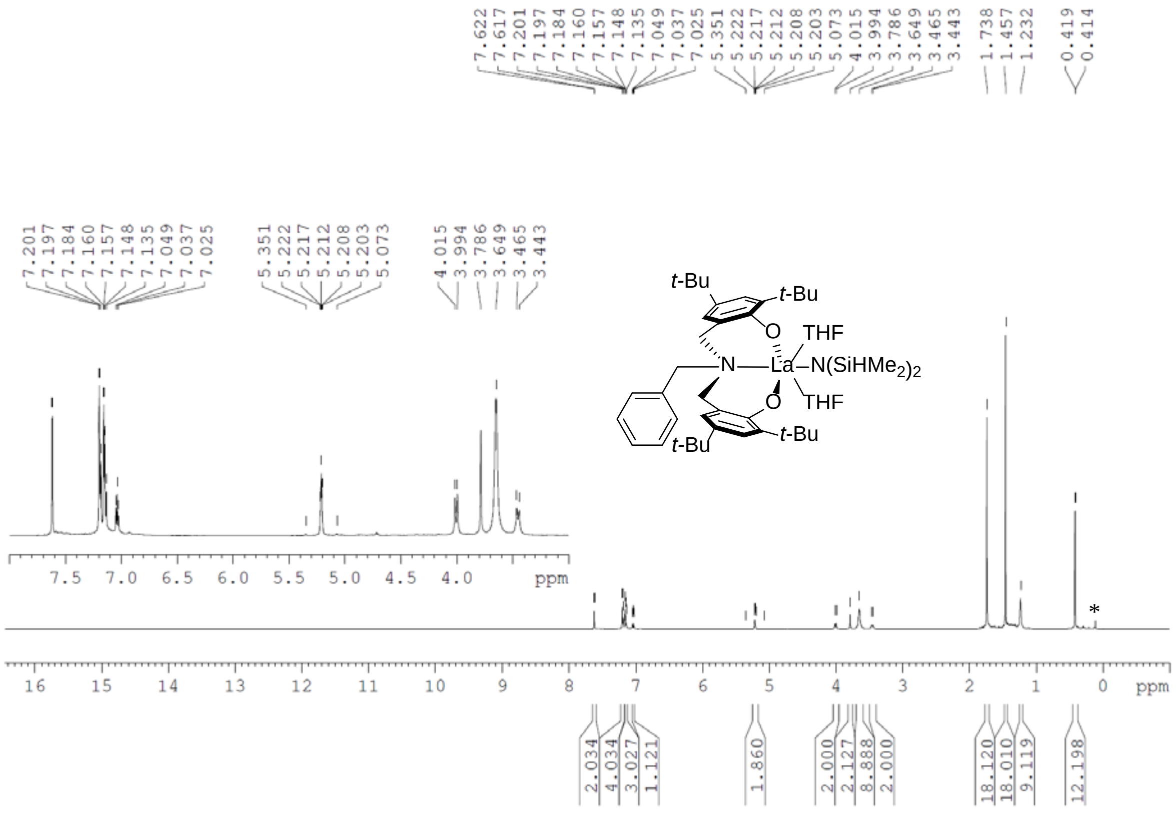

Figure S3a. ^{1}H-NMR (C_6D_6, 600 MHz) spectra of **1-La**.

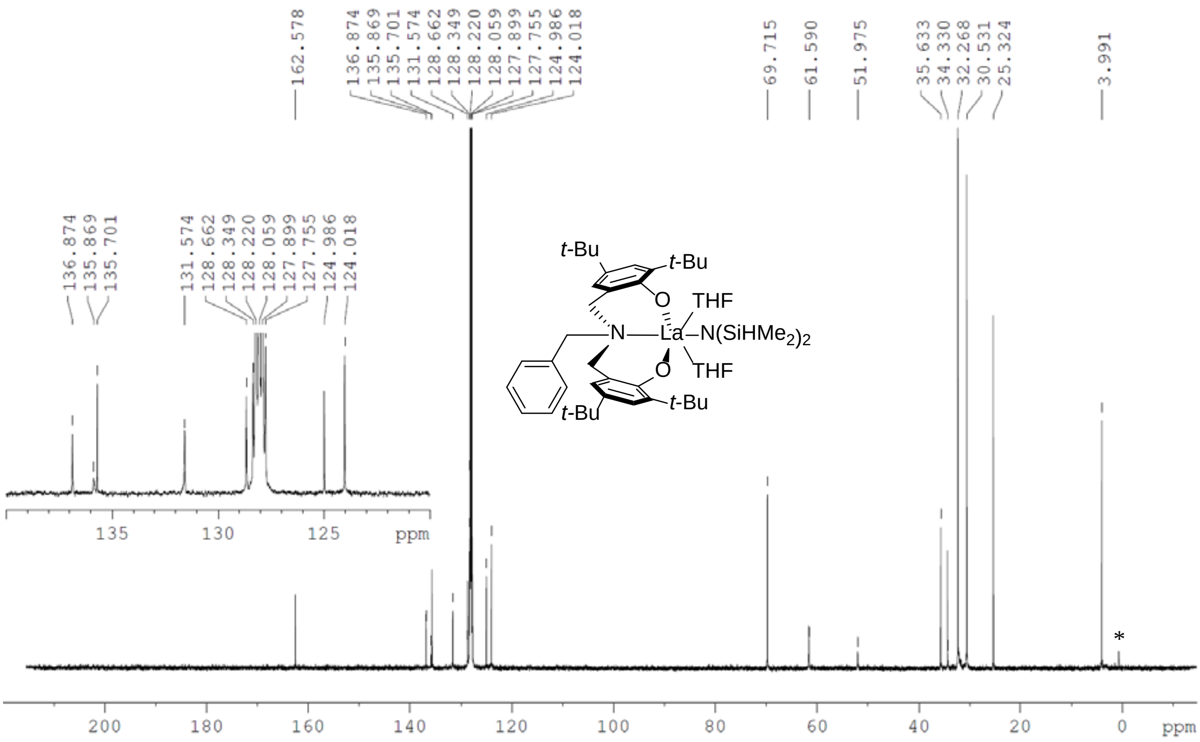

Figure S3b. ^{13}C-NMR (C_6D_6, 152 MHz) spectra of **1-La**.

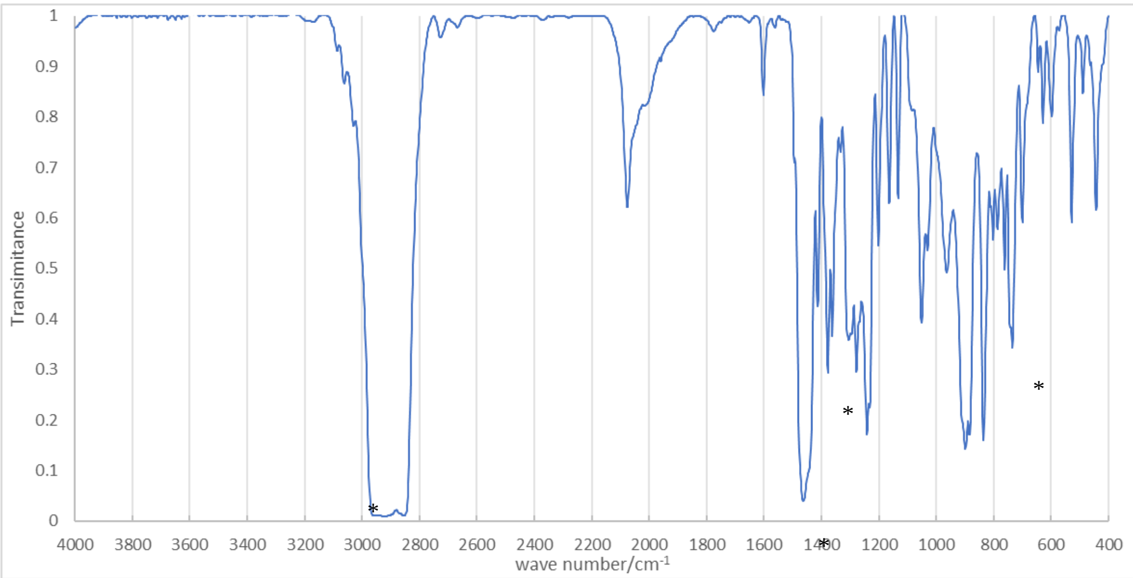

Figure S3c. IR (Nujol) spectra of **1-La**. (*: Nujol).

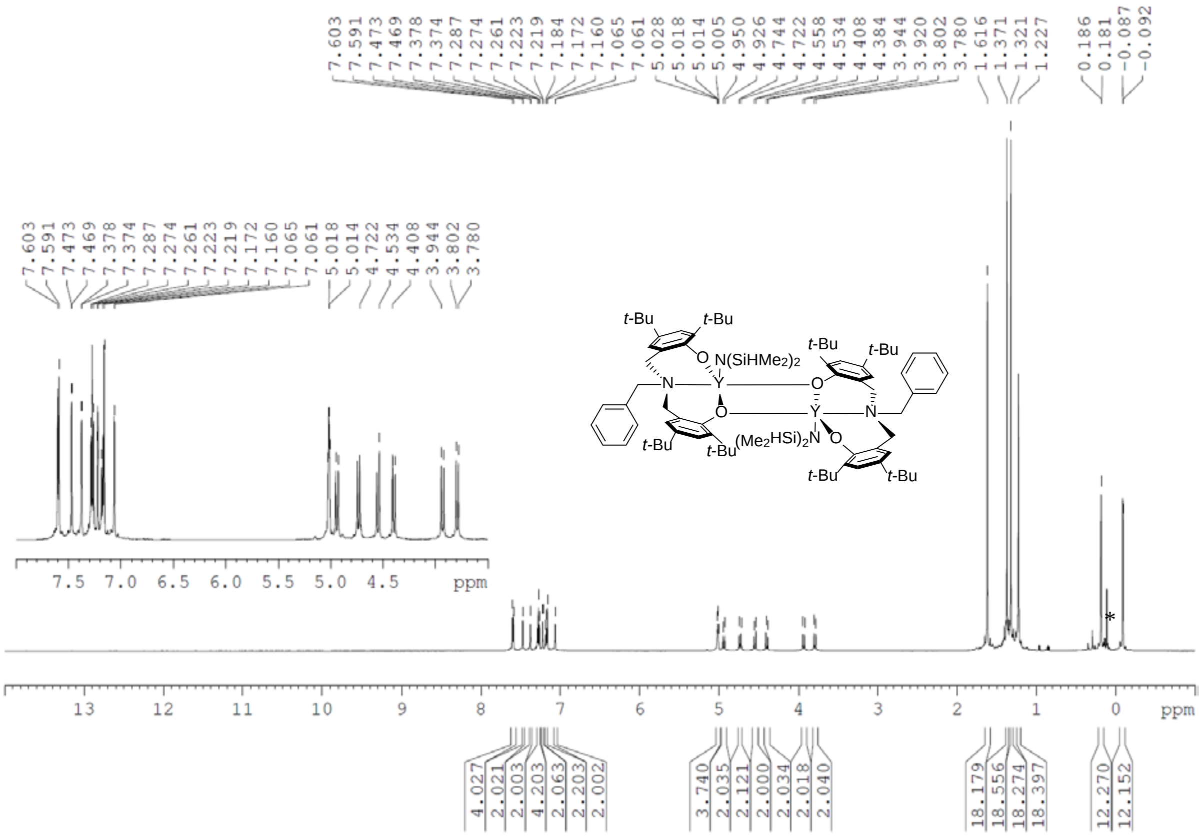

Figure S4a. ^{1}H-NMR (C_6D_6, 600 MHz) spectra of **1-Y$_2$**. (*: $HN(SiHMe_2)_2$).

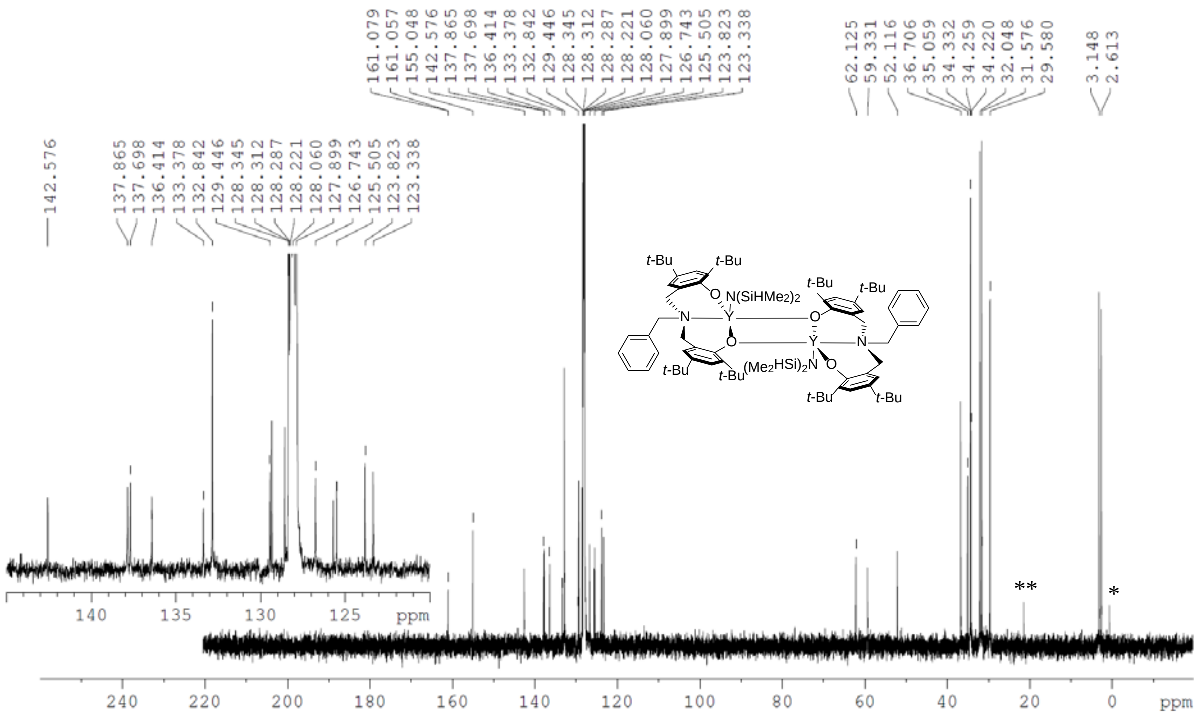

Figure S4b. ^{13}C-NMR (C_6D_6, 152 MHz) spectra of **1-Y$_2$**. (*: $HN(SiHMe_2)_2$, **: toluene).

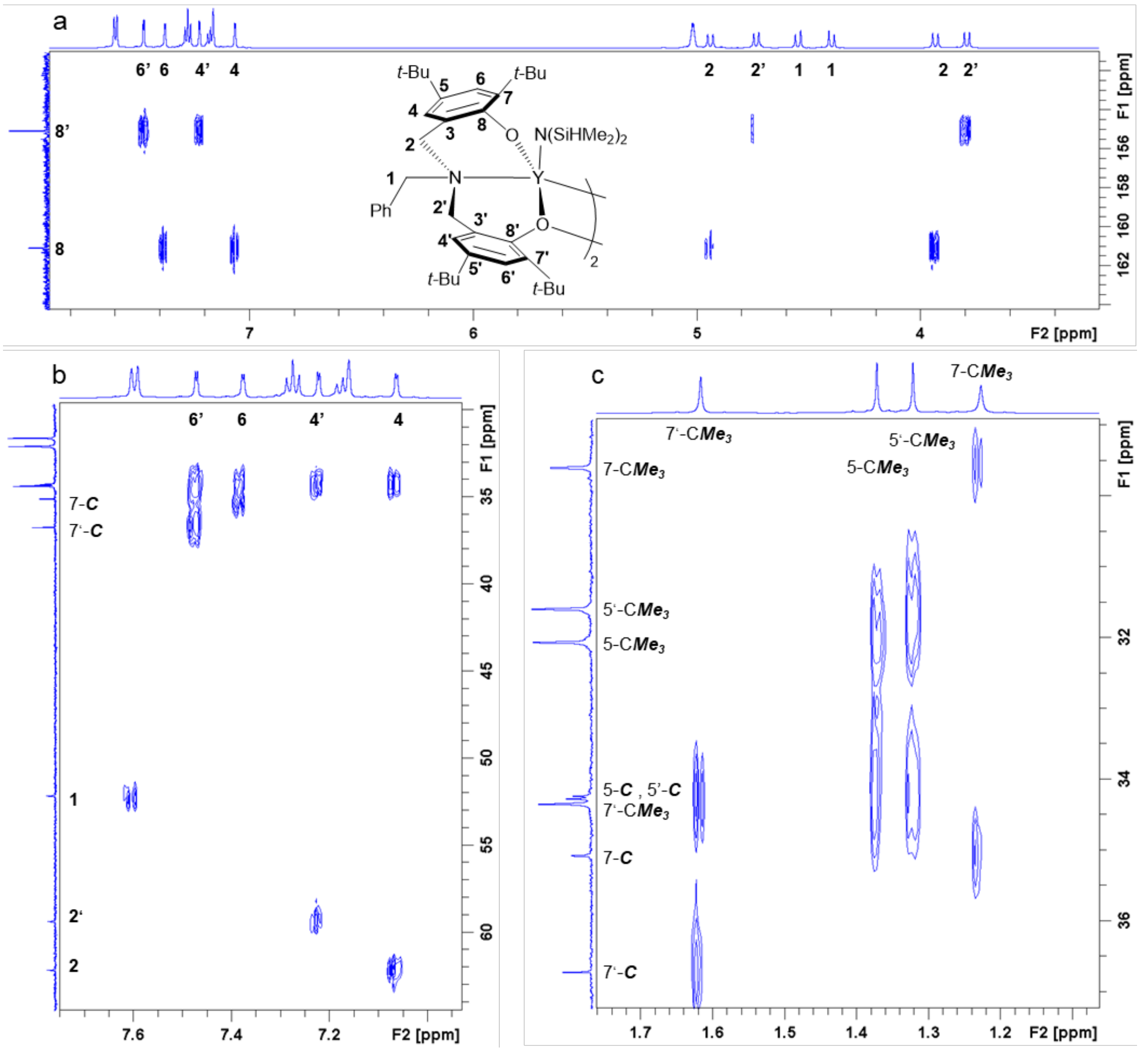

Figure S4c. Selected regions of ^1H-^{13}C HMBC (600 MHz for ^1H in C_6D_6) of **1-Y$_2$**

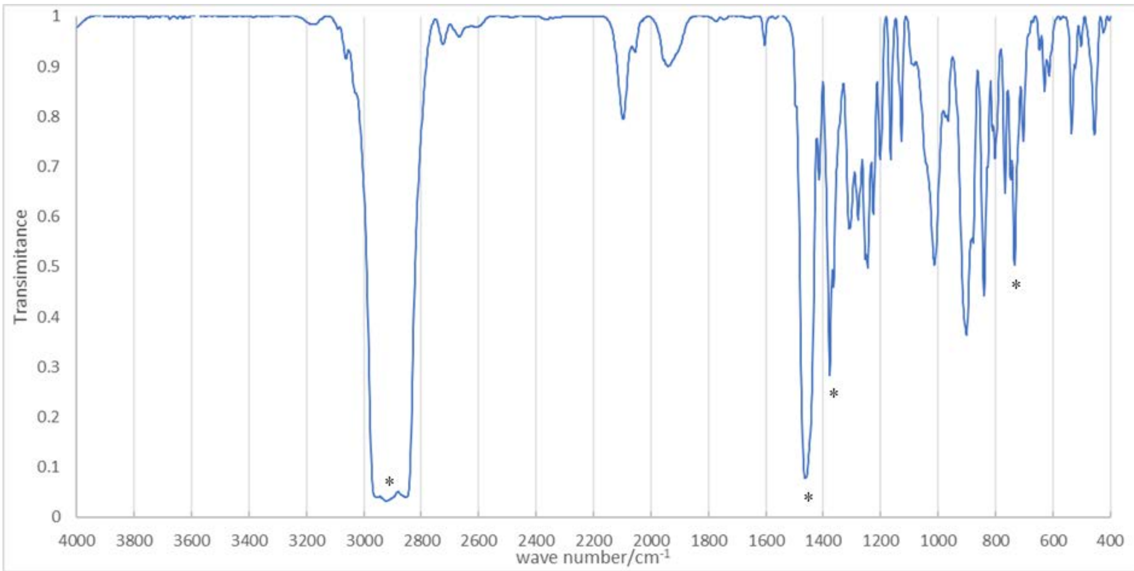

Figure S4d. IR (Nujol) spectra of **1-Y$_2$**. (*: Nujol).

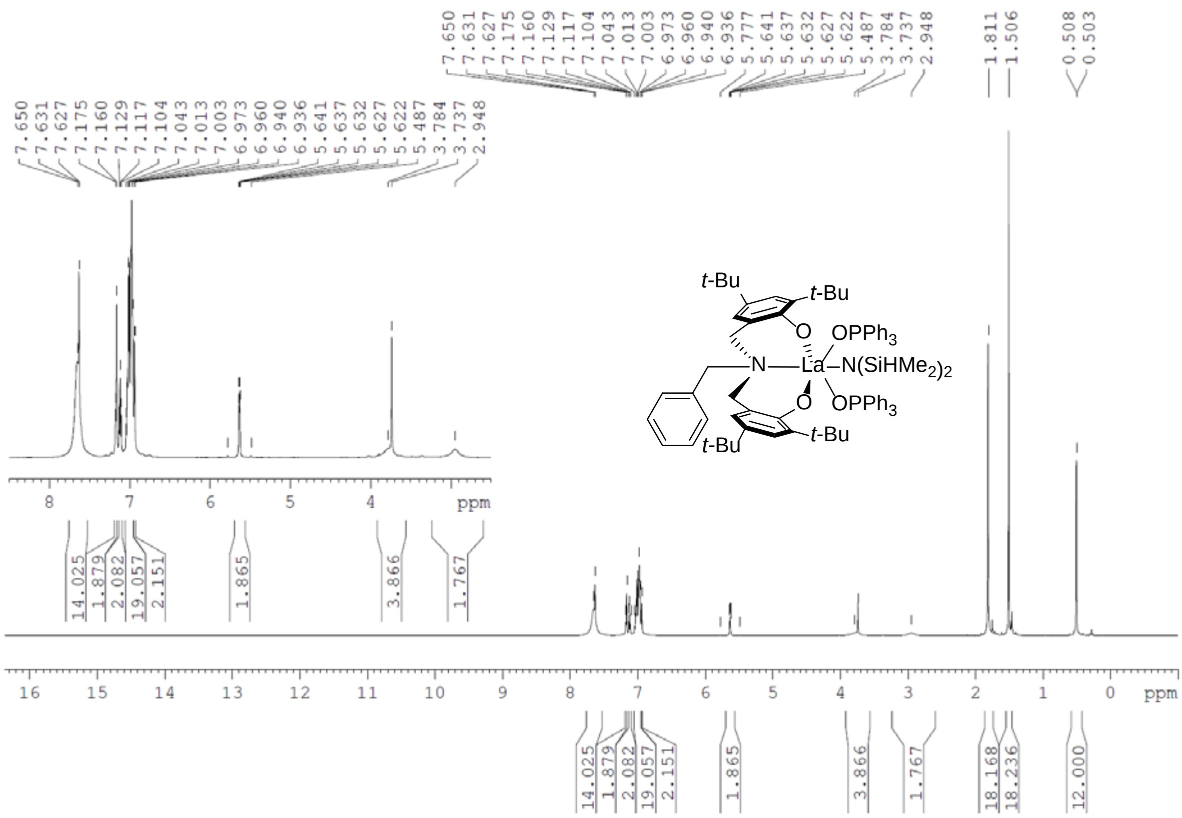

Figure S5a. [1]H-NMR (C_6D_6, 600 MHz) spectra of **1-La(TPPO)₂**.

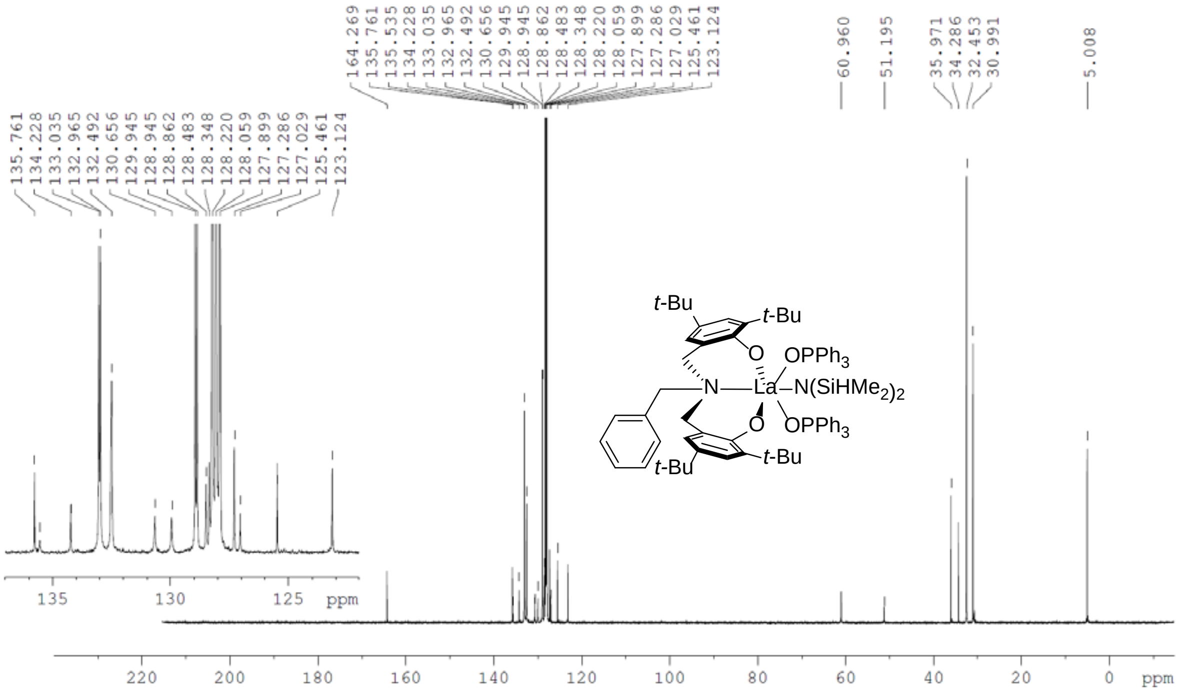

Figure S5b. [13]C-NMR (C_6D_6, 152 MHz) spectra of **1-La(TPPO)₂.**

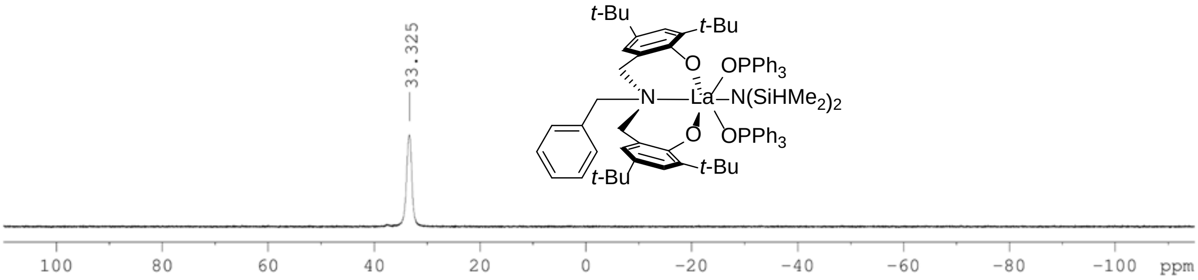

Figure S5c. $^{31}P\{^{1}H\}$-NMR (C_6D_6, 243 MHz) spectra of **1-La(TPPO)₂.**

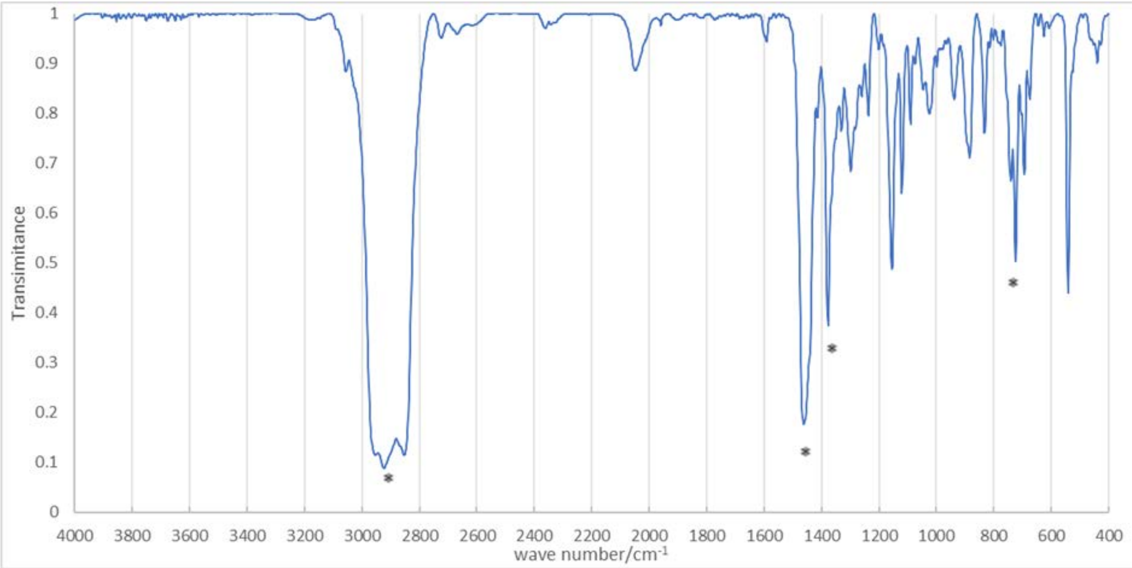

Figure S5d. IR (Nujol) spectra of **1-La(TPPO)₂**. (*: Nujol).

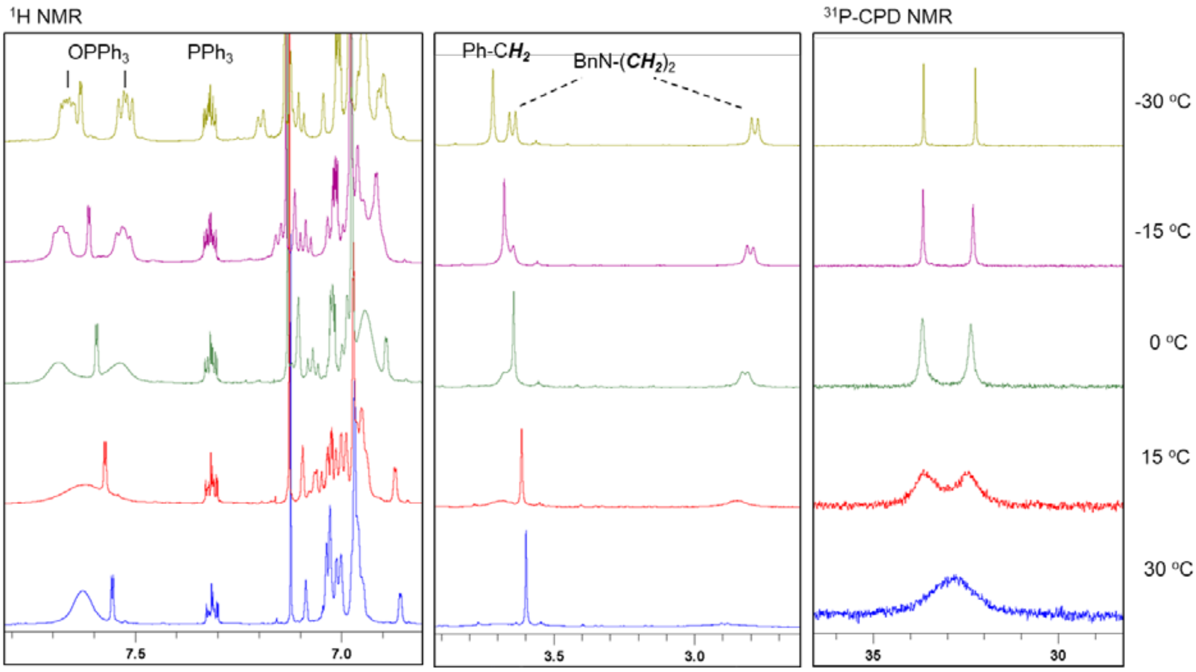

Figure S6. ^{1}H-NMR (600 MHz, toluene-d_8) and $^{31}P\{^{1}H\}$-NMR (243 MHz, toluene-d_8) of **1-La(TPPO)₂** at –30, –15, 0, 15 and 30 °C.

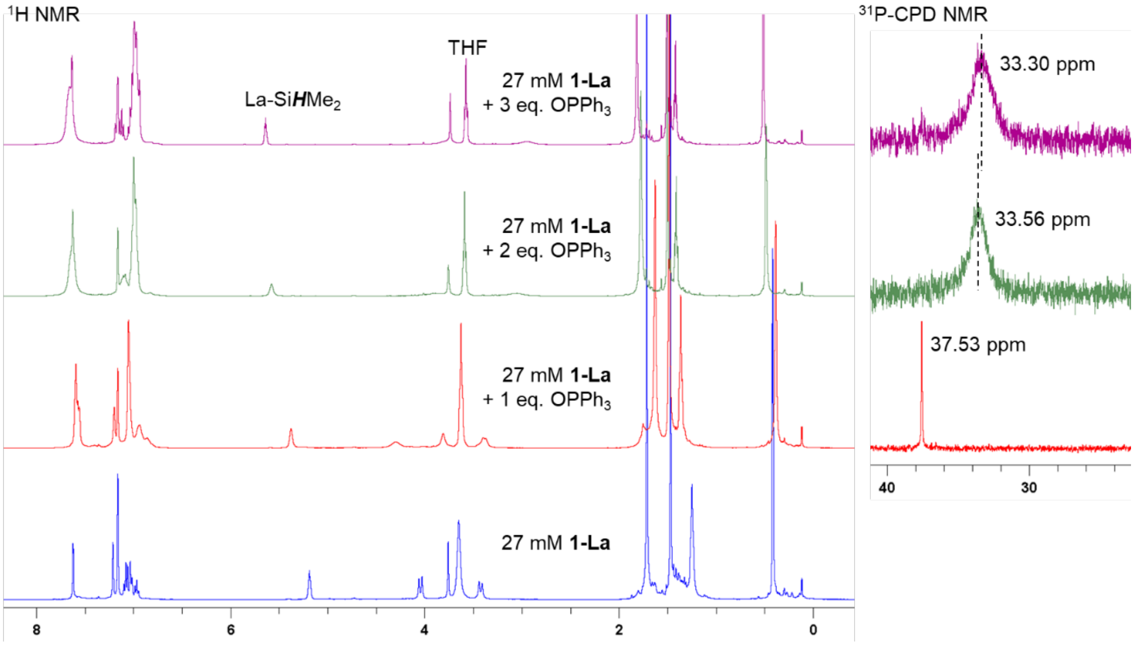

Figure S7. ^{1}H-NMR (400 MHz, C_6D_6, 298 K) and $^{31}P\{^{1}H\}$-NMR (162 MHz, C_6D_6, 298 K) of **1-La** (27 mM) in the presence of 0 (blue, bottom), 1 (red), 2 (green) and 3 (magenta, top) equiv of TPPO.

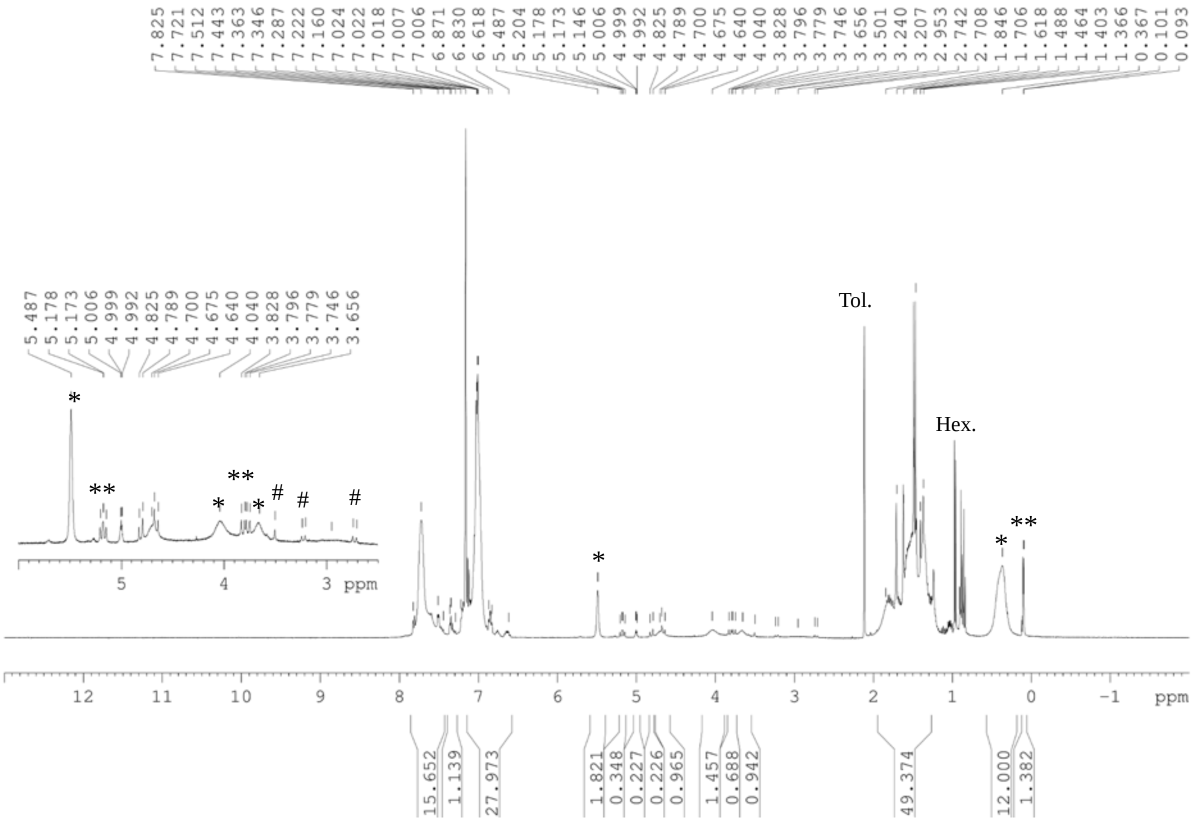

Figure S8a. ^{1}H-NMR (C_6D_6, 400 MHz, 25 mM) spectra of crystallized **1-Y(TPPO)$_2$**. (*: **1-Y(TPPO)$_2$**; **: [**1-Y(TPPO)$_2$**]$_2$; #: **1-Y(TPPO)**).

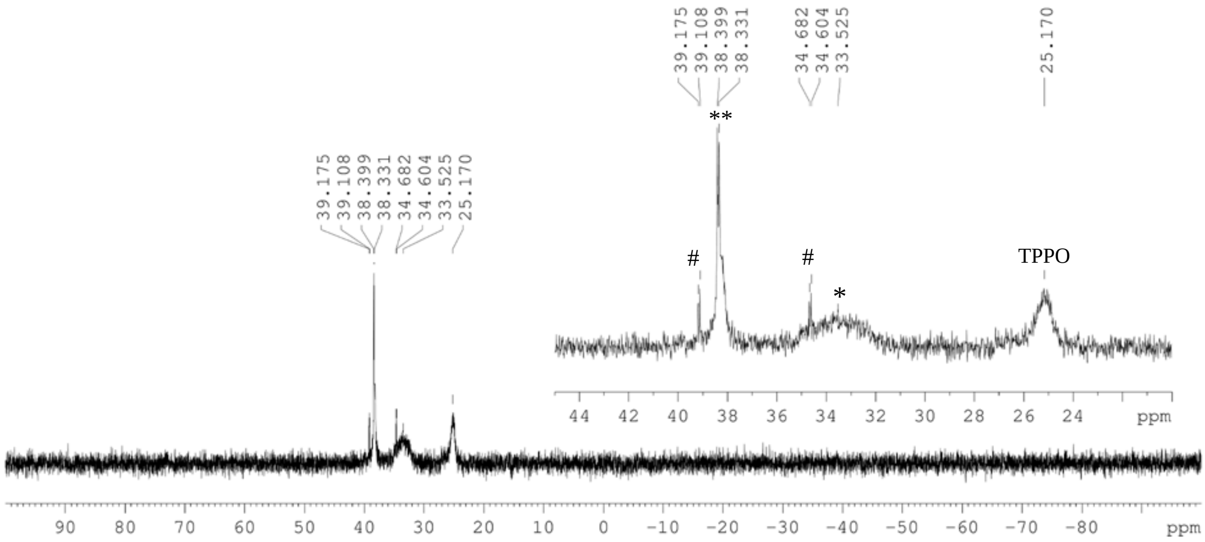

Figure S8b. $^{31}P\{^{1}H\}$-NMR (C_6D_6, 162 MHz, 25 mM) spectra of crystallized **1-Y(TPPO)$_2$**. (*: **1-Y(TPPO)$_2$**; **: [**1-Y(TPPO)$_2$]$_2$**; #: **1-Y(TPPO)**).

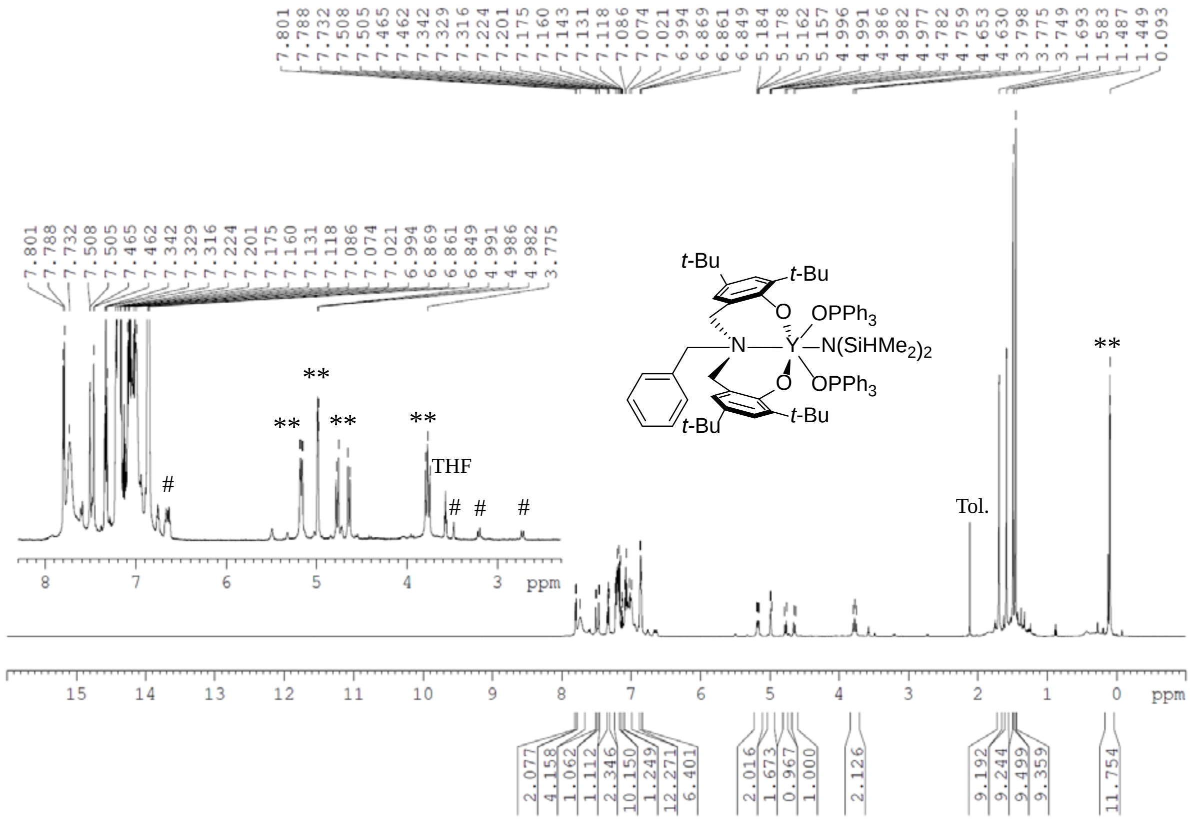

Figure S8c. ^{1}H-NMR (C_6D_6, 600 MHz, 75 mM) spectra of *in-situ* prepared **1-Y(TPPO)$_2$**. (**: [**1-Y(TPPO)$_2$]$_2$**; #: **1-Y(TPPO)**).

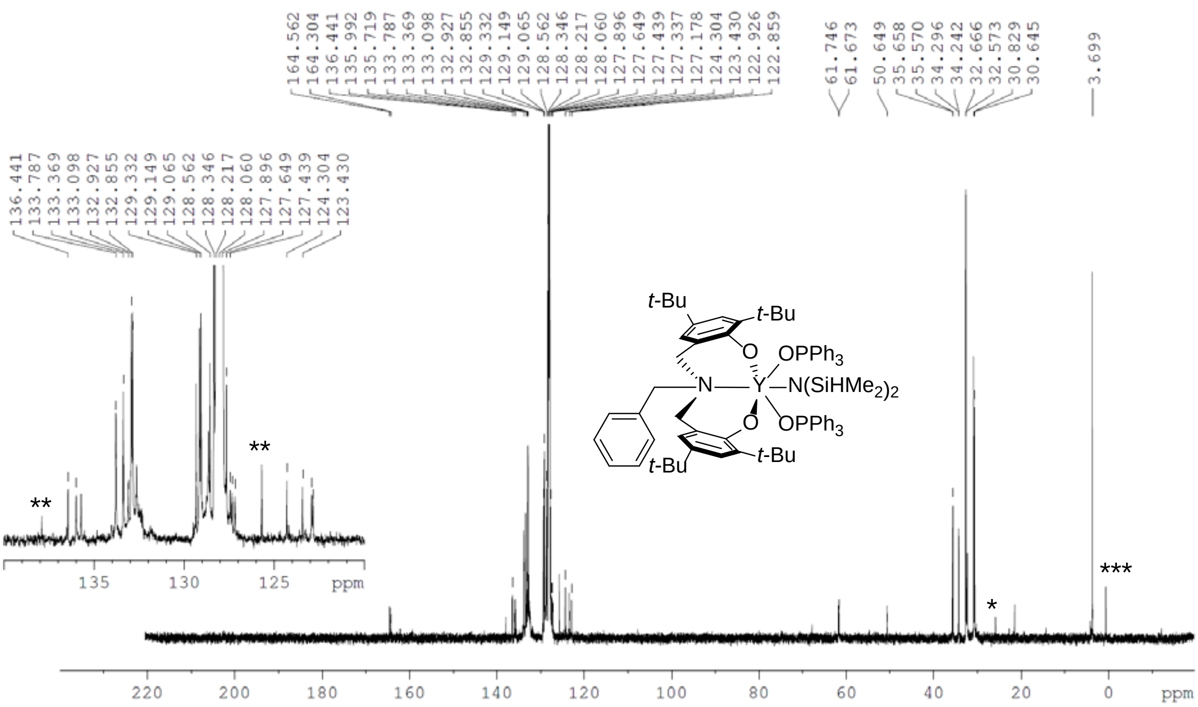

Figure S8d. ^{13}C-NMR (C_6D_6, 152 MHz, 75 mM) spectra of *in-situ* prepared **1-Y(TPPO)$_2$.** (*: THF; **: toluene; ***: $HN(SiHMe_2)_2$).

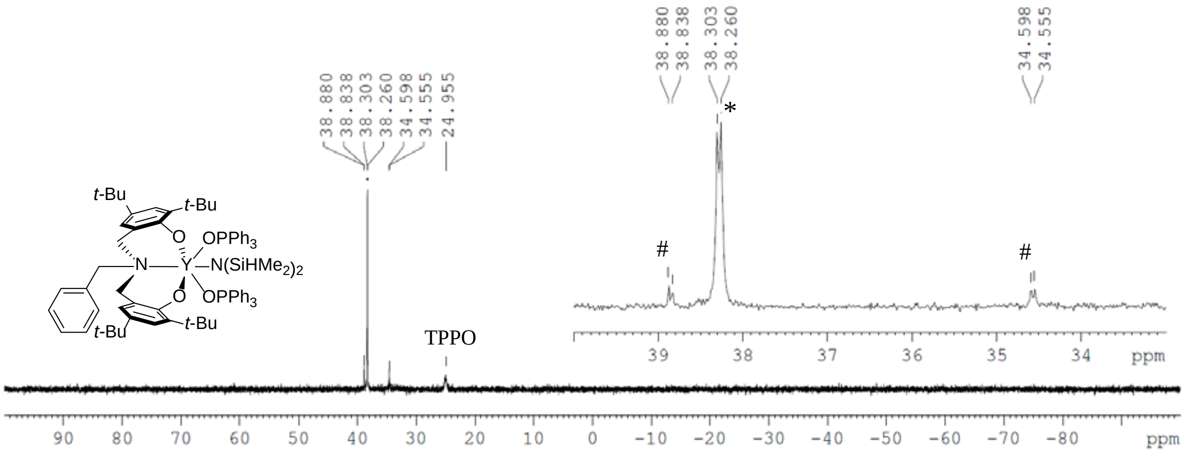

Figure S8e. ^{31}P{^{1}H}-NMR (C_6D_6, 243 MHz, 75 mM) spectra of *in-situ* prepared **1-Y(TPPO)$_2$**. (**: [**1-Y(TPPO)$_2$**]$_2$; #: **1-Y(TPPO)**).

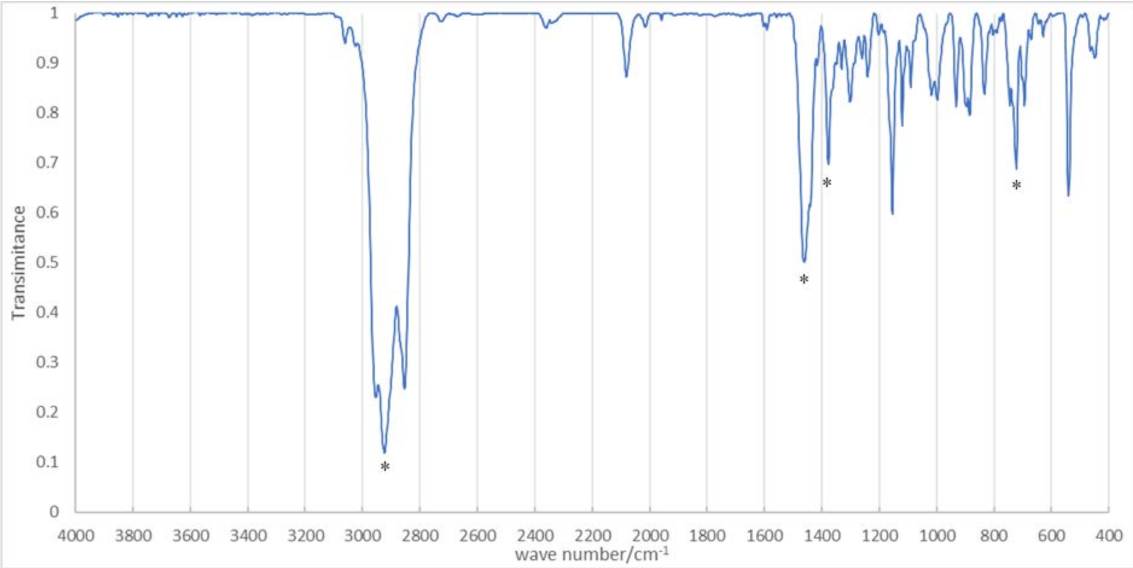

Figure S8f. IR (Nujol) spectra of **1-Y(TPPO)₂**. (*: Nujol).

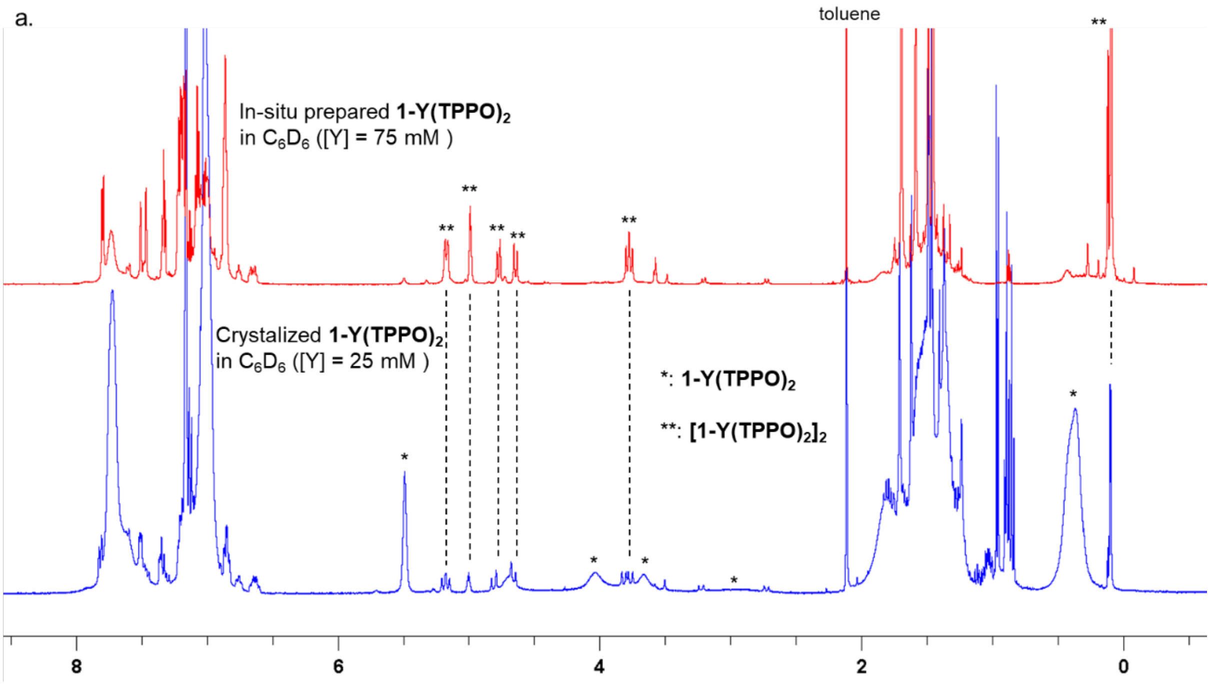

Figure S9a. ^{1}H-NMR (600 MHz, C_6D_6, 298 K) of **1-Y(TPPO)$_2$** prepared in-situ from **1-Y$_2$** and TPPO (75 mM [Y], 2 equiv TPPO / [Y]; red, top) and re-dissolved crystalline **1-Y(TPPO)$_2$** (25 mM, blue, bottom).

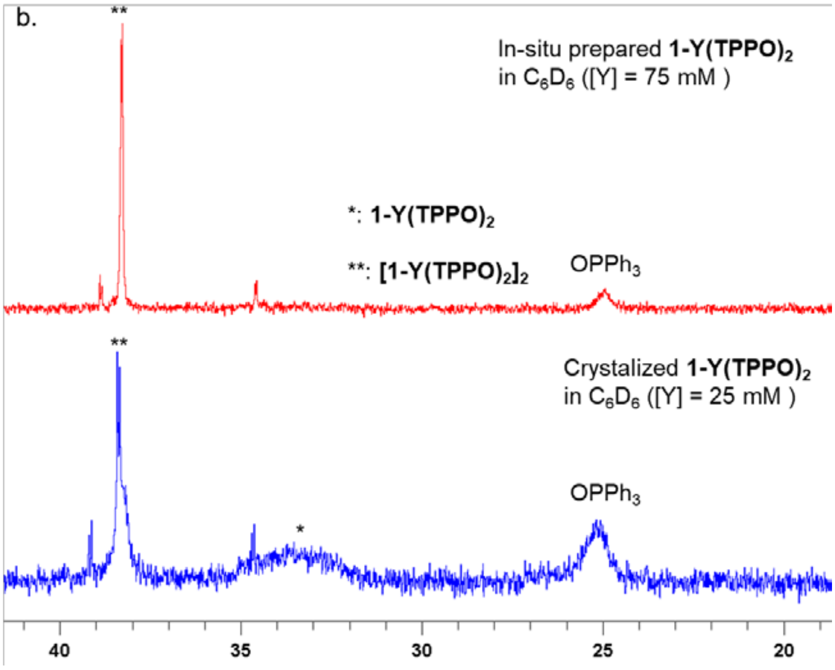

Figure S9b. $^{31}P\{^1H\}$-NMR (243 MHz, C_6D_6, 298 K) of **1-Y(TPPO)$_2$** prepared in-situ from **1-Y$_2$** and TPPO (75 mM [Y], 2 equiv TPPO / [Y]; red, top) and re-dissolved crystalline **1-Y(TPPO)$_2$** (25 mM, blue, bottom).

Table S3. Diffusion coefficients, *D*, and estimated hydrodynamic radii, r_H, measured by ^1H DOSY NMR of **1-RE** complexes (**1-La, 1-La(TPPO)$_2$, 1-Y$_2$, 1-Y(TPPO)$_2$ and [1-Y(TPPO)$_2$]$_2$**)

Species	D_{Fc} (10^{-10} m^2/s)[a]	D (10^{-10} m^2/s)	D_{Fc}/D	r_H(DOSY)[b] (Å)	r_H(theo.)[c] (Å)
Fc[d]	-	-	-	-	2.166
1-La	13.2	5.10	2.59	5.61	6.011
1-La(TPPO)$_2$	12.8	4.13	3.10	6.71	6.764
1-Y$_2$	11.8	3.56	3.31	7.18	7.361[e]
1-Y(TPPO)$_2$[f]	11.1	3.54	3.14	6.79	6.791
[1-Y(TPPO)$_2$]$_2$[f]	11.1	2.37	4.68	10.14	-

a – DOSY measured diffusion coefficient of ferrocene (Fc) in the experiment of the corresponding complex. DOSY measured diffusion coefficient of the sample *b* – $r_H = D_{Fc}/D_{sample} \cdot r_H$(Fc, theo.). *c* – r_H(theo.) is the average of half lengths of the principal axes of the homogeneous ellipsoid with the same principal moments of inertia of the molecule, which are determined from the crystal structure. *d* – Fc was added to each sample as an internal standard to cancel the fluctuation of temperature and viscosity, of which the diffusion coefficient varies. *e* – Estimated according to structure of **S1**,[17] due to the lack of X-ray structure of **1-Y$_2$**. *f* – Prepared *in-situ* with **1-Y$_2$** and addition of TPPO (2 equiv).

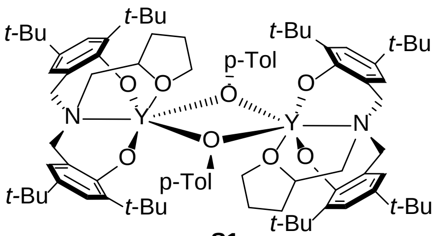

S1

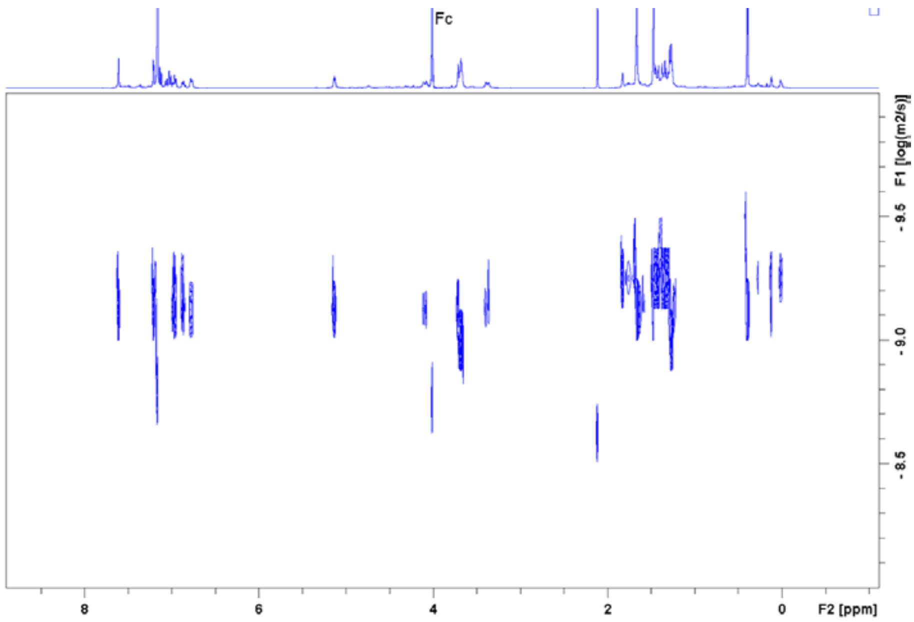

Figure S10. [1]H DOSY NMR (400 MHz, C_6D_6) of a mixture of **1-La** and ferrocene (Fc). In 0.5 mL C_6D_6, **1-La** (10 mg, 0.010 mmol, 1.0 equiv; MW: 957.27 g•mol^{-1}) and Fc (3.2 mg, 0.017 mmol, 1.7 equiv; MW: 186.04 g•mol^{-1}) were dissolved. Diffusion time was (Δ, d20) 100 ms, and the rectangular gradient pulse duration (δ, p30) was 1200 μs.

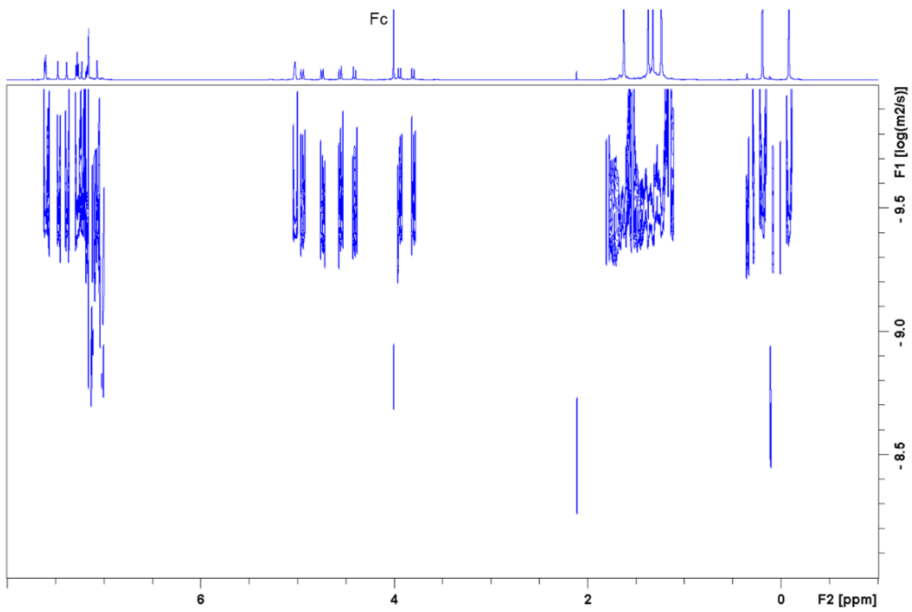

Figure S11. [1]H DOSY NMR (600 MHz, C_6D_6) of a mixture of **1-Y$_2$** and Fc. In 0.5 mL C_6D_6, **1-Y$_2$** (10 mg, 0.007 mmol, 1.0 equiv; MW: 1526.12 g•mol^{-1}) and Fc (0.4 mg, 0.002 mmol, 0.34 equiv; MW: 186.04 g•mol^{-1}) were dissolved. Diffusion time was (Δ, d20) 100 ms, and the rectangular gradient pulse duration (δ, p30) was 1000 μs.

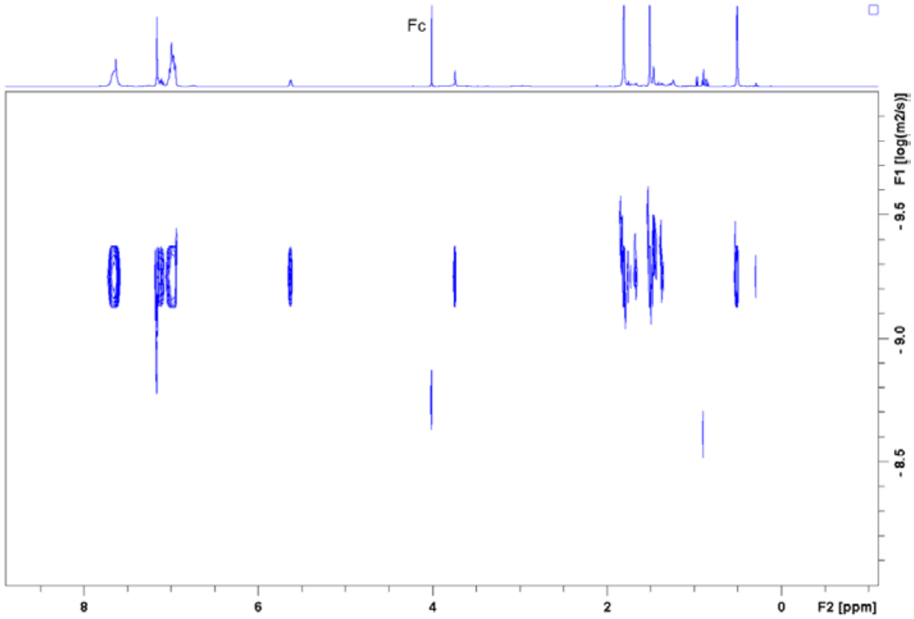

Figure S12. ^{1}H DOSY NMR (400 MHz, C_6D_6) of a mixture of **1-La(TPPO)$_2$** and Fc. In 0.5 mL C_6D_6, **1-La** (10 mg, 0.007 mmol, 1.0 equiv; MW: 1369.64 g•mol^{-1}) and Fc (0.5 mg, 0.003 mmol, 0.37 equiv; MW: 186.04 g•mol^{-1}) were dissolved. Diffusion time was (Δ, d20) 100 ms, and the rectangular gradient pulse duration (δ, p30) was 1200 μs.

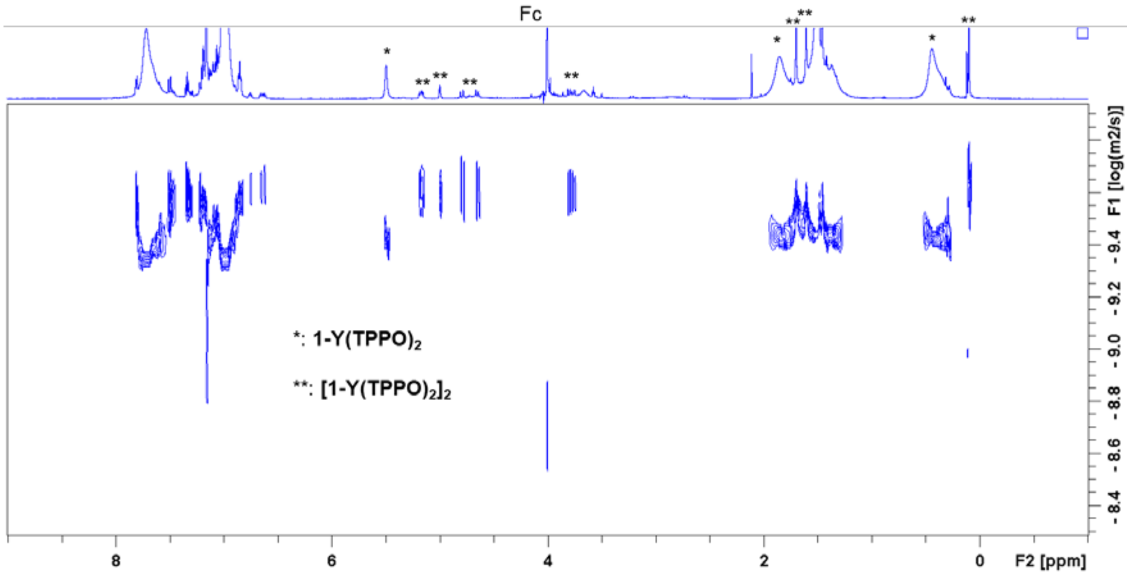

Figure S13. ^{1}H DOSY NMR (600 MHz, C_6D_6) of a mixture of **1-Y(TPPO)$_2$**, Fc, and TPPO. In 0.5 mL C_6D_6, **1-Y(TPPO)$_2$** (16 mg, 0.012 mmol, 1.0 equiv; MW: 1319.64 g•mol^{-1}), and Fc (0.4 mg, 0.002 mmol, 0.17 equiv; MW: 186.04 g•mol^{-1}) were dissolved. 1 h later, DOSY was taken. Diffusion time was (Δ, d20) 100 ms, and the rectangular gradient pulse duration (δ, p30) was 1400 μs.

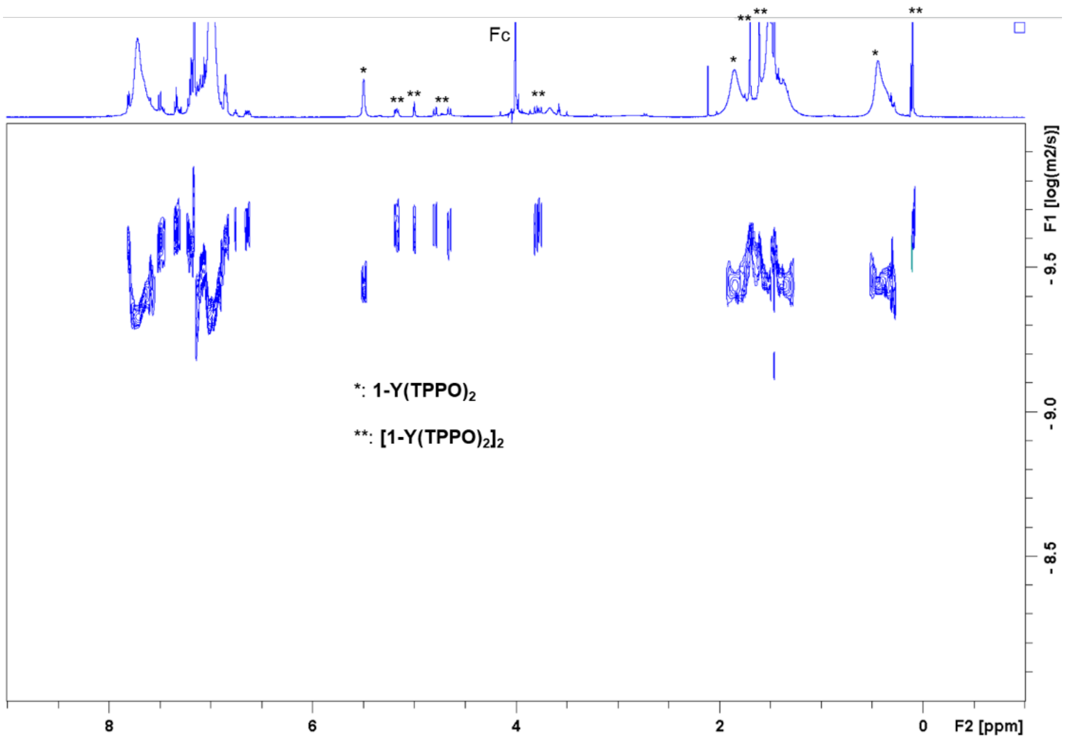

Figure S14. ^{1}H DOSY NMR (600 MHz, C_6D_6) of a mixture of **1-Y$_2$**, Fc, and TPPO. In 0.5 mL C_6D_6, **1-Y$_2$** (10 mg, 0.007 mmol, 1.0 equiv; MW: 1526.12 g•mol^{-1}), Fc (0.4 mg, 0.002 mmol, 0.34 equiv; MW: 186.04 g•mol^{-1}) and TPPO (7.3 mg, 0.007 mmol, 4.0 equiv; MW: 278.29 g•mol^{-1}) were dissolved. 7 h later, DOSY was taken. Diffusion time was (Δ, d20) 100 ms, and the rectangular gradient pulse duration (δ, p30) was 1400 µs. **Note:** Spectrum was nearly identical to authentic **1-Y(TPPO)$_2$** (Figure S13, nearly the same [Y] concentration).

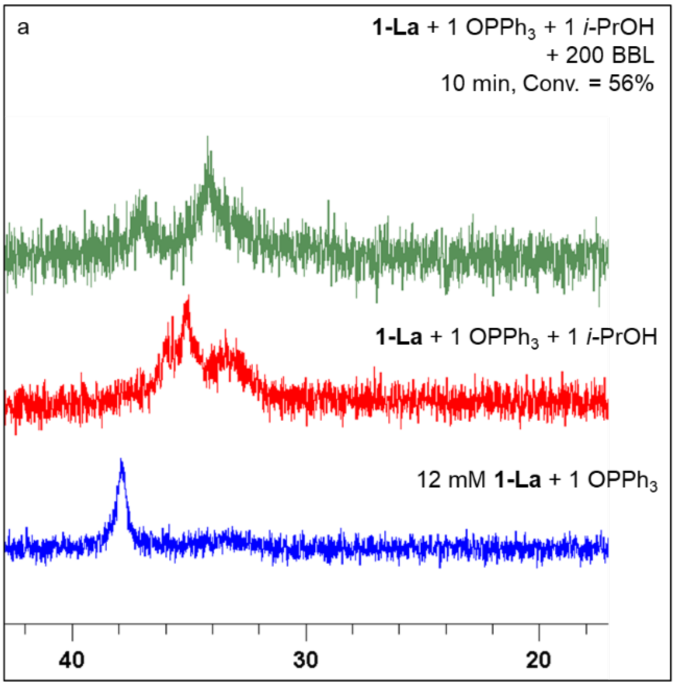

Figure S15a. ^{31}P{^{1}H}-NMR (243 MHz, toluene, 298 K) of: **1-La** + 1 TPPO (bottom, blue), **1-La** + TPPO + ^{i}PrOH (middle, red), and **1-La** + TPPO + ^{i}PrOH + 200 BBL (top, green).

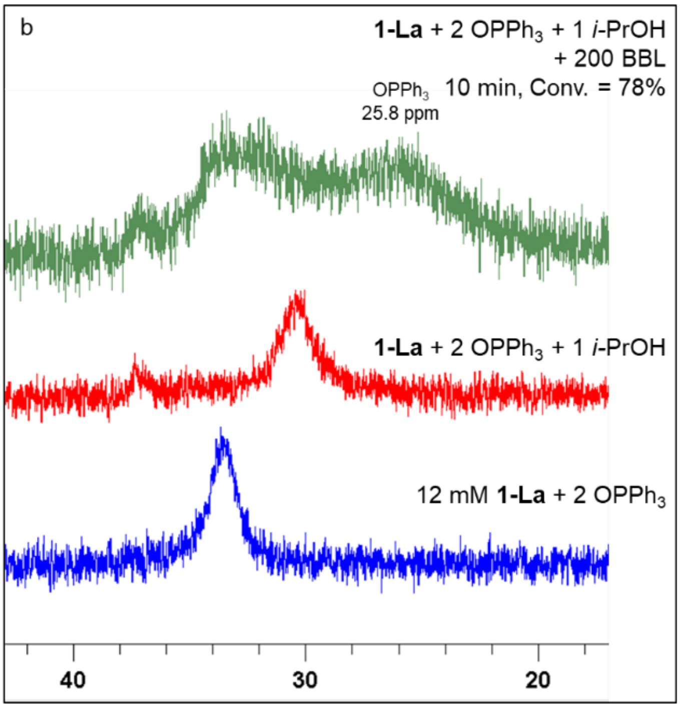

Figure S15b. $^{31}P\{^{1}H\}$-NMR (243 MHz, toluene, 298 K) of: **1-La** + 2 TPPO (bottom, blue), **1-La** + 2 TPPO + ^{i}PrOH (middle, red), and **1-La** + 2 TPPO + ^{i}PrOH + 200 BBL (top, green).

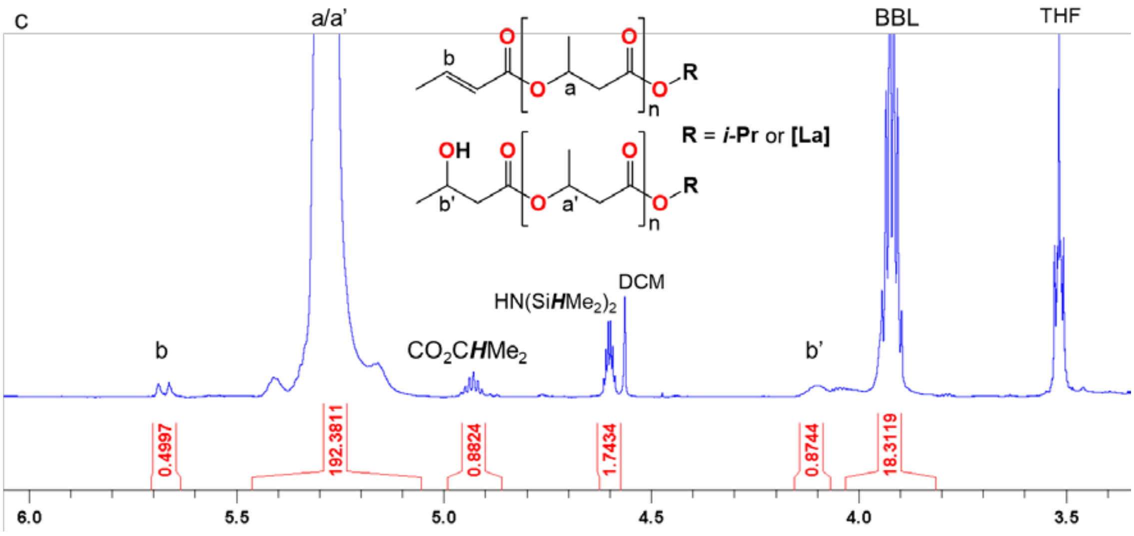

Figure S15c. ^{1}H-NMR (600 MHz, toluene, 298 K) of: **1-La** + 2 TPPO + ^{i}PrOH + 200 BBL (2.4 M). The NMR was taken after 40 min of reaction without quenching. The conversion of BBL was 91%. (The toluene as the solvent of reaction and NMR contained circa 0.05% DCM due to weak but endure vapor diffusion in the glovebox.)

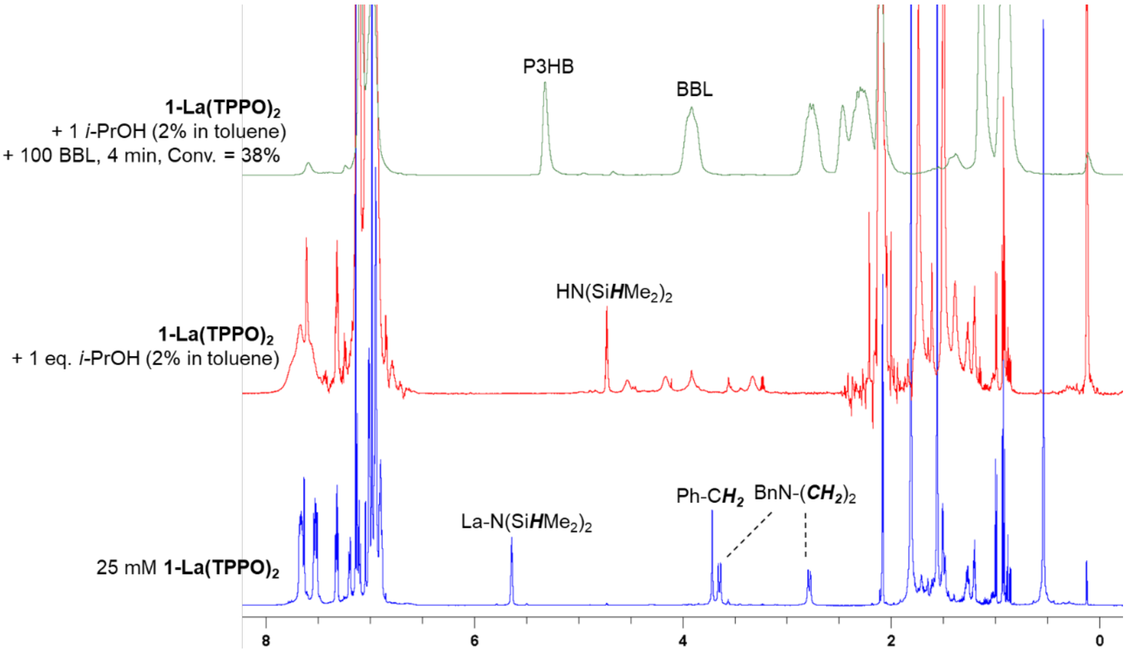

Figure S16a. ^{1}H-NMR (600 MHz, toluene-d_8, –30 °C) of **1-La(TPPO)₂** (25 mM, blue, bottom), **1-La(TPPO)₂** + ^{i}PrOH (red, middle), and **1-La(TPPO)₂** + ^{i}PrOH + 100 BBL at 4 min (green, top).

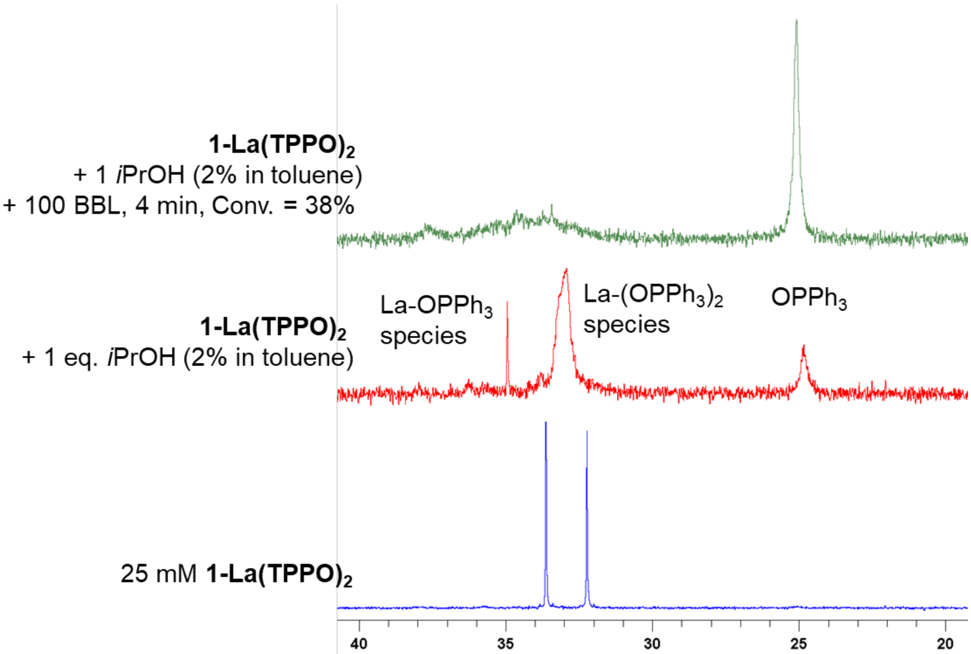

Figure S16b. ^{31}P{^{1}H}-NMR (600 MHz, toluene-d_8, –30 °C) of **1-La(TPPO)₂** (25 mM, blue, bottom), **1-La(TPPO)₂** + ^{i}PrOH (red, middle), and **1-La(TPPO)₂** + ^{i}PrOH + 100 BBL at 4 min (green, top).

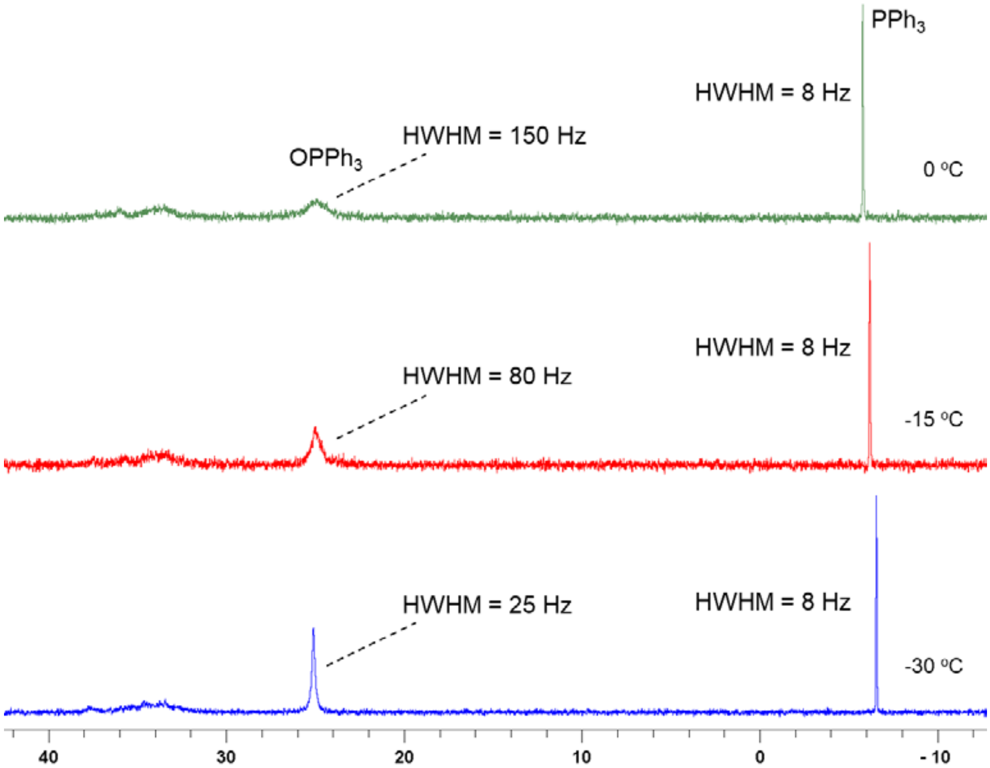

Figure S17. $^{31}P\{^{1}H\}$-NMR (600 MHz, toluene-d_8, –30 °C – 0 °C) of the ROP of BBL by **1-La(TPPO)$_2$** and ^{i}PrOH initially performed at –30 °C (38% conversion), followed by warming to –15 °C (55% conversion) and 0 °C (67% conversion).

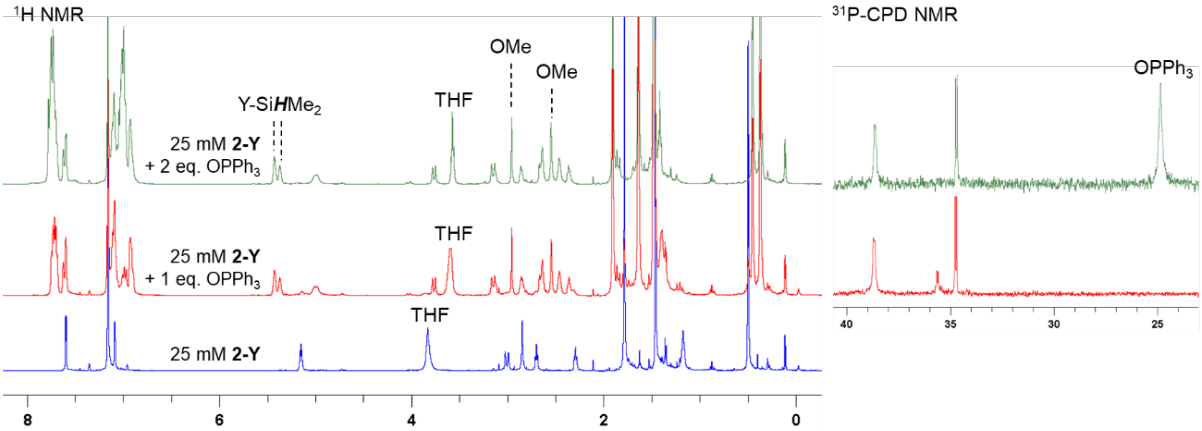

Figure S18. ^{1}H-NMR (400 MHz, C_6D_6, 298 K), $^{31}P\{^{1}H\}$-NMR (162 MHz, C_6D_6, 298 K) of adding 0, 1 and 2 equiv. of $OPPh_3$ to **2-Y**.

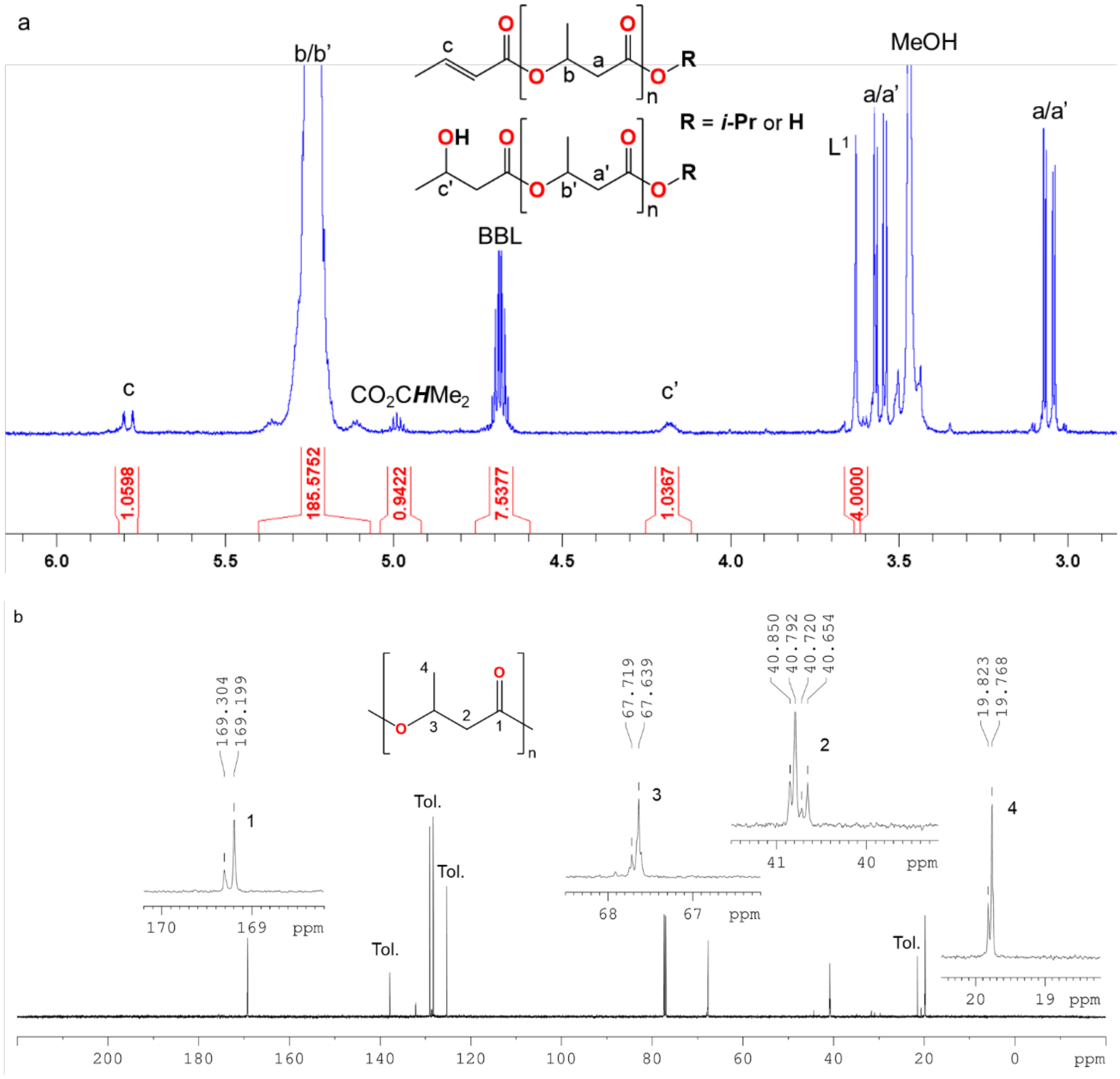

Figure S19. (*a*) ^{1}H-NMR (600 MHz, $CDCl_3$), (*b*) ^{13}C-NMR (152 MHz, $CDCl_3$) spectra of P3HB (Table 1, entry 6). Reaction was performed in toluene at ambient temperature with [BBL]/[**1-La**]/[TPPO]/[^{i}PrOH] = 200/1/2/1 and [BBL] = 2.4 M within 1 h. Conversion = 97%, M_n = 9.6 kg/mol (corrected by Mark-Houwink factor of 0.54), $Đ$ = 1.18.

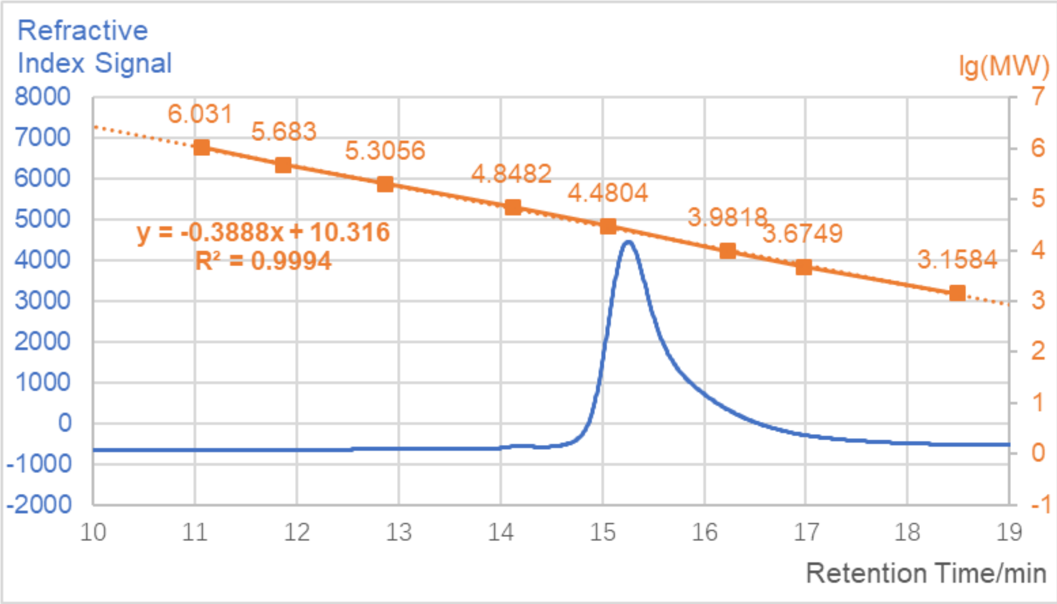

Figure S20. GPC calibration curve using polystyrene standards (orange) and GPC trace (blue) of Table 1, entry 6. Reaction was performed in toluene at ambient temperature with [BBL]/[**1-La**]/[TPPO]/[^{i}PrOH] = 200/1/2/1 and [BBL] = 2.4 M within 1 h. Conversion = 97%, M_n = 9.6 kg/mol (corrected by Mark-Houwink factor of 0.54), *Đ* = 1.18

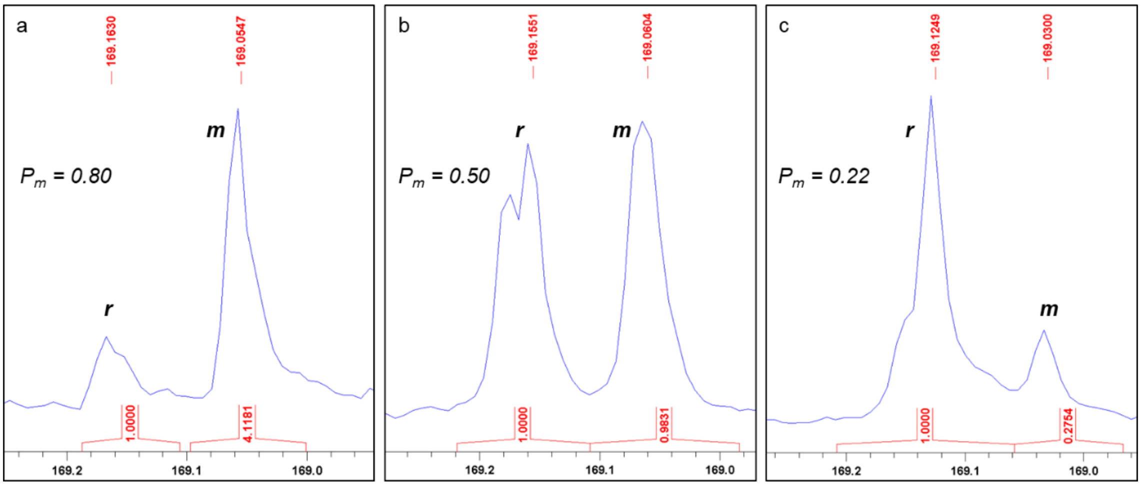

Figure S21. Carbonyl region of IG-^{13}C-NMR (152 MHz, $CDCl_3$) of P3HB with different P_m. (a) Table 1, entry 15 (**1-La** + 2 TPPO + ^{i}PrOH, –30 °C), (b) Table 2, entry 7 (**1-Y(TPPO)$_2$** + ^{i}PrOH), (c) Table 2, entry 8 (**2-Y** + ^{i}PrOH).

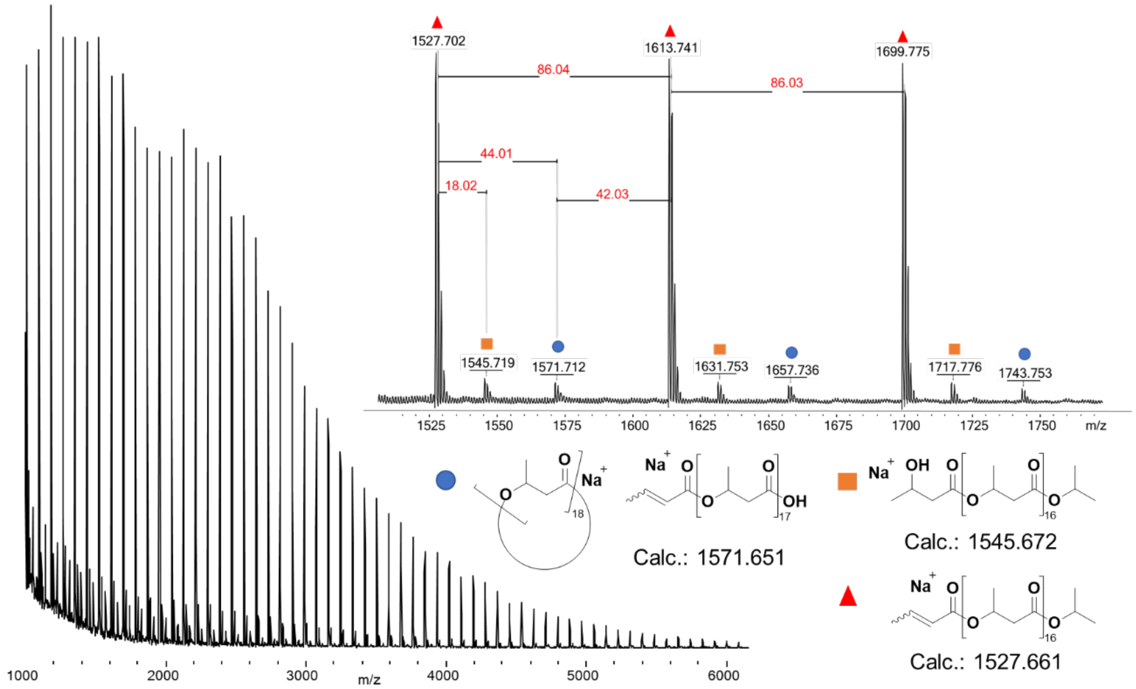

Figure S22. MALDI-TOF spectrum of P3HB, produced in toluene at ambient temperature with [BBL]/[**1-La**]/[TPPO]/[^{i}PrOH] = 40/1/2/1 and [BBL] = 2.4 M within 1 h. Conversion = 99%. M_n = 3.8 kg/mol (corrected by Mark-Houwink factor of 0.54), $Đ$ = 1.30.

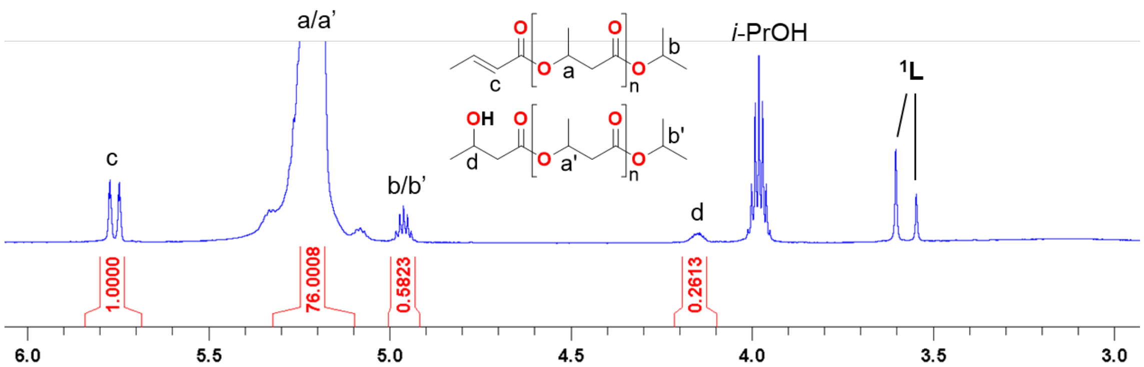

Figure S23. ^{1}H-NMR (400 MHz, $CDCl_3$) of the P3HB for MALDI analysis.

Note: The ^{i}Pr methine of 2-isopropoxyl butyrate should appear at ~3.6 ppm, analogous to that of 4-isopropoxypentan-2-one (3.60-3.66, m, $CDCl_3$)[18]. No isopropyl ether (i.e. product of O-Alkyl cleavage) is formed as there is no multiplet present in this range.

Table S4. ROP of *rac*-BBL with **1-La(TPPO)₂** + ^{i}PrOH quenched at different time points.

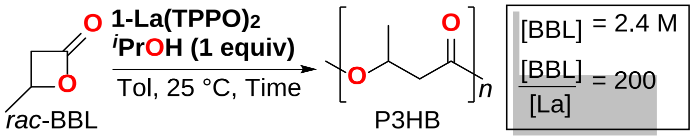

Entry	Time (min)	Conv. (%)[a]	$M_{n,\,calc}$[c] (kg/mol)	$M_{n,\,exp}$[c] (kg/mol)	$Đ$[c,d]
1	0.25	22	3.9	3.2	1.054
2	0.50	28	4.9	4.0	1.042
3	0.75	34	5.9	4.6	1.050
4	1.0	39	6.7	5.1	1.050
5	1.5	46	7.9	5.8	1.056
6	2.0	50	8.7	6.3	1.069
7	5.0	62	10.6	7.6	1.056
8	15	74	12.7	8.7	1.074
9	30	82	14.1	8.9	1.116
10	60	88	15.1	9.2	1.145

a – Determined by ^{1}H-NMR integration of BBL and PHB methine resonances in the crude reaction mixture. *b* – [BBL]/[La]/[^{i}PrOH] × Conv. × 0.08609 kg•mol^{-1}. *c* – Determined by gel permeation chromatography (GPC) at 30 °C in THF using polystyrene standards and corrected by Mark-Houwink factor of 0.54.[16] d – M_w/M_n.

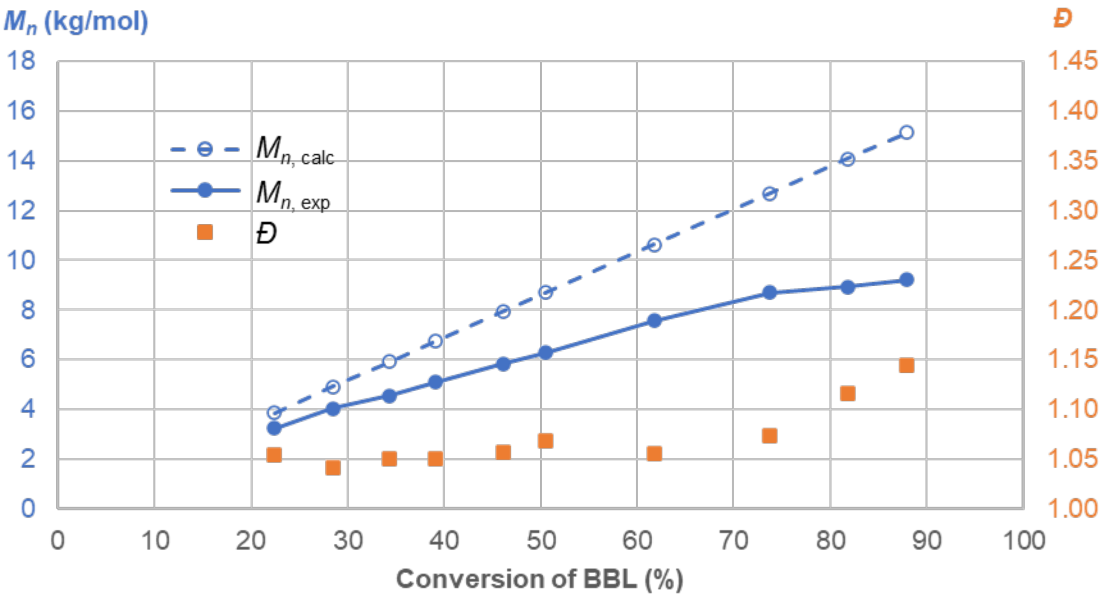

Figure S24. Calculated M_n (blue circle), Experimental M_n (blue dot) and $Đ$ (orange squares) as functions of conversion of BBL. Reaction was performed in toluene at ambient temperature with [BBL]/[**1-La(TPPO)₂**]/[^{i}PrOH] = 200/1/1 and [BBL] = 2.4 M.

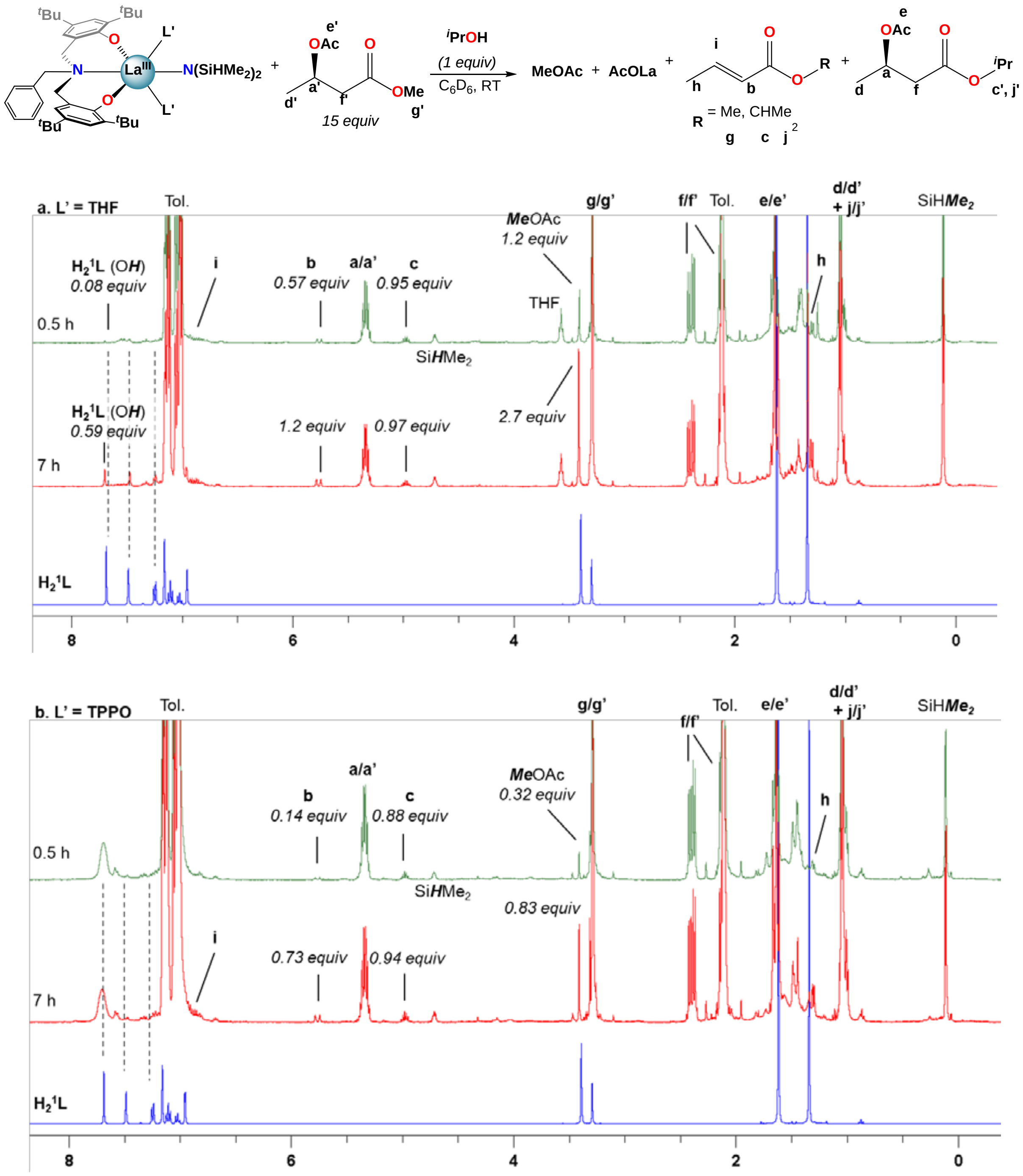

Figure S25. Reactivity studies of (a) **1-La** and (b) **1-La(TPPO)$_2$** in the presence of 1 equiv ^{i}PrOH and 15 equiv **(*R*)-3-OAcB^{Me}** in C$_6$D$_6$ followed by ^{1}H-NMR after 0.5 h, 7 h. Dashed lines provided to help track the formation of **H$_2$^{1}L** during the reaction time course.

Note:

1. MeOAc is assigned according to previously reported NMR data (3.34 ppm in C$_6$D$_6$).[19]
2. There are minor singlets, other than **(*R*)-3-OAcB^{Me}** and **(*R*)-3-OAcB^{iPr}**, from 1.6-1.7 ppm, representing La acetate species and other transesterification products, but cannot be unambiguously assigned.

Table S5. Crystallographic parameters for compounds **1-La**, **1-La(TPPO)$_2$**, and **1-Y(TPPO)$_2$**

	1-La	**1-La(TPPO)$_2$**	**1-Y(TPPO)2**
Empirical formula	$C_{49}H_{83}LaN_2O_4Si_2$	$C_{91}H_{111}LaN_2O_4P_2Si_2$	$C_{91}H_{111}N_2O_4P_2Si_2Y$
Formula weight	959.26	1553.84	1503.84
Temperature/K	173.2	173.21	173.19
Crystal system	monoclinic	monoclinic	monoclinic
Space group	$P2_1/c$	$P2_1/n$	$P2_1/n$
a/Å	17.0458(16)	15.355(2)	15.2210(16)
b/Å	16.5877(16)	15.378(2)	15.3725(15)
c/Å	19.5942(17)	35.734(5)	35.552(4)
α/°	90	90	90
β/°	112.851(3)	94.563(5)	93.759(3)
γ/°	90	90	90
Volume/Å^3	5105.5(8)	8411(2)	8300.7(15)
Z	4	4	4
ρ_{calc}g/cm^3	1.248	1.227	1.203
μ/mm^{-1}	0.925	0.624	0.820
F(000)	2032.0	3272.0	3200.0
Crystal size/mm^3	0.25 × 0.25 × 0.2	0.14 × 0.12 × 0.1	0.3 × 0.2 × 0.1
Radiation	MoKα (λ = 0.71073)	MoKα (λ = 0.71073)	MoKα (λ = 0.71073)
2Θ range for data collection/°	3.57 to 55.872	3.862 to 55.2	3.992 to 55.156
Index ranges	$-22 \le h \le 22$, $-21 \le k \le 21$, $-25 \le l \le 25$	$-19 \le h \le 20$, $-20 \le k \le 19$, $-46 \le l \le 44$	$-19 \le h \le 19$, $-19 \le k \le 19$, $-46 \le l \le 46$
Reflections collected	192582	152196	166733
Independent reflections	11709 [R_{int} = 0.1329, R_{sigma} = 0.0585]	19424 [R_{int} = 0.1040, R_{sigma} = 0.0594]	19123 [R_{int} = 0.0829, R_{sigma} = 0.0489]
Data/restraints/parameters	11709/0/549	19424/175/886	19123/164/875
Goodness-of-fit on F^2	1.022	1.046	1.018
Final R indexes [I>=2σ (I)]	R_1 = 0.0527, wR_2 = 0.0906	R_1 = 0.0528, wR_2 = 0.1315	R_1 = 0.0477, wR_2 = 0.1238
Final R indexes [all data]	R_1 = 0.0847, wR_2 = 0.1021	R_1 = 0.0659, wR_2 = 0.1399	R_1 = 0.0615, wR_2 = 0.1332
Largest diff. peak/hole / e Å^{-3}	1.17/-0.83	0.48/-0.89	0.94/-0.81
CCDC Dep. #	1980000	1980001	1980002

Table S6a. Bond distances for **1-La**.

La1	Si1	3.3497(13)	C1	C2	1.414(5)	C23	C24	1.503(5)
La1	O1	2.258(3)	C1	C14	1.405(5)	C24	C25	1.386(5)
La1	O2	2.263(2)	C2	C3	1.544(5)	C24	C37	1.406(5)
La1	O3	2.703(3)	C2	C7	1.392(5)	C25	C26	1.386(5)
La1	O4	2.650(3)	C3	C4	1.537(6)	C26	C27	1.530(5)
La1	N1	2.712(3)	C3	C5	1.536(6)	C26	C31	1.396(5)
La1	N2	2.429(3)	C3	C6	1.529(6)	C27	C28	1.517(6)
Si1	N2	1.681(4)	C7	C8	1.395(5)	C27	C29	1.525(7)
Si1	C38	1.872(5)	C8	C9	1.532(5)	C27	C30	1.516(6)
Si1	C39	1.864(6)	C8	C13	1.398(5)	C31	C32	1.390(5)
Si2	N2	1.708(3)	C9	C10	1.529(6)	C32	C33	1.533(5)
Si2	C40	1.873(5)	C9	C11	1.527(6)	C32	C37	1.424(5)
Si2	C41	1.865(5)	C9	C12	1.526(6)	C33	C34	1.539(6)
O1	C1	1.344(4)	C13	C14	1.386(5)	C33	C35	1.539(5)
O2	C37	1.333(4)	C14	C15	1.508(5)	C33	C36	1.531(6)
O3	C42	1.434(5)	C16	C17	1.524(5)	C42	C43	1.506(7)
O3	C45	1.442(5)	C17	C18	1.378(5)	C43	C44	1.503(7)
O4	C47	1.507(6)	C17	C22	1.391(5)	C44	C45	1.527(6)
O4	C48	1.388(6)	C18	C19	1.385(6)	C46	C47	1.405(8)
N1	C15	1.488(4)	C19	C20	1.373(6)	C48	C49	1.465(9)
N1	C16	1.486(4)	C20	C21	1.377(7)			
N1	C23	1.488(5)	C21	C22	1.387(6)			

Table S6b. Bond angles for **1-La**.

O1	La1	Si1	130.53(7)	C6	C3	C5	107.5(4)
O1	La1	O2	123.05(10)	C2	C7	C8	123.9(3)
O1	La1	O3	82.31(10)	C7	C8	C9	122.7(3)
O1	La1	O4	118.24(10)	C7	C8	C13	116.4(4)
O1	La1	N1	74.84(9)	C13	C8	C9	120.8(3)
O1	La1	N2	102.24(11)	C10	C9	C8	109.0(3)
O2	La1	Si1	96.16(7)	C11	C9	C8	112.0(3)
O2	La1	O3	75.49(9)	C11	C9	C10	108.2(4)
O2	La1	O4	101.62(10)	C12	C9	C8	111.2(4)
O2	La1	N1	70.39(9)	C12	C9	C10	109.1(4)
O2	La1	N2	121.18(11)	C12	C9	C11	107.4(4)
O3	La1	Si1	141.03(7)	C14	C13	C8	121.9(3)
O3	La1	N1	117.10(9)	C1	C14	C15	120.5(3)
O4	La1	Si1	75.62(8)	C13	C14	C1	120.1(3)
O4	La1	O3	69.23(10)	C13	C14	C15	119.3(3)
O4	La1	N1	166.75(10)	N1	C15	C14	115.8(3)
N1	La1	Si1	94.39(7)	N1	C16	C17	119.2(3)
N2	La1	Si1	28.53(8)	C18	C17	C16	122.3(3)
N2	La1	O3	152.34(10)	C18	C17	C22	117.8(4)

N2	La1	O4	85.01(11)	C22	C17	C16	119.7(4)
N2	La1	N1	90.22(10)	C17	C18	C19	121.3(4)
N2	Si1	La1	43.67(11)	C20	C19	C18	120.6(4)
N2	Si1	C38	116.2(3)	C19	C20	C21	118.8(4)
N2	Si1	C39	116.6(2)	C20	C21	C22	120.8(4)
C38	Si1	La1	123.4(2)	C21	C22	C17	120.6(4)
C39	Si1	La1	129.54(19)	N1	C23	C24	116.8(3)
C39	Si1	C38	107.1(3)	C25	C24	C23	117.9(3)
N2	Si2	C40	113.5(2)	C25	C24	C37	120.4(3)
N2	Si2	C41	114.5(2)	C37	C24	C23	121.6(3)
C41	Si2	C40	107.8(2)	C26	C25	C24	122.2(3)
C1	O1	La1	141.0(2)	C25	C26	C27	122.2(3)
C37	O2	La1	148.1(2)	C25	C26	C31	116.7(3)
C42	O3	La1	138.7(3)	C31	C26	C27	121.1(3)
C42	O3	C45	108.2(3)	C28	C27	C26	112.4(3)
C45	O3	La1	112.7(2)	C28	C27	C29	107.1(4)
C47	O4	La1	118.0(3)	C29	C27	C26	108.5(4)
C48	O4	La1	127.4(4)	C30	C27	C26	110.3(4)
C48	O4	C47	114.5(4)	C30	C27	C28	108.0(4)
C15	N1	La1	108.4(2)	C30	C27	C29	110.5(5)
C16	N1	La1	104.9(2)	C32	C31	C26	123.9(3)
C16	N1	C15	110.3(3)	C31	C32	C33	121.4(3)
C16	N1	C23	114.1(3)	C31	C32	C37	117.9(3)
C23	N1	La1	110.4(2)	C37	C32	C33	120.7(3)
C23	N1	C15	108.6(3)	C32	C33	C34	110.4(3)
Si1	N2	La1	107.80(16)	C32	C33	C35	112.7(3)
Si1	N2	Si2	129.1(2)	C34	C33	C35	106.6(3)
Si2	N2	La1	122.81(18)	C36	C33	C32	109.1(3)
O1	C1	C2	122.4(3)	C36	C33	C34	110.4(3)
O1	C1	C14	118.4(3)	C36	C33	C35	107.5(3)
C14	C1	C2	119.2(3)	O2	C37	C24	119.6(3)
C1	C2	C3	121.2(3)	O2	C37	C32	121.6(3)
C7	C2	C1	117.8(3)	C24	C37	C32	118.9(3)
C7	C2	C3	121.0(3)	O3	C42	C43	105.7(4)
C4	C3	C2	108.6(3)	C44	C43	C42	102.0(4)
C5	C3	C2	110.7(3)	C43	C44	C45	104.6(4)
C5	C3	C4	110.2(4)	O3	C45	C44	106.6(4)
C6	C3	C2	112.1(3)	C46	C47	O4	115.1(5)
C6	C3	C4	107.7(4)	O4	C48	C49	108.8(5)

Table S7a. Bond distances for 1-La(TPPO)$_2$.

La1	Si1	3.3964(10)	C8	C13	1.391(4)	C43	C44	1.388(5)
La1	O1	2.276(2)	C9	C10	1.504(10)	C44	C45	1.379(6)
La1	O2	2.267(2)	C9	C11	1.501(10)	C45	C46	1.351(6)
La1	O3	2.4821(19)	C9	C12	1.519(10)	C46	C47	1.377(5)
La1	O4	2.456(2)	C9	C10A	1.506(10)	C48	C49	1.378(4)
La1	N1	2.828(2)	C9	C11A	1.507(10)	C48	C53	1.388(4)
La1	N2	2.459(3)	C9	C12A	1.546(10)	C49	C50	1.386(5)
P1	O3	1.502(2)	C13	C14	1.392(4)	C50	C51	1.358(6)
P1	C42	1.792(3)	C14	C15	1.511(4)	C51	C52	1.378(6)
P1	C48	1.808(3)	C16	C17	1.516(4)	C52	C53	1.377(5)
P1	C54	1.805(3)	C17	C18	1.385(5)	C54	C55	1.383(4)
P2	O4	1.502(2)	C17	C22	1.391(5)	C54	C59	1.397(4)
P2	C60	1.797(3)	C18	C19	1.382(5)	C55	C56	1.374(5)
P2	C66	1.795(3)	C19	C20	1.387(7)	C56	C57	1.389(5)
P2	C72	1.792(3)	C20	C21	1.359(6)	C57	C58	1.374(5)
Si1	N2	1.681(3)	C21	C22	1.380(5)	C58	C59	1.379(5)
Si1	C38	1.853(4)	C23	C24	1.513(4)	C60	C61	1.382(5)
Si1	C39	1.865(4)	C24	C25	1.384(4)	C60	C65	1.381(5)
Si2	N2	1.686(3)	C24	C37	1.407(4)	C61	C62	1.379(5)
Si2	C40	1.851(4)	C25	C26	1.388(4)	C62	C63	1.378(6)
Si2	C41	1.728(8)	C26	C27	1.526(5)	C63	C64	1.357(6)
Si2	C41A	1.685(8)	C26	C31	1.390(5)	C64	C65	1.387(5)
O1	C1	1.329(4)	C27	C28	1.614(9)	C66	C67	1.389(4)
O2	C37	1.325(4)	C27	C29	1.557(10)	C66	C71	1.388(4)
N1	C15	1.494(3)	C27	C30	1.468(11)	C67	C68	1.378(4)
N1	C16	1.477(4)	C27	C28A	1.541(9)	C68	C69	1.380(5)
N1	C23	1.491(3)	C27	C29A	1.485(8)	C69	C70	1.369(5)
C1	C2	1.420(4)	C27	C30A	1.487(10)	C70	C71	1.371(5)
C1	C14	1.403(4)	C31	C32	1.398(5)	C72	C73	1.392(5)
C2	C3	1.527(5)	C32	C33	1.534(5)	C72	C77	1.386(5)
C2	C7	1.401(5)	C32	C37	1.423(4)	C73	C74	1.384(5)
C3	C4	1.528(5)	C33	C34	1.529(5)	C74	C75	1.359(7)
C3	C5	1.534(5)	C33	C35	1.526(6)	C75	C76	1.364(6)
C3	C6	1.539(5)	C33	C36	1.538(5)	C76	C77	1.382(5)
C7	C8	1.382(5)	C42	C43	1.387(5)			
C8	C9	1.535(4)	C42	C47	1.371(5)			

Table S7b. Bond angles for **1-La(TPPO)$_2$**.

O1	La1	Si1	89.35(5)	N1	C16	C17	119.8(2)
O1	La1	O3	96.73(7)	C18	C17	C16	121.8(3)
O1	La1	O4	84.03(8)	C18	C17	C22	117.5(3)
O1	La1	N1	71.33(7)	C22	C17	C16	120.6(3)
O1	La1	N2	109.07(9)	C19	C18	C17	121.4(4)
O2	La1	Si1	125.22(5)	C18	C19	C20	119.8(4)

O2	La1	O1	144.91(7)	C21	C20	C19	119.4(4)
O2	La1	O3	85.42(7)	C20	C21	C22	120.9(4)
O2	La1	O4	87.84(8)	C21	C22	C17	121.0(4)
O2	La1	N1	73.91(7)	N1	C23	C24	117.9(2)
O2	La1	N2	105.42(9)	C25	C24	C23	118.6(3)
O3	La1	Si1	79.42(5)	C25	C24	C37	120.5(3)
O3	La1	N1	85.96(7)	C37	C24	C23	120.2(3)
O4	La1	Si1	111.34(5)	C24	C25	C26	122.6(3)
O4	La1	O3	169.24(7)	C25	C26	C27	122.2(3)
O4	La1	N1	84.11(7)	C25	C26	C31	116.0(3)
O4	La1	N2	93.24(8)	C31	C26	C27	121.8(3)
N1	La1	Si1	154.26(5)	C26	C27	C28	114.3(5)
N2	La1	Si1	27.94(7)	C26	C27	C29	109.7(5)
N2	La1	O3	96.63(8)	C26	C27	C28A	106.3(4)
N2	La1	N1	177.28(7)	C29	C27	C28	104.3(8)
O3	P1	C42	114.42(14)	C30	C27	C26	111.7(8)
O3	P1	C48	109.78(13)	C30	C27	C28	107.2(9)
O3	P1	C54	110.62(13)	C30	C27	C29	109.3(10)
C42	P1	C48	107.67(15)	C29A	C27	C26	106.8(4)
C42	P1	C54	105.69(14)	C29A	C27	C28A	107.0(7)
C54	P1	C48	108.43(14)	C29A	C27	C30A	116.7(8)
O4	P2	C60	111.28(13)	C30A	C27	C26	110.7(7)
O4	P2	C66	112.55(13)	C30A	C27	C28A	108.7(9)
O4	P2	C72	110.65(15)	C26	C31	C32	124.8(3)
C66	P2	C60	107.45(15)	C31	C32	C33	121.5(3)
C72	P2	C60	108.17(15)	C31	C32	C37	117.3(3)
C72	P2	C66	106.51(14)	C37	C32	C33	121.1(3)
N2	Si1	La1	43.26(9)	C32	C33	C36	110.2(3)
N2	Si1	C38	116.0(2)	C34	C33	C32	112.8(3)
N2	Si1	C39	115.45(17)	C34	C33	C36	106.4(3)
C38	Si1	La1	129.53(17)	C35	C33	C32	108.8(3)
C38	Si1	C39	106.3(2)	C35	C33	C34	107.1(3)
C39	Si1	La1	124.18(15)	C35	C33	C36	111.5(4)
N2	Si2	C40	112.26(17)	O2	C37	C24	119.3(3)
N2	Si2	C41	120.1(4)	O2	C37	C32	121.9(3)
C41	Si2	C40	112.0(4)	C24	C37	C32	118.9(3)
C41A	Si2	N2	124.4(5)	C43	C42	P1	118.6(3)
C41A	Si2	C40	111.8(4)	C47	C42	P1	122.1(3)
C1	O1	La1	148.58(18)	C47	C42	C43	119.3(3)
C37	O2	La1	141.29(18)	C42	C43	C44	119.5(4)
P1	O3	La1	167.60(13)	C45	C44	C43	119.9(4)
P2	O4	La1	162.97(14)	C46	C45	C44	120.2(4)
C15	N1	La1	106.97(16)	C45	C46	C47	120.4(4)
C16	N1	La1	112.18(16)	C42	C47	C46	120.7(4)
C16	N1	C15	112.5(2)	C49	C48	P1	118.2(2)

C16	N1	C23	113.7(2)	C49	C48	C53	119.1(3)
C23	N1	La1	106.23(15)	C53	C48	P1	122.7(3)
C23	N1	C15	104.7(2)	C48	C49	C50	120.1(3)
Si1	N2	La1	108.81(13)	C51	C50	C49	120.8(4)
Si1	N2	Si2	123.12(16)	C50	C51	C52	119.4(4)
Si2	N2	La1	126.39(15)	C53	C52	C51	120.7(4)
O1	C1	C2	121.3(3)	C52	C53	C48	119.9(4)
O1	C1	C14	119.7(3)	C55	C54	P1	119.3(2)
C14	C1	C2	118.9(3)	C55	C54	C59	119.1(3)
C1	C2	C3	121.6(3)	C59	C54	P1	121.6(2)
C7	C2	C1	117.8(3)	C56	C55	C54	120.4(3)
C7	C2	C3	120.4(3)	C55	C56	C57	120.4(3)
C2	C3	C4	111.4(3)	C58	C57	C56	119.5(3)
C2	C3	C5	109.1(3)	C57	C58	C59	120.6(3)
C2	C3	C6	112.1(3)	C58	C59	C54	120.0(3)
C4	C3	C5	109.6(3)	C61	C60	P2	122.3(3)
C4	C3	C6	106.8(3)	C65	C60	P2	117.9(2)
C5	C3	C6	107.7(3)	C65	C60	C61	119.7(3)
C8	C7	C2	124.0(3)	C62	C61	C60	119.6(3)
C7	C8	C9	121.4(3)	C63	C62	C61	120.5(4)
C7	C8	C13	116.6(3)	C64	C63	C62	120.1(4)
C13	C8	C9	121.9(3)	C63	C64	C65	120.3(4)
C8	C9	C12A	109.6(7)	C60	C65	C64	119.9(3)
C10	C9	C8	108.7(7)	C67	C66	P2	121.9(2)
C10	C9	C12	110.2(10)	C67	C66	C71	119.1(3)
C11	C9	C8	108.5(6)	C71	C66	P2	118.9(2)
C11	C9	C10	110.0(9)	C68	C67	C66	120.7(3)
C11	C9	C12	108.9(9)	C67	C68	C69	119.4(3)
C12	C9	C8	110.6(6)	C70	C69	C68	120.3(3)
C10A	C9	C8	113.7(6)	C69	C70	C71	120.8(3)
C10A	C9	C11A	111.7(8)	C70	C71	C66	119.9(3)
C10A	C9	C12A	104.8(7)	C73	C72	P2	121.9(3)
C11A	C9	C8	110.3(6)	C77	C72	P2	118.8(3)
C11A	C9	C12A	106.2(8)	C77	C72	C73	119.3(3)
C8	C13	C14	122.3(3)	C74	C73	C72	119.7(4)
C1	C14	C15	122.4(2)	C75	C74	C73	120.2(4)
C13	C14	C1	120.1(3)	C74	C75	C76	120.8(4)
C13	C14	C15	116.5(3)	C75	C76	C77	120.2(4)
N1	C15	C14	119.9(2)	C76	C77	C72	119.8(4)

Table S8a. Bond distances for **1-Y(TPPO)$_2$**.

Y1	Si1	3.3926(8)	C8	C13	1.393(3)	C42	C47	1.392(3)
Y1	O1	2.1610(15)	C9	C10	1.546(8)	C43	C44	1.385(4)
Y1	O2	2.1557(15)	C9	C11	1.513(9)	C44	C45	1.375(4)
Y1	O3	2.3160(15)	C9	C12	1.513(9)	C45	C46	1.377(5)
Y1	O4	2.2948(15)	C9	C10A	1.511(9)	C46	C47	1.376(4)
Y1	N1	2.6578(18)	C9	C11A	1.509(8)	C48	C49	1.381(3)
Y1	N2	2.301(2)	C9	C12A	1.494(9)	C48	C53	1.399(3)
P1	O3	1.5060(15)	C13	C14	1.396(3)	C49	C50	1.389(4)
P1	C42	1.806(2)	C14	C15	1.507(3)	C50	C51	1.375(4)
P1	C48	1.807(2)	C16	C17	1.517(3)	C51	C52	1.386(4)
P1	C54	1.796(2)	C17	C18	1.390(4)	C52	C53	1.374(4)
P2	O4	1.5019(16)	C17	C22	1.392(4)	C54	C55	1.395(4)
P2	C60	1.797(2)	C18	C19	1.389(4)	C54	C59	1.377(4)
P2	C66	1.796(2)	C19	C20	1.377(5)	C55	C56	1.384(4)
P2	C72	1.798(2)	C20	C21	1.366(5)	C56	C57	1.380(5)
Si1	N2	1.696(2)	C21	C22	1.388(4)	C57	C58	1.360(5)
Si1	C38	1.868(3)	C23	C24	1.507(3)	C58	C59	1.383(4)
Si1	C39	1.873(3)	C24	C25	1.389(3)	C60	C61	1.396(3)
Si2	N2	1.723(2)	C24	C37	1.415(3)	C60	C65	1.389(3)
Si2	C40	1.865(3)	C25	C26	1.388(3)	C61	C62	1.384(3)
Si2	C41	1.816(4)	C26	C27	1.534(3)	C62	C63	1.375(4)
O1	C1	1.332(3)	C26	C31	1.388(4)	C63	C64	1.385(4)
O2	C37	1.320(3)	C27	C28	1.599(7)	C64	C65	1.376(4)
N1	C15	1.491(3)	C27	C29	1.495(6)	C66	C67	1.390(3)
N1	C16	1.493(3)	C27	C30	1.495(7)	C66	C71	1.390(4)
N1	C23	1.496(3)	C27	C28A	1.546(9)	C67	C68	1.379(4)
C1	C2	1.423(3)	C27	C29A	1.537(9)	C68	C69	1.359(5)
C1	C14	1.411(3)	C27	C30A	1.450(10)	C69	C70	1.371(5)
C2	C3	1.538(4)	C31	C32	1.394(3)	C70	C71	1.389(4)
C2	C7	1.390(3)	C32	C33	1.538(3)	C72	C73	1.385(3)
C3	C4	1.536(4)	C32	C37	1.421(3)	C72	C77	1.387(3)
C3	C5	1.536(4)	C33	C34	1.532(4)	C73	C74	1.386(4)
C3	C6	1.527(4)	C33	C35	1.524(4)	C74	C75	1.371(4)
C7	C8	1.390(4)	C33	C36	1.537(4)	C75	C76	1.365(4)
C8	C9	1.533(3)	C42	C43	1.382(3)	C76	C77	1.382(4)

Table S8b. Bond angles for **1-Y(TPPO)$_2$**.

O1	Y1	Si1	86.00(4)	C18	C17	C16	121.4(2)
O1	Y1	O3	95.21(6)	C18	C17	C22	117.9(2)
O1	Y1	O4	85.47(6)	C22	C17	C16	120.4(2)
O1	Y1	N1	75.57(6)	C19	C18	C17	120.5(3)
O1	Y1	N2	104.91(7)	C20	C19	C18	120.7(3)
O2	Y1	Si1	120.94(4)	C21	C20	C19	119.3(3)
O2	Y1	O1	152.65(6)	C20	C21	C22	120.6(3)

O2	Y1	O3	87.44(6)	C21	C22	C17	120.9(3)
O2	Y1	O4	88.30(6)	N1	C23	C24	117.15(17)
O2	Y1	N1	77.39(5)	C25	C24	C23	118.76(19)
O2	Y1	N2	102.06(7)	C25	C24	C37	120.6(2)
O3	Y1	Si1	76.52(4)	C37	C24	C23	120.00(19)
O3	Y1	N1	87.15(5)	C26	C25	C24	122.2(2)
O4	Y1	Si1	111.55(4)	C25	C26	C27	121.6(2)
O4	Y1	O3	171.93(5)	C25	C26	C31	116.5(2)
O4	Y1	N1	85.23(5)	C31	C26	C27	121.9(2)
O4	Y1	N2	93.84(6)	C26	C27	C28	107.1(3)
N1	Y1	Si1	154.17(4)	C26	C27	C28A	113.2(4)
N2	Y1	Si1	26.86(5)	C26	C27	C29A	109.7(5)
N2	Y1	O3	93.75(6)	C29	C27	C26	108.7(3)
N2	Y1	N1	178.93(6)	C29	C27	C28	106.7(4)
O3	P1	C42	110.02(10)	C29	C27	C30	112.7(6)
O3	P1	C48	110.76(10)	C30	C27	C26	112.6(4)
O3	P1	C54	115.22(10)	C30	C27	C28	108.8(6)
C42	P1	C48	108.54(11)	C29A	C27	C28A	102.3(8)
C54	P1	C42	107.20(12)	C30A	C27	C26	111.0(5)
C54	P1	C48	104.79(11)	C30A	C27	C28A	107.8(9)
O4	P2	C60	112.55(10)	C30A	C27	C29A	112.7(9)
O4	P2	C66	110.68(10)	C26	C31	C32	124.3(2)
O4	P2	C72	111.87(10)	C31	C32	C33	120.9(2)
C60	P2	C72	107.27(11)	C31	C32	C37	118.2(2)
C66	P2	C60	105.99(10)	C37	C32	C33	120.8(2)
C66	P2	C72	108.20(11)	C34	C33	C32	112.6(2)
N2	Si1	Y1	37.81(7)	C34	C33	C36	106.2(2)
N2	Si1	C38	115.11(16)	C35	C33	C32	108.9(2)
N2	Si1	C39	115.60(13)	C35	C33	C34	107.4(2)
C38	Si1	Y1	129.97(13)	C35	C33	C36	111.4(2)
C38	Si1	C39	105.17(17)	C36	C33	C32	110.3(2)
C39	Si1	Y1	124.12(12)	O2	C37	C24	119.05(18)
N2	Si2	C40	112.96(12)	O2	C37	C32	122.8(2)
N2	Si2	C41	116.6(2)	C24	C37	C32	118.2(2)
C41	Si2	C40	106.16(19)	C43	C42	P1	118.05(19)
C1	O1	Y1	146.10(14)	C43	C42	C47	118.8(2)
C37	O2	Y1	140.54(13)	C47	C42	P1	123.1(2)
P1	O3	Y1	169.93(10)	C42	C43	C44	120.5(3)
P2	O4	Y1	164.03(10)	C45	C44	C43	120.0(3)
C15	N1	Y1	107.66(12)	C44	C45	C46	120.0(3)
C15	N1	C16	111.60(16)	C47	C46	C45	120.2(3)
C15	N1	C23	104.54(15)	C46	C47	C42	120.4(3)
C16	N1	Y1	112.60(12)	C49	C48	P1	119.58(17)
C16	N1	C23	112.88(17)	C49	C48	C53	118.9(2)
C23	N1	Y1	107.07(12)	C53	C48	P1	121.48(18)

Si1	N2	Y1	115.33(11)	C48	C49	C50	120.3(2)
Si1	N2	Si2	117.77(12)	C51	C50	C49	120.3(2)
Si2	N2	Y1	124.71(11)	C50	C51	C52	119.7(2)
O1	C1	C2	122.0(2)	C53	C52	C51	120.2(2)
O1	C1	C14	119.35(19)	C52	C53	C48	120.4(2)
C14	C1	C2	118.6(2)	C55	C54	P1	119.03(19)
C1	C2	C3	121.8(2)	C59	C54	P1	121.9(2)
C7	C2	C1	118.2(2)	C59	C54	C55	119.1(2)
C7	C2	C3	119.8(2)	C56	C55	C54	119.4(3)
C4	C3	C2	111.1(2)	C57	C56	C55	120.6(3)
C4	C3	C5	109.8(2)	C58	C57	C56	120.0(3)
C5	C3	C2	108.6(2)	C57	C58	C59	120.1(3)
C6	C3	C2	112.5(2)	C54	C59	C58	120.9(3)
C6	C3	C4	107.5(2)	C61	C60	P2	121.39(17)
C6	C3	C5	107.4(2)	C65	C60	P2	119.37(18)
C8	C7	C2	124.1(2)	C65	C60	C61	119.2(2)
C7	C8	C9	121.5(2)	C62	C61	C60	120.3(2)
C7	C8	C13	116.5(2)	C63	C62	C61	119.7(2)
C13	C8	C9	121.9(2)	C62	C63	C64	120.3(2)
C8	C9	C10	110.0(6)	C65	C64	C63	120.3(2)
C11	C9	C8	111.0(5)	C64	C65	C60	120.2(2)
C11	C9	C10	107.3(7)	C67	C66	P2	121.6(2)
C11	C9	C12	109.2(7)	C71	C66	P2	119.01(19)
C12	C9	C8	114.4(5)	C71	C66	C67	119.3(2)
C12	C9	C10	104.4(7)	C68	C67	C66	120.1(3)
C10A	C9	C8	111.9(5)	C69	C68	C67	120.5(3)
C11A	C9	C8	108.2(4)	C68	C69	C70	120.3(3)
C11A	C9	C10A	109.4(7)	C69	C70	C71	120.5(3)
C12A	C9	C8	107.8(5)	C70	C71	C66	119.3(3)
C12A	C9	C10A	110.0(9)	C73	C72	P2	122.31(19)
C12A	C9	C11A	109.4(7)	C73	C72	C77	119.3(2)
C8	C13	C14	122.2(2)	C77	C72	P2	118.37(19)
C1	C14	C15	122.54(19)	C72	C73	C74	119.8(3)
C13	C14	C1	120.0(2)	C75	C74	C73	120.4(3)
C13	C14	C15	116.6(2)	C76	C75	C74	120.1(3)
N1	C15	C14	119.76(17)	C75	C76	C77	120.4(3)
N1	C16	C17	119.38(18)	C76	C77	C72	120.1(3)

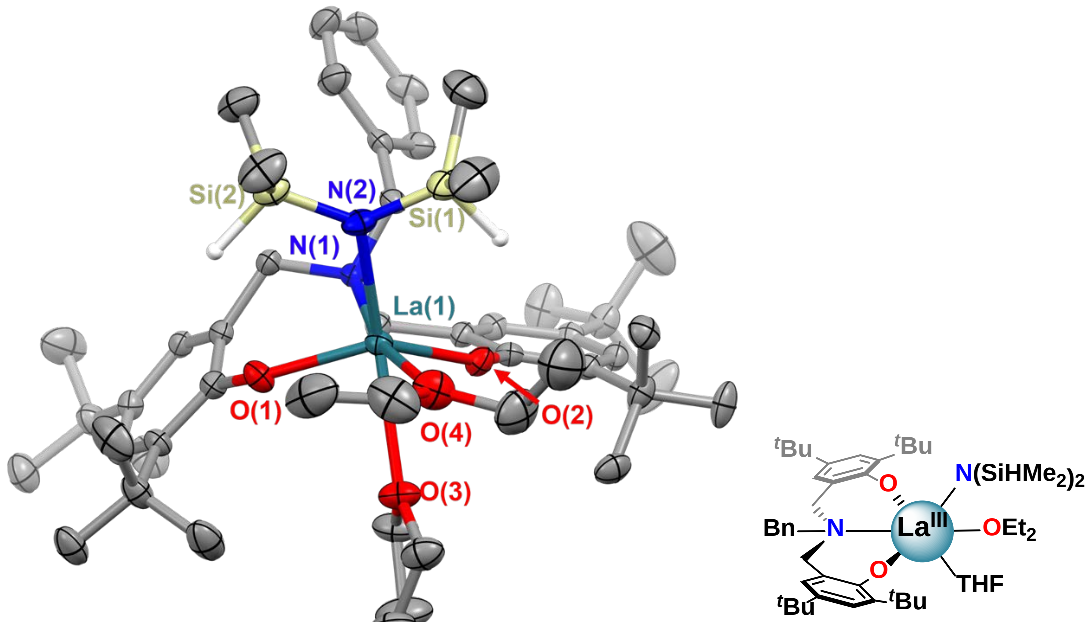

1-La

Figure S26. Thermal ellipsoid plot of **1-La** ([La(^{1}**L**)(N(SiHMe$_2$)$_2$)(Et$_2$O)(THF)]) shown at 50% probability. Hydrogen atoms other than those attached to Si(1) and Si(2) have been removed for clarity.

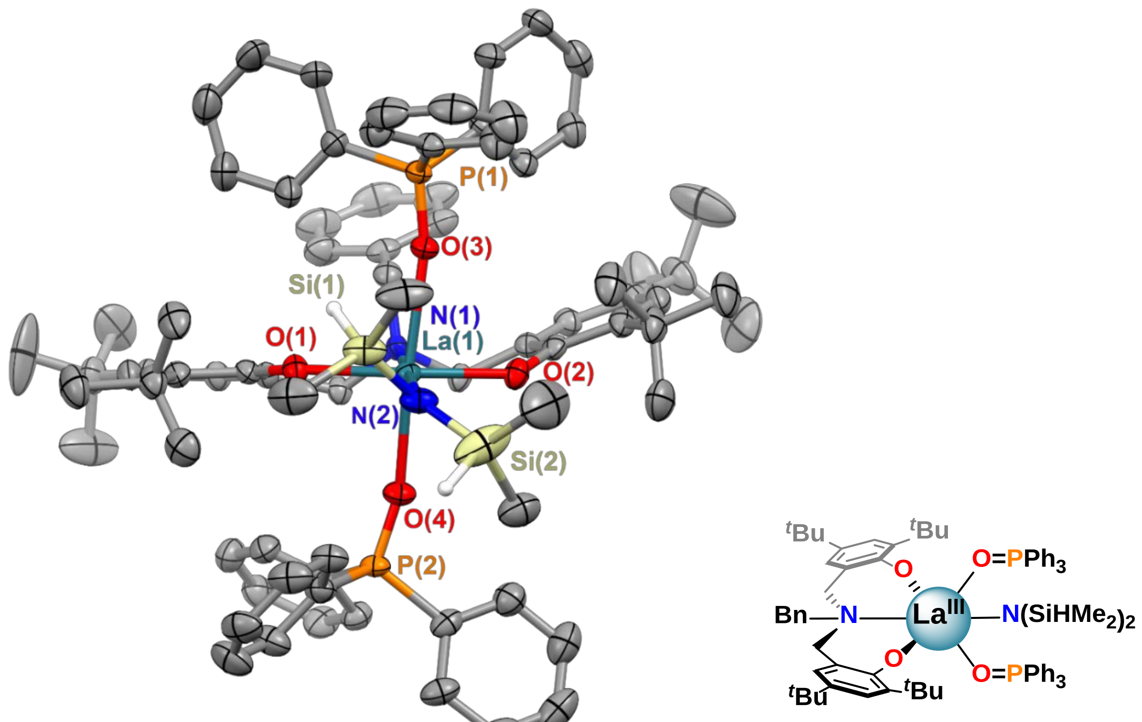

1-La(TPPO)2

Figure S27. Thermal ellipsoid plot of **1-La(TPPO)$_2$** ([La(^{1}**L**)(N(SiHMe$_2$)$_2$)(TPPO)$_2$]) shown at 50% probability. Second components of the two disordered tert-butyl groups and the (Me$_2$H) unit on Si(2) have been removed for clarity. Hydrogen atoms other than those attached to Si(1) and Si(2) have been removed for clarity.

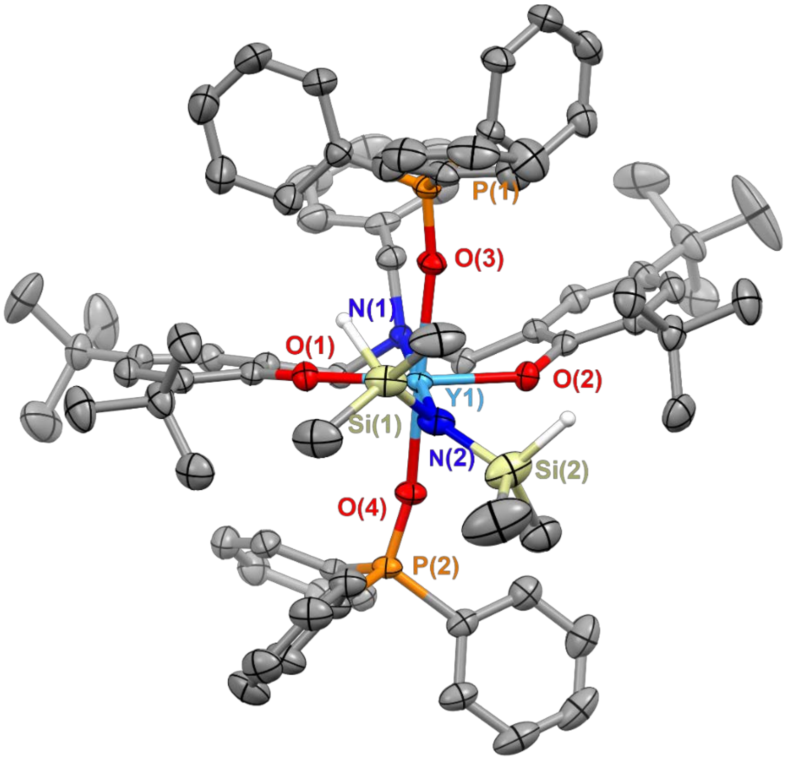

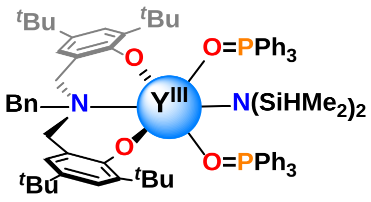

1-Y(TPPO)2

Figure S28. Thermal ellipsoid plot of **1-Y(TPPO)₂** ([Y([1]L)(N(SiHMe₂)₂)(TPPO)₂]) shown at 50% probability. Second components of the two disordered tert-butyl groups have been removed for clarity. Hydrogen atoms other than those attached to Si(1) and Si(2) have been removed for clarity.

5. References

1. Sandström, J. *Dynamic NMR Spectroscopy*; Academic Press: New York, **1982**.
2. Amgoune, A.; Thomas, C. M.; Ilinca, S.; Roisnel, T.; Carpentier, J.-F. *Angew. Chem., Int. Ed.* **2006**, *45*, 2782−2784.
3. Save, M.; Schappacher, M.; Soum, A. *Macromol. Chem. Phys.* **2002**, *203*, 889-899.
4. Bradley, D. C.; Ghotra, J. S.; Hart, F. A. *J. Chem. Soc., Dalton Trans.* **1973**, 1021−1023.
5. Smith, A. R.; Livinghouse, T. *Organometallics* **2013**, *32*, 1528−1530.
6. Amgoune, A.; Thomas, C. M.; Roisnel, T.; Carpentier, J.-F. *Chem. - Eur. J.* **2006**, *12*, 169−179.
7. Cai, C.-X.; Amgoune, A.; Lehmann, C. W.; Carpentier, J.-F. *Chem. Commun.* **2004**, 330−331.
8. Bruker SAINT, v8.37a; Bruker AXS Inc.: Madison, Wisconsin, 2012.
9. Sheldrick, G. M. SHELXT – Integrated space-group and crystal-structure determination, *Acta Crystallogr. Sect. A: Found. Crystallogr.* **2015**, *71*, 3–8.
10. Bruker SADABS, v2014/5; Bruker AXS Inc.: Madison, Wisconsin, 2001.
11. Sheldrick, G. M. Crystal structure refinement with SHELXL, *Acta Crystallogr. Sect. C: Cryst. Struct. Commun.* **2015**, *71*, 3–8.

12. Müller, P.; Herbst-Irmer, R.; Spek, A. L.; Schneider, T. R.; Sawaya, M. R. Crystal Structure Refinement: A Crystallographer's Guide to SHELXL; Oxford University Press, New York, 2006.
13. Thorn, A.; Dittrich, B.; Sheldrick, G. M. Enhanced rigid-bond restraints, *Acta Cryst.* **2012**, *A68*, 448-451.
14. Spek, A. L. PLATON SQUEEZE: a tool for the calculation of the disordered solvent contribution to the calculated structure factors. *Acta Cryst.* **2015**, *C71*, 9-18.
15. Fleming, W. J.; Muller-Bunz, H.; Lillo, V; Fernandez, E; Guiry, P. J., *Org. Biomol. Chem.*, **2009**, *7*, 2520–2524.
16. Save, M.; Schappacher, M.; A. Soum, *Macromol. Chem. Phys* **2002,** *203*, 889-899.
17. Ouyang, H.; Nie, K.; Yuan, D.; Yao, Y. *Dalton Trans.*, **2017**, *46*, 15928−15938.
18. Han, F.; Yang, L.; Li, Z.; Xia, C. *Org. Biomol. Chem.*, **2012**, *10*, 346-354.
19. Griesbaum, K.; Zwick, G. *Chem. Ber.*, **1986**, *119*, 229-243.